ATOMIC SCALE CHEMISTRY ON SILICON SURFACES STUDIED WITH A VARIABLE TEMPERATURE SCANNING TUNNELING MICROSCOPE

A Dissertation

Presented to the Faculty of the Graduate School

of Cornell University

in Partial Fulfillment of the Requirements for the Degree of

Doctor of Philosophy

by

Mohammad Ali Rezaei

August 1998

ATOMIC SCALE CHEMISTRY ON SILICON SURFACES STUDIED WITH A VARIABLE TEMPERATURE SCANNING TUNNELING MICROSCOPE

Mohammad Ali Rezaei, Ph.D.

Cornell University 1998

Using a variable temperature scanning tunneling microscope, we have studied several adsorbates on silicon surfaces. We have studied the adsorption characteristics of H_2S on Si(111)-(7×7). H_2S adsorbs dissociatively at sub-monolayer coverage, from 50 to 300 K, with HS bonded to an adatom and H bonded to a rest atom. The adsorption is site selective and the adsorption site preference is temperature dependent. At 50 K, the faulted center sites are most favored for adsorption, followed by unfaulted center sites, faulted corner sites, and unfaulted corner sites. As the temperature is increased, the differences between the faulted and unfaulted halves diminish, but the center sites remain more reactive than the corner sites. We present an explanation to account for the non-Langmuir kinetics involved in this system.

We have induced and imaged the dissociation of HS and DS on Si(111)-(7×7). Individual HS (or DS) fragments can be dissociated with the STM at low temperatures without affecting neighboring adsorbates. Near room temperature (297 K)

and above, DS dissociates thermally, with an activation barrier of 0.73 ± 0.15 eV. The activation barrier was calculated from atomistic studies of the dissociation rates at temperatures between 297 and 312 K.

We have induced and imaged the dissociation of D_2S on Si(100). D_2S dissociates into DS and D below 200 K. Individual DS fragments can be dissociated with the STM at low temperatures. At 200 K or above, D_2S dissociates into S and two D's. D_2S adsorption affects the surface reconstruction on Si(100), from the buckled dimer configuration to the dynamically flipping configuration and vice versa.

We have studied the adsorption and STM induced desorption of NO from Si(111)-(7×7). NO adsorbs preferentially on faulted corner sites, followed by faulted center sites, unfaulted corner sites and unfaulted center sites. The preference for the different adsorption sites is independent of temperature and correlates well with the local density of states at these sites. NO can be desorbed from Si(111) by the STM. The data suggest the desorption is induced by the electric field under the STM tip. The threshold positive electric field for desorption of NO is 0.114 ± 0.009 V/Å.

Biographical Sketch

He was born two months premature by c-section on the nineteenth day of the first month of the Persian calendar. At the age of fourteen, he left Teheran for Vienna, Austria. He spent four years in Vienna attending high school at the American International School. He then ventured to the United States of America to earn two degrees in four years from the University of Pennsylvania with high honors (*magna cum laude*). He then decided to pursue graduate studies in physics at Cornell University. After six years of study and research, he may yet graduate with a Ph.D. in physics.

To my parents and my sister.

Acknowledgements

For the past four years, I have been fortunate enough to have the support and guidance of my advisor, Professor Wilson Ho. His unconditional confidence in my ability to overcome problems has been almost unreal at times. I appreciate his support which has been strongest when I needed some direction. I would also like to thank the members of my Special Committee, Professors Geoffrey Chester and Robert Buhrman for administering my A and B exams as well as putting up with all the required bureaucracy. Professor Harold Craighead has cordially agreed to serve as a proxy during my B exam for Professor Buhrman, for which I am grateful.

My co-worker, Barry Stipe, has been instrumental in designing and building the scanning tunneling microscope (STM) used for the research described here. His excellent command of electronics as well as his meticulous attention to every detail have made this project possible. Four years is a long time to spend with another person in a small room, but we somehow managed to keep everything sane. He has my eternal gratitude and I wish him the best of luck in his future endeavors.

This work was greatly facilitated by the excellent support staff at Cornell. A special thanks goes to Sned (Bob Snedeker) for all the hours in the shop and the machine shop crew for their precise and timely work, especially Stan Carpenter, Rodney Bowman and Jeff Koski. I would like to thank Rick Cochran and Daniel

Blakeley for upgrading and maintaining a complex computing infrastructure. Many of the equipment used in the course of my studies at Cornell was at the Technical Operations Lab of the Cornell Center for Materials Research and my thanks goes to Gerhard Schmidt and Ron Kemp for teaching me how to use the equipment.

I would like to express my sincerest thanks to Lincoln Lauhon for allowing me to use and modify his AutoCad diagrams (Fig. B.1, Fig. B.3, Fig. B.4, Fig. B.5, Fig. B.6, Fig. B.7, Fig. B.8). He also proofread large portions of this thesis, for which I am grateful. I also thank Hyojune Lee for drawing Fig. B.9 and allowing me to use it.

I would like to thank the older graduate students in the Ho group for showing me the ropes and the younger students for helping me throughout the past four years. Kyle Brown, Darryl Busch, Robert Pelak, Amanda Killen, Scott Ustin, Lincoln Lauhon and Li Yang are but a few names that I will remember fondly.

Support for this research by the Division of Chemical Sciences, Office of Basic Energy Sciences, Office of Energy Research, U.S. Department of Energy under Grant No. DE-FG02-91ER14025 is gratefully acknowledged.

Table of Contents

List of Tables

List of Figures

Chapter 1

Introduction

Chemical reactions on solid surfaces have spurred scientific research and subsequent industrial applications for over 150 years [1]. Catalysis on metal surfaces is an important subclass of these reactions and has been studied extensively [2]. Reactions on semiconducting surfaces have become an important avenue of research in the past few decades due to their wide array of applications. The major thrust of the present work is to understand the atomic scale chemistry between adsorbates and silicon surfaces.

Solids are held together by the chemical bonds between the atoms in the solid. If these bonds are broken in a crystal plane, a well ordered and highly reactive surface will result. The surface atoms have a lower coordination number compared to the bulk atoms and can readily react with a variety of substances. Performing experiments on highly reactive surfaces under best done under ultrahigh vacuum (UHV) because the experiment can be better controlled and the surface would otherwise react with ambient gases. For covalent solids with highly oriented bonds, such as silicon, the broken bond energy at the surface is often large. To minimize the energy at the surface, the atoms rearrange or "reconstruct" under suitable conditions. For

example, heating silicon in UHV will result in a variety of reconstructions depending on the crystal orientation and temperature [3]. The reconstruction, however, does not pacify the surface entirely. The remaining dangling bonds are good candidates for reaction sites and often react before other bonds are broken. The arrangement of the dangling bonds is critical for understanding the chemistry ensuing on the surface. A brief description of Si(111) and Si(100) reconstructions are included in this introduction.

There are a number of questions that when answered further our understanding of a particular reaction. The reaction pathway may be elucidated by determining the reaction site on the surface as well as the adsorption geometry. Different adsorption sites and different reactivities can reveal the effect of local chemistry on the reaction. Incoming molecules may search for reaction sites via a mobile precursor state. A precursor state is defined by lower binding energy and further distance from the surface compared to the more strongly bonded, chemisorbed state. The availability of reaction sites as a function coverage and the maximum coverage can determine whether a mobile precursor exists for a particular reaction. Interactions between neighboring adsorbates may be important in determining the high coverage behavior of the system. The scanning tunneling microscope has been instrumental in studying reactions on surfaces at the atomic scale due to its ability to answer the questions defined above [4–7].

Since its inception in 1982 [8], the STM has found wide acceptance in study of surface science. Perhaps the most attractive feature of this instrument is its extremely high spatial resolution and real space imaging capability. Although theoretical modeling of STM images is often helpful, it is rarely necessary for interpreting the STM images if the adsorbates and substrate material are known. The

ability of the STM to resolve single atoms makes the study of chemical reactions at the low coverage (about one adsorbate per 100 substrate atoms or 0.01 monolayer) regime possible. At low coverage, the reaction involves only the adsorbate and the substrate and is not complicated by adsorbate-adsorbate interactions. The STM is also effective at medium coverages (0.1 to 0.5 monolayer), where the effect of adsorbate-adsorbate interactions may be directly compared with the low coverage results. At high coverage, however, the interaction of the adsorbates with the STM tip can cause difficulties, especially for reactive adsorbates, mobile adsorbates or loose multilayer adsorbate systems.

Not only can the STM be used to observe surfaces, it can also be used to directly modify the surface or adsorbates [9, 10]. Interactions between the STM tip and the adsorbate or substrate include Van der Waal's forces [11], the electric field under the STM tip [12], and the tunneling electrons interacting with the adsorbate or substrate [13]. This capability is often touted as a novel approach to nanolithography, although there been have no commercial applications that use STMs in such a capacity. The more important use of this capability to date is inducing chemical changes in a system that may reveal the basic physical phenomenon underlying the interaction of the adsorbate with the substrate. By studying the dependence of the interaction on the various parameters (bias voltage, current and tip-surface distance), we learn about the mechanisms involved in the reaction.

The chemistry on silicon surfaces is strongly influenced by the arrangement of atoms at the surface. The (7×7) reconstruction of the Si(111) surface is one of the most complicated reconstructions known. The STM was instrumental in the determination of the exact surface structure [14]. In the dimer adatom stacking fault (DAS) model of the reconstruction, there are 12 atoms at the topmost layer,

called adatoms. All of these atoms have a dangling bond. The reconstruction is not limited to the first layer; the top four layers are significantly different from the bulk arrangement. There are 19 dangling bonds, 12 at the adatom layer, 6 at the rest atom (second) layer and 1 at the corner hole. That is a significant reduction as compared to the 49 dangling bonds of the bulk terminated surface.

Figure 1.1a shows a schematic of the reconstructed surface. The adatom positions in one half of the unit cell have a stacking fault with respect to the bulk arrangement. Although the stacking fault does not introduce a net height difference between the two halves of the unit cell, it does change the local density of states (LDOS). With a negative sample bias, the STM images the filled state LDOS. As can be seen in Fig. 1.1b, the faulted half of the unit cell appears brighter, indicating a higher LDOS. The adatoms on the faulted half are found to be more reactive under a wide range of experimental conditions (Ch. 2, Ch. 5). In the adatom layer, there are four different types of atoms: faulted and unfaulted corner sites and faulted and unfaulted center sites. These sites have different reactivities even within the same half of the unit cell, in part due to the different electronic density at these sites. The dangling bonds in the rest atom layer are also potential reaction sites and can strongly influence adsorption behavior (Ch. 2). This unique arrangement of atoms allows us to study the effects of local chemistry.

The defects on Si(111) tend to be fairly simple: usually one or two missing adatoms. When a center site adatom is missing, a neighboring adatom will often move to minimize the surface energy. Figure 1.2a shows examples of a missing adatom defect. The marked defect is one where the neighboring adatom has moved to the midpoint of where the two atoms would have been. We have not found any systematic preference of adsorbates for these defect sites possibly because our sur-

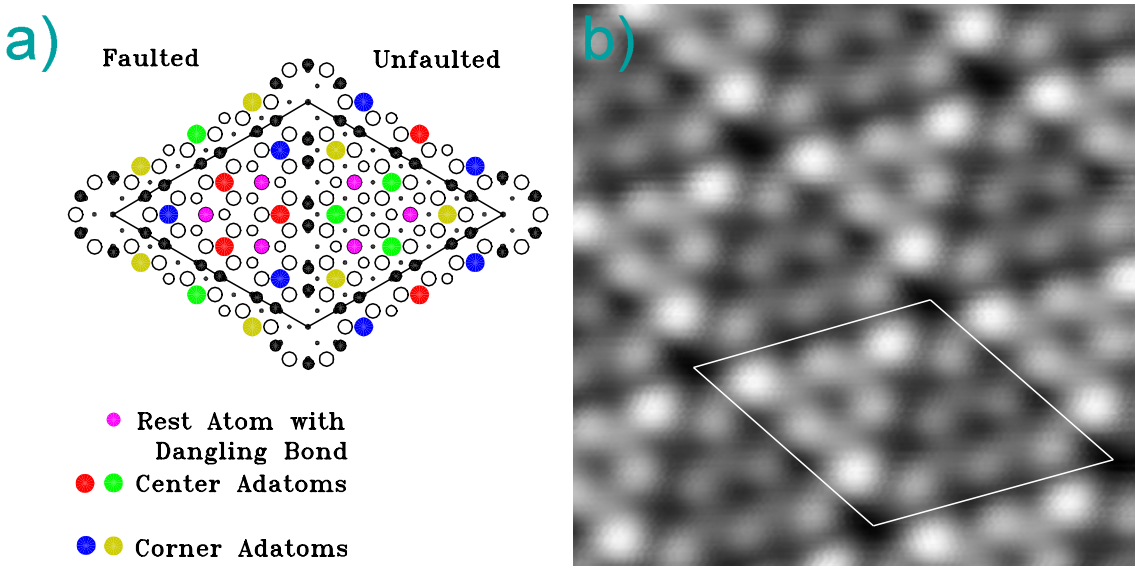

Figure 1.1: a) Schematic drawing of the (7×7) reconstructed Si(111) surface. b) Room temperature STM image of the filled states (sample bias −2 V, tunneling current 1 nA) of Si(111)-(7×7). The brighter half of the unit cell is the faulted half. The diamond outlines the (7×7) unit cell.

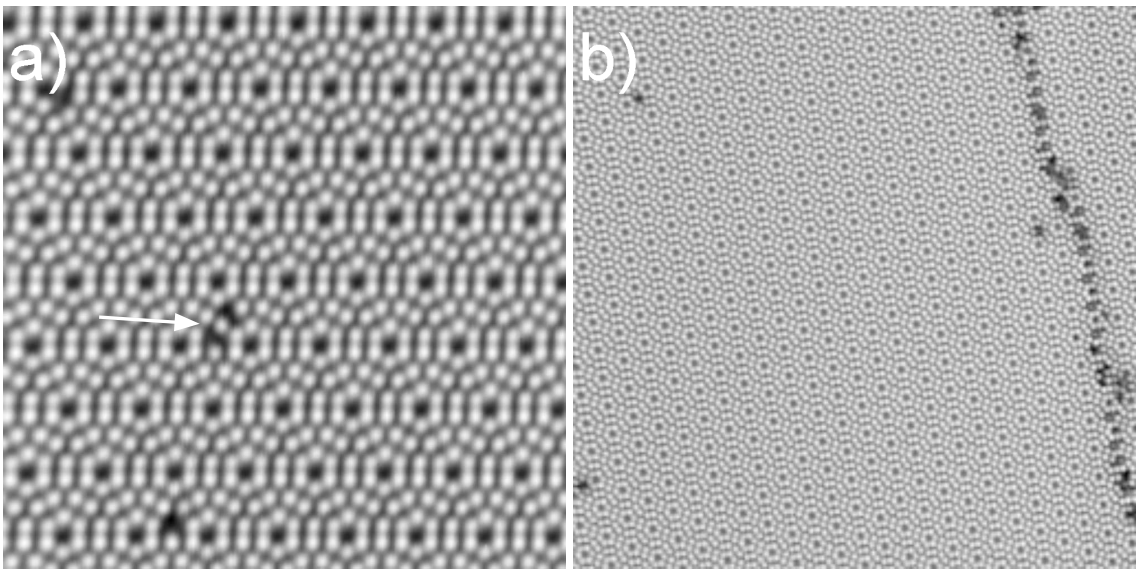

Figure 1.2: a) Examples of defects on Si(111). The marked defect shows how an adatom can move to the midpoint of its position and the position of missing adatom. b) Domain phase boundary defect is visible on the right edge of the image.

face have very low defect density (less than 1%). There is one other defect on the surface that is readily observable with the STM: the domain phase boundary [15]. Figure 1.2b shows an example of a domain phase boundary defect on Si(111). Although we have not studied the domain phase boundary and its interaction with adsorbates in great detail, it is a very visible feature on the surface and can be used to locate the same area even after heavy dosing.

Si(100) has a much simpler reconstruction than Si(111). The unreconstructed square lattice is dimerized to form rows of dimers. The inter-dimer distance is 3.84 Å and the distance between the atoms in the dimer is 2.4 Å [16]. These atoms are much closer together than the 6.7 to 7.7 Å distance between adatoms on Si(111). Imaging closely spaced atoms, especially the atoms within the dimer, is therefore more difficult. The STM has also been important in determining the

ground state configuration of the dimerized surface. At room temperature, the dimers appear symmetric and the reconstruction was thought to be a simple (2×1) arrangement. Low temperature STM studies revealed the existence of centered 4×2 and primitive 2×2 reconstructions on the surface [17], wherein alternating dimers are buckled differently and the dimers appear asymmetric. The p(2×2) reconstruction does not occur as frequently as the c(4×2) reconstruction. The (2×1) appearance at room temperature is attributed to rapidly oscillating buckled dimers. Theoretical calculations have confirmed the lowest energy configuration to be the c(4×2) arrangement with p(2×2) a close second.

The appearance of Si(100) in STM images is both temperature and bias dependent. Figure 1.3a shows a large area scan of Si(100) at 300 K with a 2 V bias voltage. With a positive sample bias, the empty states are imaged; the dimer bonds appear dark and the remaining dangling bond on each surface atom appears bright. A close up view of the reconstructed dimers (Fig. 1.3b) shows the dark dimer bond and the dangling bond on each Si atom. Below 200 K, domains of centered 4×2 reconstruction appear if the surface defect density is low enough (Fig. 1.3c). Figure 1.3d shows the Si(100) surface scanned at 150 K with a 2 V bias. Silicon atoms that are buckled down are visible in this image.

The defects on Si(100) influence the surface reconstruction to a greater degree than those on Si(111). Although the ground state arrangement is c(4×2), defects can pin regions of rapidly flipping (symmetric) dimers and are also found at the boundary of p(2×2) reconstructed regions. The defects on Si(100) are often attributed to missing silicon dimers which appear dark in STM images, but it has also been suggested that some of the defects may be adsorbed water [18].

We have studied the adsorption of H_2S and D_2S on Si(111). Chapter 2 will

Figure 1.3: a) Clean Si(100) scanned at 300 K, with 2 V sample bias. The dimers appear symmetric because they are dynamically flipping up and down at this temperature. b) High resolution scan at 300 K and 2 V sample bias. A silicon dimer is outlined. The dimer bond appears dark. c) Si(100) scanned at 150 K and 0.7 V sample bias. The c(2×4) reconstruction shows a typical "honeycomb" pattern because alternating Si atoms are not visible. The dynamically flipping dimers appear symmetric, much like the room temperature images. d) High resolution scan at 150 K and 2 V sample bias. A c(2×4) unit cell is outlined. At this bias voltage, all Si atoms are visible.

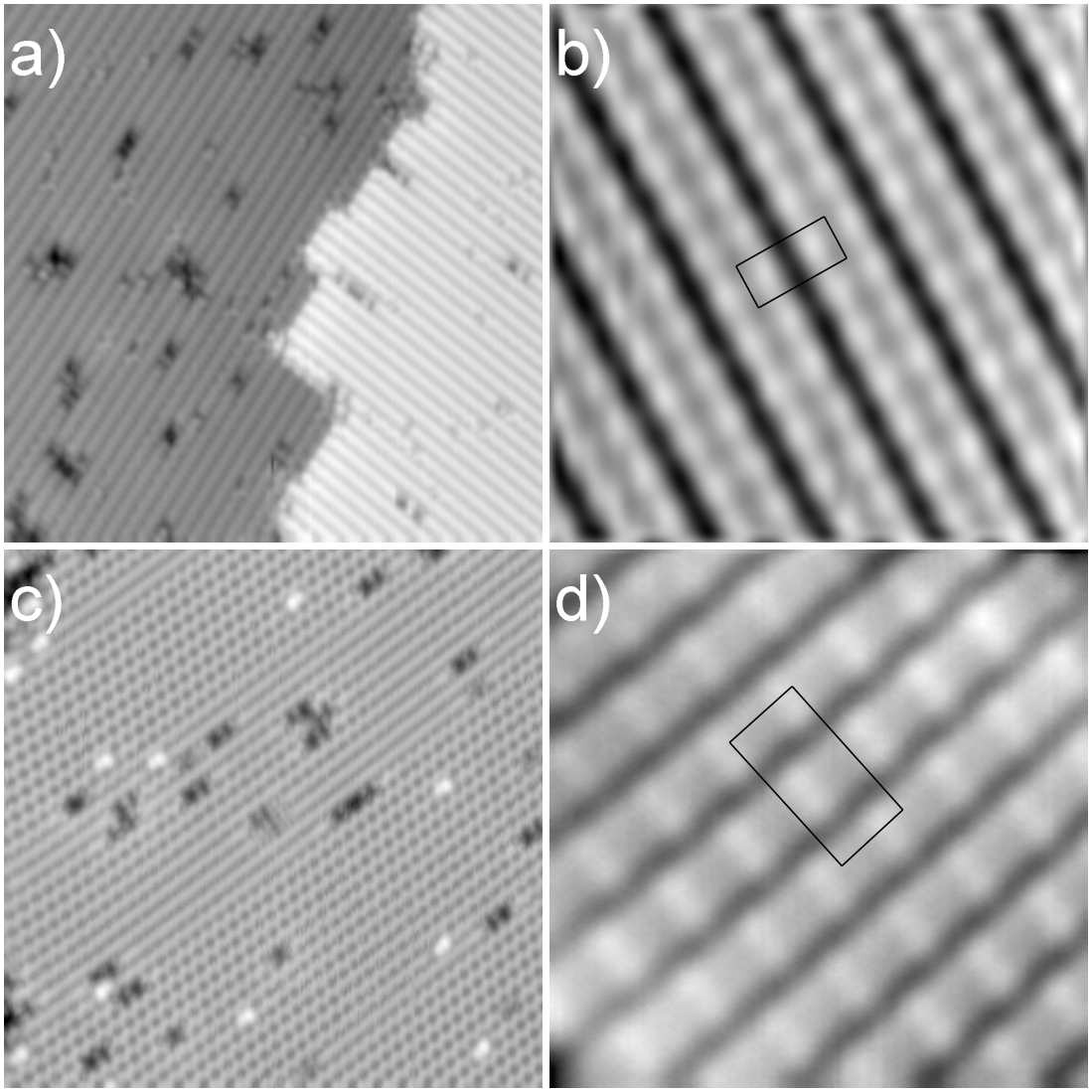
a)
b)
c)
d)

discuss the adsorption characteristics of H_2S and D_2S on Si(111). Chapter 3 will discuss DS dissociation as induced by STM or by heat. Chapter 4 will discuss the adsorption of D_2S on Si(100). The differences between the two surfaces as related to D_2S adsorption are explored in Ch. 4. Chapter 5 discusses the adsorption as well as the STM induced desorption of NO on Si(111).

Our instrument has been described in detail elsewhere [19, 20]. Appendix A describes the philosophy behind the computer program that controls the STM. Appendix B is a guide to building an STM scanning head.

Bibliography

[1] J. Trofast, J. J. Berzelius and the Concept of Catalysis' in *Perspectives in Catalysis*, Liberaromodel, Lund (1981).

[2] T. J. Yates Jr., *The Activation of Chemical Bonds; Solvay Conference on Surface Science* (Springer Series in Surface Science 14, p. 74-108, 1988).

[3] Kubby, J. A.; Boland, J. J. *Surf. Sci. Rep.* **1996**, *26*, 61.

[4] G. Binnig and H. Rohrer, Rev. Mod. Phys. **65**, 615 (1987).

[5] P. K. Hansma, V. B. Elings, O. Marti, and C. E. Bracker, Science **242**, 157 (1988).

[6] Ph. Avouris, J. Phys. Chem. **94**, 2246 (1990).

[7] C. Joachim and S. Gauthier, Annales de Chimie **17**, 179 (1992).

[8] G. Binnig, H. Rohrer, Ch. Gerber, and E. Weibel, Phys. Rev. Lett. **49**, 57 (1982).

[9] J. A. Stroscio and D. M. Eigler, Science **254**, 1319 (1991).

[10] Ph. Avouris, Acc. Chem. Res. **28**, 95 (1995).

[11] D. M. Eigler and E. Schweizer, Nature **344**, 524 (1990).

[12] L. J. Whitman, J. A. Strosci, R. A. Dragoset, and R. J. Cellota, Science **251**, 1206 (1991).

[13] B. C. Stipe, M. A. Rezaei, W. Ho, S. Gao, M. Persson, and B. I. Lundqvist, Phys. Rev. Lett. **78**, 4410 (1997).

[14] K. Takayanagi, Y. Tanishiro, M. Takahashi, and S. Takahashi, J. Vac. Sci. Tech. A **3**, 1502 (1985).

[15] K. Miyake, H. Shigekawa, and R. Yoshizaki, Appl. Phys. Lett. **66**, 3468 (1995).

[16] Z. Jing and J. L. Witten, Surf. Sci. **274**, 106 (1992).

[17] R. A. Wolkow, Phys. Rev. Lett. **68**, 2636 (1992).

[18] M. Chander, Y. Z. Li, J. C. Patrin, and J. H. Weaver, Phys. Rev. B **48**, 2493 (1993).

[19] B. C. Stipe, M. A. Rezaei, and W. Ho, Rev. Sci. Instrum. to be published.

[20] B. C. Stipe, Ph.D. Dissertation, Cornell University, August 1998.

Chapter 2

Atomically Resolved Determination of the Adsorption Sites as a Function of Temperature and Coverage: H_2S on Si(111)-(7×7)[†]

2.1 Abstract

Using a variable-temperature ultrahigh vacuum scanning tunneling microscope (STM), we have studied the adsorption characteristics of H_2S on Si(111)-(7×7). The data suggest that H_2S adsorbs dissociatively at sub-monolayer coverage, from 50 to 300 K, with HS bonded to an adatom and H bonded to a rest atom. The adsorption is

[†]This chapter by M. A. Rezaei, B. C. Stipe, and W. Ho has been submitted to *Journal of Physical Chemistry* under the same title for publication.

site selective and the adsorption site preference is temperature dependent. At 50 K, the faulted center sites are most favored for adsorption, followed by unfaulted center sites, faulted corner sites, and unfaulted corner sites. As the temperature is increased, the differences between the faulted and unfaulted halves diminish, but the center sites remain more reactive than the corner sites. At room temperature, the ratio of adsorbates on center sites versus corner sites is 2:1. We present an explanation to account for the non-Langmuir kinetics involved in this system.

2.2 Introduction

The dissociative adsorption of gas molecules on solid surfaces is a fundamental chemical reaction. The dissipation of the kinetic energy of the gas can involve energy transfer to the excited states of the solid, such as phonon and electronic excitations. Furthermore, the reactivity at the surface is influenced by the local properties of the surface. These local properties include the positions of the atoms at the surface, the electronic properties at different sites based on dangling bond configurations, and non-bulk collective effects, such as electronic surface states. By studying chemisorption at the atomic scale, we hope to understand the dynamics of the adsorption process and the effects of the local environment on this process.

The Si(111)-(7×7) surface provides an opportunity for studying the effects of the local environment on adsorption and dissociation. In the top (adatom) layer, the unit cell contains four different types of sites with dangling bonds and the second (rest atom) layer also contains dangling bonds that are potentially reaction sites. The complexity of this surface makes it difficult to model theoretically, which emphasizes the need to investigate this surface experimentally. To elucidate the

nature of the adsorption of H_2S on silicon, we have performed our experiments at different temperatures and coverages. We will also suggest an explanation of the results. We hope that our data can spur *ab initio* theoretical studies of this system.

Our instrument is a home-made STM based on the Besocke design. [1] It is housed inside an ultrahigh vacuum (UHV) chamber with a base pressure of 3×10^{-11} Torr. The STM and sample assembly is cooled with a continuous flow cryostat. The helium flow rate is adjustable and the cold head can be heated. By setting the flow rate and controlling the heater with a temperature controller, the temperature can be held constant from 8 to 350 K to within 0.1 K. The silicon used in these experiments is cut from a *p*-type, boron-doped, 1 Ω cm, prime grade wafer. The sample is mounted on a molybdenum sample holder. Both the sample and sample holder are out-gassed at 1000 K for 10 to 12 hours. The sample is further cleaned by repeated sputtering with 1 keV Ne^+ ions and annealing (1200 to 1500 K) cycles.

2.3 Experimental Results

It is generally accepted that the initial adsorption of H_2S on Si(111) is dissociative [2] even at low temperatures. Our experiments indicate that the adsorption characteristics change as a function of temperature and coverage. We will discuss the low temperature results first and then describe the effects of increasing the sample temperature. We will denote the surface coverage as the percentage of adatoms that have adsorbates, because that is what we directly observe with the STM.

Figure 2.1a shows the Si(111)-(7×7) reconstruction. [3] The topmost layer has twelve atoms in the unit cell, which, depending on their position, are called center

or corner adatoms. The adatoms have a dangling bond, which is readily observed in STM images (Fig. 2.1b). The unit cell has two halves, faulted and unfaulted, which refer to the faulted stacking of the adatom layer with respect to the fourth layer atoms. The stacking fault increases the local density of states in the faulted half of the unit cell, [4] as can be seen in the filled state STM images (Fig. 2.1b). The second layer, called the rest atom layer, has six atoms with dangling bonds, as shown in Fig. 2.1a. Note that each center adatom has two neighboring rest atoms with dangling bonds, whereas the corner adatoms have one. There are four inequivalent adatom sites: faulted/unfaulted center sites and faulted/unfaulted corner sites. The sticking probability of H_2S on these sites changes as a function of temperature and coverage.

At 50 K, the low coverage regime is dominated by one species: HS adsorbed on faulted center adatom sites. At 2.3% coverage, 96% of the adsorbates were on faulted center sites, while the other 4% were on unfaulted center sites; there were no adsorbates on corner sites. We cannot see any atomic hydrogen, which is quite distinct when bonded to silicon adatoms. H reduces the local density of states (LDOS) and appears like a missing adatom. [5] Even at higher coverage, there is no hydrogen bonded to the adatom layer. We propose that the hydrogen atoms are all adsorbed at the rest atoms adjacent to the HS adsorption sites. We will present evidence for this assignment and offer an explanation for this behavior. HS reduces the LDOS significantly, as it appears darker than the silicon atoms, even though it is above the surface (Fig. 2.2a).

If two HS adsorbates are nearest neighbors, one in the faulted half, the other in the unfaulted half, the LDOS is further reduced (Fig. 2.2b). Although the appearance of these darker neighboring sites could be interpreted as a different species,

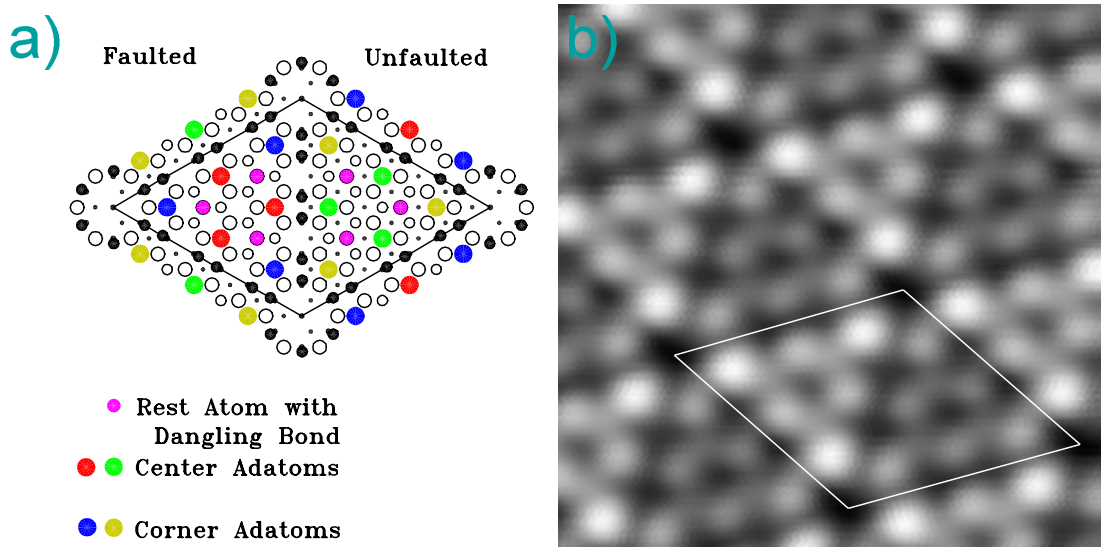

Figure 2.1: a) Schematic drawing of the (7×7) reconstructed Si(111) surface. The same color coding is used for the other figures. Note the position of the rest atoms with dangling bonds and the stacking fault. b) Room temperature STM image of the filled states (sample bias −2 V, tunneling current 1 nA) of Si(111)-(7×7). The brighter half of the unit cell is the faulted half. The diamond outlines the (7×7) unit cell.

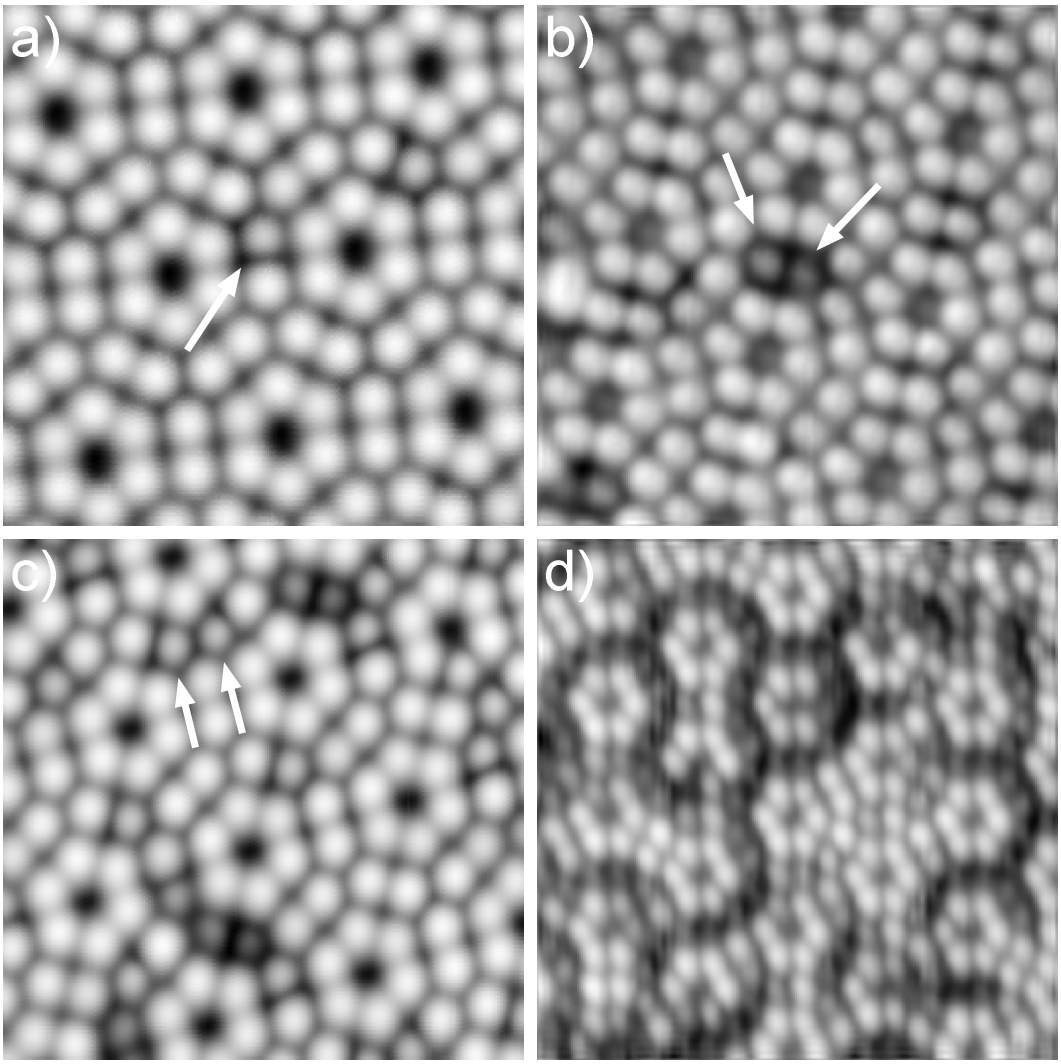

Figure 2.2: Effects of coverage on adsorbate appearance. a) At low coverage, the single adsorbate appears slightly darker than the Si adatoms. b) Two neighboring adsorbates, one on each half of the unit cell, appear much darker than the single adsorbate. c) Two neighboring adsorbates in the same half of the unit cell. These appear only slightly darker than the single adsorbate. d) High coverage (47%) limit. The appearance of chain-like structures results from the preference of neighboring adsorbates to be on two different halves of the unit cell. Images scanned at 200 K, with 1 V sample bias a 0.1 nA tunneling current.

we verified by two different methods that the two molecules are HS. First, by successive in-situ dosing, we found that sites with one adsorbate would turn darker if their nearest neighbor became occupied in the next dose. Second, we can dissociate HS molecules using the STM. [6] By dissociating each presumed HS molecule separately, we found features consistent with the reaction products being sulfur and hydrogen. If the two neighboring adsorbates are in the same half of the unit cell, the reduction in the LDOS is not as great (Fig. 2.2c). From our dissociation experiments, it is clear that HS bonds with sulfur attached to silicon and the hydrogen is presumably on top of sulfur.

Given that the two neighboring HS molecules do not form a new species, that is, the major chemical bonds are not rearranged, we attribute the reduction in the LDOS to the dipole-dipole interaction between the two HS molecules. It is possible that the HS molecules bend slightly, so that the dipole moments are no longer parallel, thereby reducing the strain on the bonds by reducing the dipole-dipole force. Bending of the HS molecules would also explain the darker appearance in the STM images. We note that the distance between two center sites in opposite halves of the unit cell is 6.7 Å, and 7.7 Å for the same half of the unit cell. Since dipole-dipole interactions fall off as $1/r^3$, where r is the distance between the dipoles, the dipole force should be smaller in the same half of the unit cell. This is consistent with our interpretation of the STM images. Furthermore, the center to center distance of the two HS neighbors is 0.3 Å less than the silicon adatom distance (6.7 Å), possibly signifying a shift in the atomic positions.

As we increased the coverage, the ratio of occupied faulted to occupied unfaulted center sites decreased. At 30% coverage, 53% of the adsorbates were on faulted center sites, 30% were on unfaulted center sites, 15% were on faulted corner sites

and only 2% were on unfaulted corner sites. At first, we attributed the increase in unfaulted center site population to a simple saturation effect: the more faulted center sites had adsorbates, the less the probability of a new molecule sticking to these sites. But upon careful analysis, it became clear that there exists a nearest neighbor interaction between adsorbates on faulted and unfaulted center sites which affects the sticking probability.

Figure 2.3d shows a typical scan at 50 K with 30% HS coverage. By combining statistics from several images, we found that in 254 unit cells, 474 (62% ± 3%) of faulted center sites have adsorbates, and 275 (36%) of the unfaulted center sites have adsorbates. Each faulted center adatom has exactly one nearest neighbor unfaulted center adatom. Therefore, if there were no interaction, we would expect about 170 (62%) of the adsorbates in the unfaulted half to have adsorbate neighbors in the faulted half. But 234 (85% ± 5.5%) of the adsorbates in the unfaulted half have neighbors in the faulted half. The probability of N unit cells with f occupied faulted center sites and u occupied unfaulted center sites to have u_n occupied unfaulted center sites with neighbors is given by:

$$P(u_n) = \frac{\begin{pmatrix} f \\ u_n \end{pmatrix} \begin{pmatrix} 3N-f \\ u-u_n \end{pmatrix}}{\begin{pmatrix} 3N \\ u \end{pmatrix}} \tag{2.1}$$

The probability of a random configuration of adsorbates with more than 203 (74%, which is two standard deviations from 85.5%) nearest neighbor occupancy is given by $\sum_{i=203}^{275} P(i)$ which is less than 10^{-6}. Although by looking at the image it is difficult to notice the change in sticking probability due to nearest neighbor interaction, there is clear evidence for this effect. This interaction and the low probability of

sticking to the corner adatoms produces chain-like structures that can be seen in Fig. 2.2d.

Figures 2.3a and 2.3b show typical scanned images of H_2S adsorbed on silicon at 200 K. At low coverage, there are many more unfaulted center site adsorbates at 200 K as compared to 50 K, with more adsorbates on corner sites as well. At near saturation dosage, there are equal number of adsorbates on faulted and unfaulted center sites, as one would expect. When the experiment is performed at 300 K (2.3c), the same trend continues: more adsorbates bond to corner sites and unfaulted center sites. At coverages of 30% and above, the ratio of adsorbates on center sites to adsorbates on corner sites is 2:1. Figure 2.4 summarizes the site specific sticking probability as a function coverage and temperature.

2.4 Adsorption Geometry

It is clear from our experimental results that H_2S adsorption on Si(111)-(7×7) does not follow simple Langmuir kinetics. We are studying this system on the atomic scale, and we would like to understand the adsorption characteristics from a dynamic point of view. Given the complex nature of the (7×7) silicon surface reconstruction, the adsorption geometry is of particular importance. By knowing the adsorption geometry, we can predict the maximum coverage and verify the prediction experimentally.

From previous experiments, we know that the sub-monolayer adsorption is dissociative. [2] We do not observe any hydrogen bonded to the adatom layer, even though atomic hydrogen bonds strongly to both the rest atoms and adatoms on silicon. [5] We can also dissociate the HS fragment further with the STM. [6] We

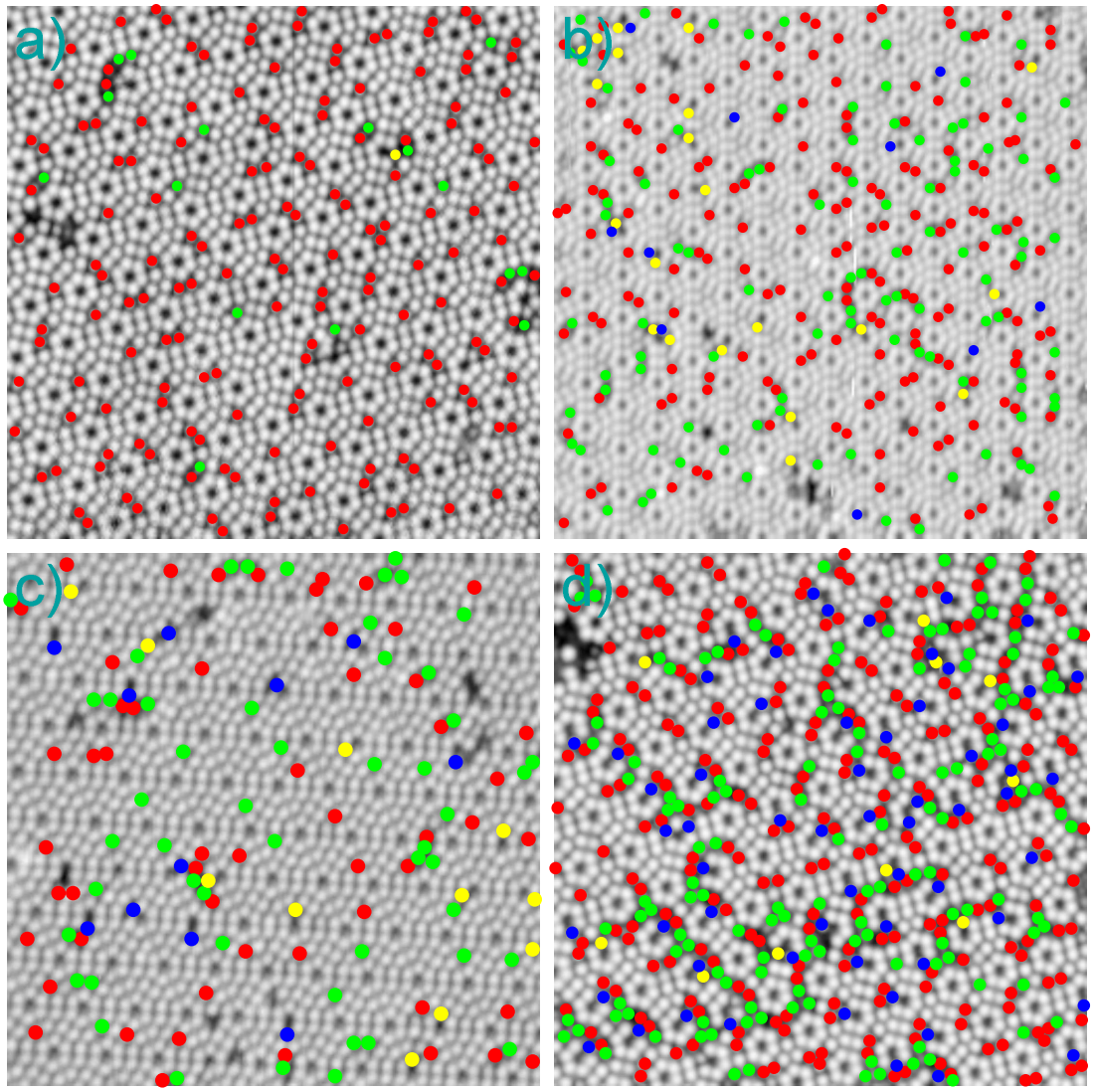

Figure 2.3: The color coding is the same as Fig. 2.1a. 10% HS coverage at a) 50 K, b) 200 K and c) 300 K, respectively. d) 30% HS coverage at 50 K. Images scanned at 1 V sample bias and 0.1 nA tunneling current.

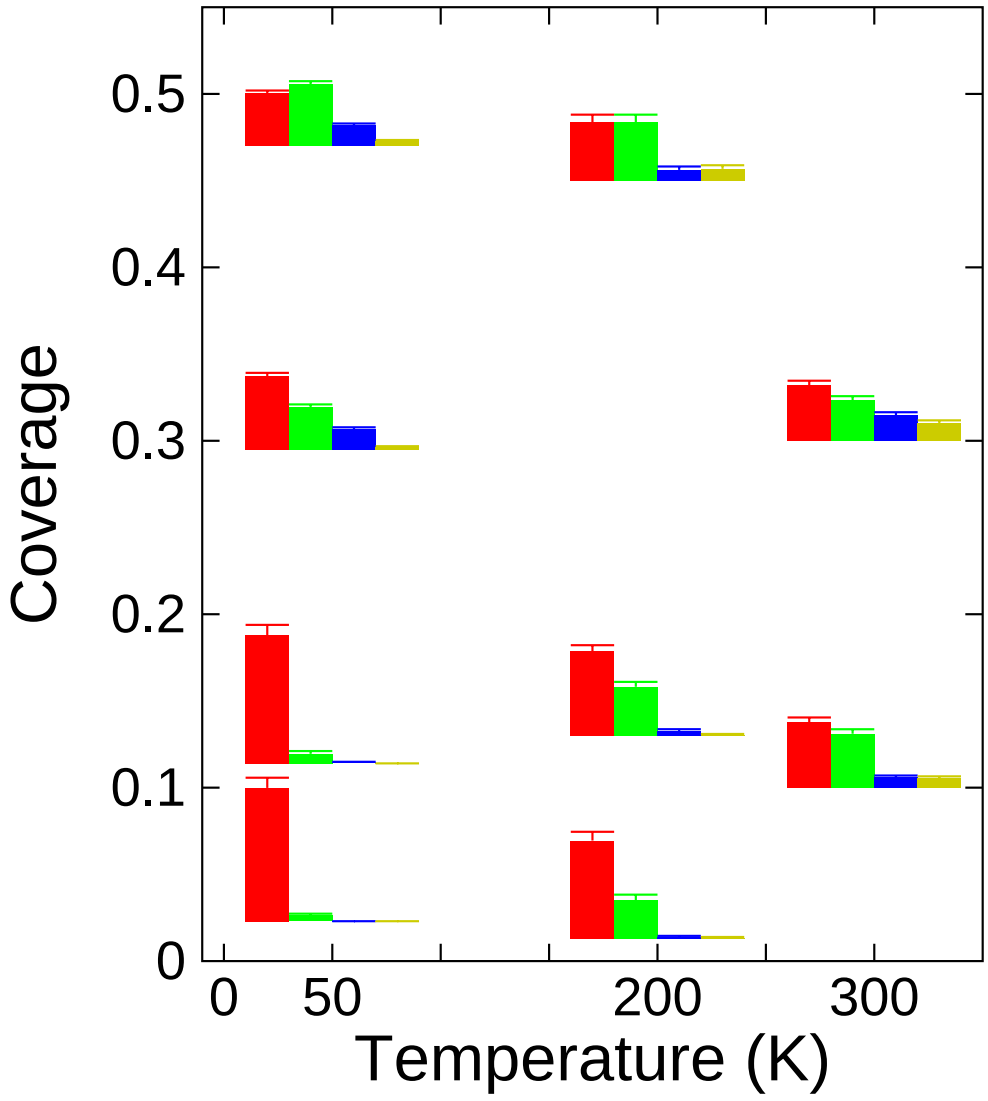

Figure 2.4: Summary of the temperature and coverage dependence of the site selectivity. The height of the histogram represents the percentage of HS adsorbed on different sites. The sum of the four heights for each temperature and coverage is 100%. The color scheme is the same as Fig. 2.1a. The error bars start from the top of each histogram.

have never observed more than one hydrogen after the STM induced dissociation, which provides further evidence for the dissociative adsorption of H_2S, to form HS and H at and below 300 K.

With a sharp tip, we consistently observe an asymmetry in the scanned images. Figure 2.5a shows an example of two adsorbates, bonded to the surface at the same relative location in two different unit cells. Since center adatoms have two neighboring rest atoms (Fig. 2.1a), it should be possible for H_2S to dissociate, with the hydrogen atom attached to either of these rest atoms. From the line profiles (Fig. 2.5c and d), we can see that the upper adsorbate has an asymmetry associated with the left rest atom, whereas the bottom adsorbate has the same asymmetry on the right side. The false color image (Fig. 2.5b) also reveals this asymmetry. We note that this cannot be a tip effect, because the adsorbates are in the same relative position in the unit cell. We attribute this asymmetry to the hydrogen atom adsorbed at one of the two possible rest atom sites.

The adsorption of H_2S depends critically on the the rest atom - adatom pair. Since there are only three rest atoms in each half of the unit cell, the maximum number of adsorbates in each half is three. Therefore, the maximum coverage is 50%. Figure 2.3d shows 30% H_2S coverage at 50 K. There are no unit cells with more than three adsorbates in each half. This fact also explains the adsorption behavior at high coverage and low temperature, where fewer faulted center sites are occupied compared to unfaulted center sites even though the low coverage adsorption probability is much higher for faulted sites. Since the adsorption on a corner site inhibits adsorption on a center site in the same unit cell, and also because the adsorption probability is higher for faulted corner sites, near saturation coverage, more faulted center sites can no longer act as adsorption sites compared to the unfaulted center

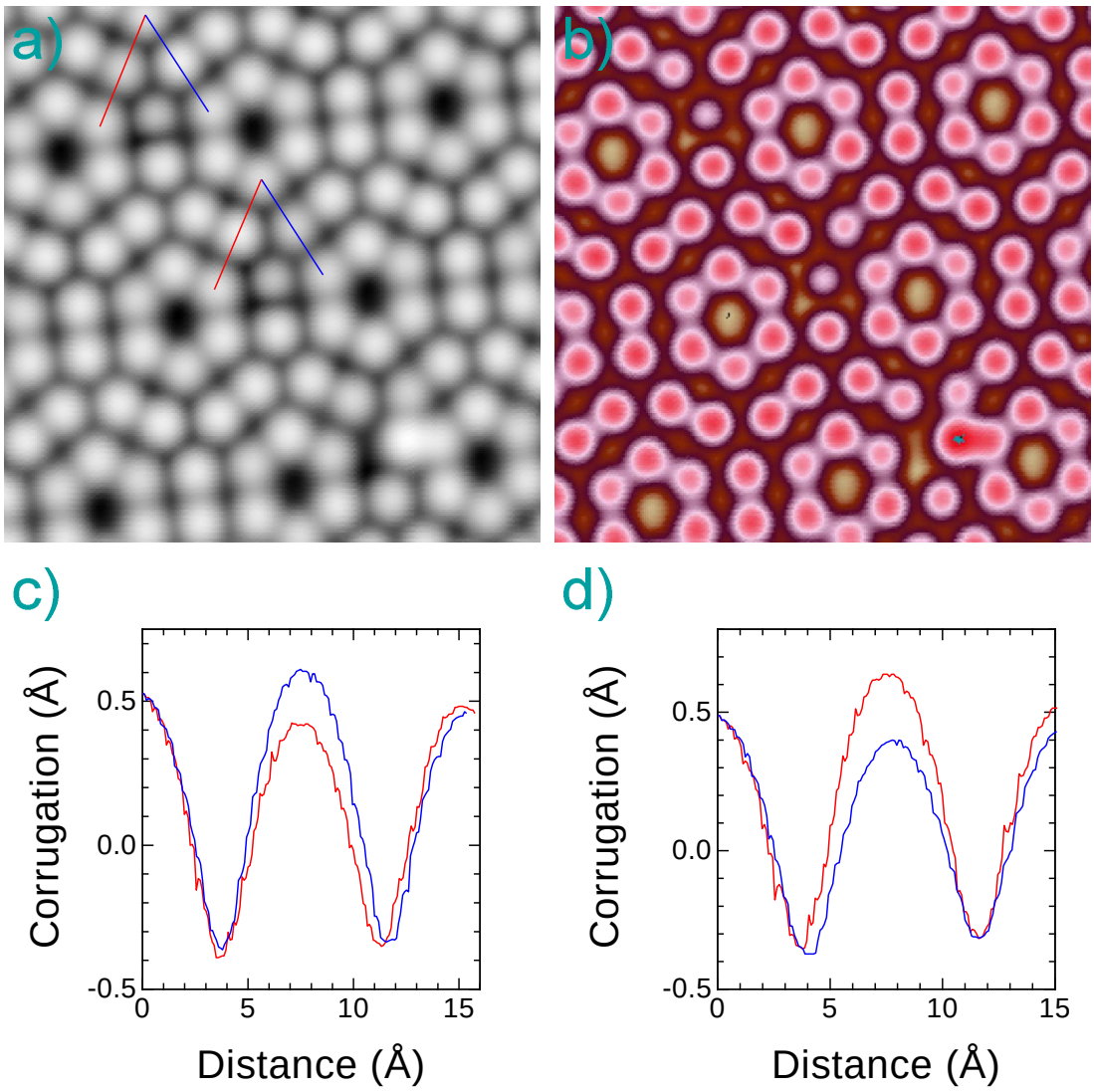

Figure 2.5: a) Gray scale STM image, with two adsorbates bonded to the same center adatom site in two different unit cells. b) False color image of the same data. Note the asymmetry in the appearance of the neighboring adatoms to the adsorption site. c) Profile cuts through the upper adsorbate position, as shown in (a). d) Profile cuts through the lower adsorbate. Images scanned at 50 K with 1 V sample bias and 0.1 nA tunneling current.

sites. At high dosage, H_2S is known to form molecular multi-layers, [2] which are difficult to observe with the STM, as the molecules are either partially mobile or interact with the tip. Heavy dosing also often leads to an unstable STM tip, due to the molecules being adsorbed on the tip. The maximum coverage we have been able to observe is 47%, which is consistent with our prediction of 50%.

We do not know of any theoretical studies of the adsorption of H_2S on Si(111)-(7×7). There is, however, an extended Huckel calculation [7] done for H_2O on Si(111)-(7×7), which is a very similar system. Results from this calculation suggest that the lowest energy state for dissociative adsorption of H_2O is OH attached to center site and H bonded to a corner site. STM experiments with H_2O on Si(111) have shown that this is not the preferred bonding arrangement. [8] H_2O adsorbs much like H_2S. Even if the adsorption site is restricted to adatom−rest atom pairs, OH bonded to the rest atom is favored over H bonded to the rest atom in the theoretical results. The adsorption process is a non-equilibrium process that involves more than just final state energies. The adsorption geometry is better explained in terms of the local electronic properties of the surface and the kinetics of the adsorption process.

From theoretical calculations [10] and spectroscopy measurements, [11] it can be concluded that the adatoms have an excess of charge and can act as electron donors, whereas the rest atoms with dangling bonds have a charge deficit. The electron affinity of H_2S is well known. [12] One possible reaction pathway is for H_2S to become partially negatively charged as it interacts with the adatom, which will attract the molecule to the rest atom, leading to dissociation. The rest atom - adatom pair act as molecular bond cleavers due to their opposite charge states. This also explains the lack of hydrogen adsorbed on the adatom layer, which may

be energetically favored. Therefore, the adsorption of H_2S on the adatom layer is consistent with the electronic properties of the surface and the molecule. The adsorbate dissociation by the adatom-rest atom pair was suggested earlier for NH_3 on Si(111). [8]

2.5 Adsorption Site Temperature Dependence

The preference of adsorbates for the faulted half of the (7×7) unit cell has been observed for many systems. These adsorbates include H, [9] O_2, [13] Li, [14] P, [15] Cu, [16] Pb, [17] Ag, [18, 19] Ti, [20] Pd, [21] C_2H_2, [22] C_2H_4, [23] and C_{60}. [24] All but one [19] of the cited experiments are performed with STM's as the determination of site selectivity is difficult by other means. Furthermore, these experiments were performed at room temperature or higher and the low temperature dependence of this effect has not been explored. We have not found any references to adsorbates that prefer the unfaulted half of the unit cell.

The site preference of O_2 on Si has been explained in terms of the local properties of the surface. [13] O_2 prefers corner sites over center sites and also the faulted half over the unfaulted half. The LDOS on the Si(111)-(7×7) surface varies from site to site; the faulted half has a higher LDOS, and within each half the corner sites have higher LDOS than the center sites. O_2 becomes adsorbed through charge transfer and interaction with the electron-hole pairs in the S1 surface state. Therefore, O_2 has a higher probability of sticking to sites with higher LDOS. Although this is a reasonable explanation for O_2, it does not fit our data for H_2S. We do not see a preference for the corner sites, especially at low temperatures. Furthermore, we have not seen any change in the LDOS as a function of temperature as measured

by the STM. Since the probability of adsorption to different sites is temperature dependent, we need a different explanation for our system.

A simple explanation for the adsorption behavior is a mobile precursor state, such as the precursor state observed for benzene on Si(111). [25] The molecule adsorbs loosely on the surface, and becomes thermally equilibrated with the surface. The molecule then dissociatively adsorbs based on the temperature and the dissociation barrier at the different sites. At higher temperatures, higher energy barriers are more easily overcome, whereas at low temperatures only the lowest energy barriers are surmountable. The barrier to dissociation is site dependent. Given this explanation, we can conclude that the lowest energy barrier to dissociation is associated with the faulted center sites, followed by unfaulted center sites, faulted corner sites and finally unfaulted corner sites.

We can estimate the difference between the energy barriers by assuming the same pre-exponential factor in Arrhenius law from which we obtain:

$$R = \frac{f}{u} = e^{\Delta E/kT},\ \Delta E = E_u - E_f, \tag{2.2}$$

where R is the ratio between the two populations, f is the number of adsorbates on the faulted center sites, u is the number of adsorbates on the unfaulted center sites, k is Boltzmann's constant, T is the temperature, E_f is the energy barrier at faulted center sites, E_u is the energy barrier at unfaulted center sites and ΔE is the energy difference. Using our low coverage (1 to 2%) results to avoid saturation and nearest neighbor effects, we obtain $\Delta E = 14 \pm 2$ meV at 50 K and $\Delta E = 16 \pm 2$ meV at 200 K, which are in reasonable agreement with each other.

We note that at room temperature and moderate coverage, the ratio of the center site adsorbates to corner site adsorbates is 2:1. This ratio can be attributed to the fact that the corner adatoms have one neighboring rest atom, but center

adatoms have two such neighbors and therefore the dissociation probability is twice as high at center sites. Although there is no evidence for a mobile precursor state, the adsorbate does not have to move far to find a suitable site. Every adatom on the silicon surface has a neighboring faulted center site adatom. The furthest an adsorbate would have to move to find a faulted center site is about 13 Å from the corner hole. It is also possible that a gas molecule will not adsorb if it cannot find a suitable site. Although that would change the overall sticking probability, we cannot measure the sticking probability accurately enough to notice a temperature dependence.

Finally, we would like to explain the change in the sticking probability as a function of coverage. Like O_2, H_2S has a high electron affinity [12] and may become charged in the process of adsorbing. HS fragments already adsorbed on the surface act like dipoles, which can interact with the charged precursor. Electrostatic interaction between the adsorbate and the precursor may lead to a higher probability of dissociation near the adsorbate. One other possibility is for the adsorbate to lower the energy barrier to dissociation by changing the local properties of the surface. We can estimate the change in the energy barrier by modifying Eq. 2.2 to compensate for the expected unequal occupation of sites with and without neighbors:

$$R = R_0 \frac{u_n}{u - u_n} = e^{\Delta\epsilon/kT}, \ \Delta\epsilon = \epsilon - \epsilon_n \tag{2.3}$$

where u_n is the number of unfaulted center site adsorbates with neighbors in the faulted half, u is the total number of unfaulted center site adsorbates, R_0 is the expected ratio of the two populations, ϵ is the energy barrier for adsorbates without neighbors, ϵ_n is the energy barrier for adsorbates with neighbors, and $\Delta\epsilon$ is the energy difference. At 30% coverage, 62% of the faulted center sites have adsorbates and therefore $R_0 = 0.38/0.62 = 0.61$. Using $u_n = 234$, and $u = 275$, we obtain

$\Delta\epsilon = 5.2 \pm 0.6$ meV.

This nearest neighbor attraction is most pronounced between faulted and unfaulted center sites, otherwise the change in adsorption behavior as a function of coverage would not be evident. It might seem unlikely that the probability of adsorption is higher on two center sites in opposite halves of the unit cell, as compared to two center sites in the faulted half of the unit cell. But by looking at the silicon rest atom positions, we can see that when a center site is bonded to an adsorbate, it automatically reduces the chances of one of the other center sites in the same half, because the other center site adatom now has only one unoccupied rest atom neighbor. It follows that the center site in the unfaulted half of the unit cell would be more favorable, because it still has two rest atom neighbors to accommodate the H atom. If the attraction is electrostatic in nature, then the further distance of the sites in the same half of the unit cell may contribute to this effect as well.

2.6 Conclusion

Further theoretical study of the dissociative adsorption of H_2S on Si(111)-(7×7) is necessary for a better understanding of the physical phenomena underlying the observed behavior. *Ab initio* calculations, however, are very difficult to perform for this system. The reconstructed unit cell has over 100 atoms in the first three layers, and any calculation would have to include additional layers in the bulk (1×1) configuration, which adds 49 atoms per layer. The shear size of the problem makes it difficult to solve. Adding an impinging adsorbate to this system makes it an even more complex problem.

By varying the temperature, we can probe different aspects of the adsorption

behavior. The site selectivity is more evident at low temperatures and the determination of the small energy differences is only possible at low temperatures. Our estimates of energy barriers elucidate the effects of the local surface chemistry in the adsorption process.

We have studied the dissociative chemisorption of H_2S on Si(111)-(7×7) from 50 to 300 K. The adsorption is both site selective and temperature dependent. We have determined the adsorption geometry by careful analysis of the data and by dissociating the HS fragment using the STM. The adsorption geometry is a consequence of the dangling bond structure on the reconstructed surface. HS bonds to the adatom sites, which have an abundance of electrons and H bonds to the neighboring rest atom. To some extent, the adsorption preference for center adatoms is dictated by the surface reconstruction, because these sites have two neighboring rest atom dangling bonds. The temperature dependence of the adsorption site preference points to a thermally activated adsorption and dissociation process on different adatom sites.

Bibliography

[1] B. S. Stipe, M. A. Rezaei, and W. Ho, Rev. Sci. Instrum., to be published.

[2] D. V. Chakarov and W. Ho, Surf. Sci. **323**, 57 (1995).

[3] K. Takayanagi, Y. Tanishiro, M. Takahashi, and S. Takahashi, J. Vac. Sci. Tech. A **3**, 1502 (1985).

[4] G. Binnig, H. Rohrer, Ch. Gerber, and E. Weibel, Phys. Rev. Lett. **50**, 120 (1983).

[5] J. J. Boland, Surf. Sci. **244**, 1 (1991).

[6] M. A. Rezaei, B. C. Stipe and W. Ho, J. Chem. Phys., to be published.

[7] H. Ezzehar, L. Stauffer, J. Leconte, and C. Minot, Surf. Sci. **388**, 220 (1997).

[8] I.-W. Lyo and Ph. Avouris, J. Chem. Phys. **93**, 4479.

[9] H. Tokumoto, K. Miki, H. Murakami, H. Bando, M. Ono, and K. Kajimura, J. Vac. Sci. Tech. A. **8**, 255 (1990).

[10] I. Stich, M. C. Payne, R. D. King-Smith, J.-S. Lin and L. J. Clarke, Phys. Rev. Lett. **68**, 1351 (1992).

[11] J. A. Kubby and J. J. Boland, Surf. Sci. Rep. **26**, 61 (1996).

[12] N. E. Bradbury, and H.E. Tatel, J. Chem. Phys. **2**, 835 (1934).

[13] Ph. Avouris, I.-W. Lyo, and F. Bozso, J. Vac. Sci. Tech. B. **9**, 424 (1991).

[14] Y. Hasegawa, I. Kamiya, T. Hashizume, T. Sakurai, H. Tochihara, M. Kubota, and Y. Murata, J. Vac. Sci. Tech. A. **8**, 238 (1990).

[15] L. Vitali, M. G. Ramsey, and F. P. Netzer, Phys. Rev. B **57**, 15376 (1998).

[16] S. Tomimatsu, T. Hasegawa, M. Kohno, and S. Nosoki, Jap. J. of Appl. Phys. **35**, 3730 (1996).

[17] D. Tang, H. E. Elsayed-Ali, H. Wendelken and J. Xu, Phys. Rev. B **52**, 1481 (1995).

[18] S. Tosch and H. Neddermeyer, Phys. Rev. Lett. **61**, 349 (1988).

[19] A. Endo and S. Ino, Surf. Sci. **293**, 165 (1993).

[20] H. Kuriyama, S. Ohara, K. Ezoe, T. Yamamoto, S. Tatsukawa, M. Umekawa, and S. Matsumoto, Atomic Res. Micros. of Surf. and Int. Symp. **ix+282**, 79 (1997).

[21] U. K. Köhler, J. E. Demuth, and R. J. Hamers, Phys. Rev. Lett. **60**, 2499 (1988).

[22] J. Yoshinobu, and M. Aono, RIKEN Rev. **7**, 11 (1994).

[23] M. N. Piancastelli, N. Motta, A. Sgarlata, A. Balzarotti, and M. De Crescenzi, Phys. Rev. B **48**, 17892 (1993).

[24] T. Sakurai, X. D. Wang, T. Hashizume, Y. Nishina, H. Shinohara, and Y. Saito, Appl. Surf. Sci. **67**, 281 (1993).

[25] D. E. Brown, D. J. Moffatt, and R. A. Wolkow, Science **279**, 542 (1998).

Chapter 3

Inducing and Imaging Single Molecule Dissociation on a Semiconductor Surface: H_2S and D_2S on Si(111)-(7×7)[†]

3.1 Abstract

Using a variable-temperature, ultrahigh vacuum scanning tunneling microscope (STM), we have induced and imaged the dissociation of H_2S and D_2S on Si(111)-(7×7). H_2S and D_2S adsorb dissociatively at low coverage, from 50 to 300 K. Individual HS (or DS) fragments can be further dissociated with the STM at low temperatures without affecting neighboring adsorbates. The hydrogen (deuterium)

[†]This chapter by M. A. Rezaei, B. C. Stipe, and W. Ho will be published under the same title in *Journal of Chemical Physics*.

atom either desorbs or re-attaches to a nearby silicon atom. Near room temperature (297 K) and above, DS dissociates thermally, with an activation barrier of 0.73 ± 0.15 eV. The activation barrier was calculated from atomistic studies of the dissociation rates at temperatures between 297 and 312 K.

3.2 Introduction

Dissociation of molecules at solid surfaces is a fundamental catalytic reaction and as such is of great importance to both basic science and industrial applications. In part due to its relevance to the semiconductor industry, Si(111)-(7×7) is a well studied surface. Hydrogen sulfide (H_2S) is a common gas in many natural and synthetic processes. For example, H_2S is a byproduct in many metallurgical processes and is a major pollutant in the environment. Thus the development of H_2S sensors is an active field of study [1, 2]. Sulfidation, much like oxidation, is a corrosive process that affects the materials properties of important alloys, such as steel [3]. Sulfidation can also be used for passivation of chemically reactive surfaces, such as silicon or gallium arsenide [4]. The detection of H_2S and its conversion to other chemicals is therefore essential for a healthy environment and a safe industry. Moreover, H_2S occurs naturally in diverse settings, especially in earth sciences and astrophysics. It can be found throughout the solar system, from Neptune [5] to comet Hale-Bopp [6]. Understanding the dissociation of H_2S on Si(111)-(7×7) also provides insight to other reactions, such as water (H_2O) on silicon.

Our instrument is a home-made STM based on the Besocke design. It is housed inside an ultrahigh vacuum (UHV) chamber with a base pressure of 3×10^{-11} Torr. The STM and sample assembly is cooled with a continuous flow cryostat. The he-

lium flow rate is adjustable and the cold head can be heated. By setting the flow rate and controlling the heater with a temperature controller, the temperature can be held constant from 8 to 350 K to within 0.1 K. The silicon used in these experiments is cut from a *p*-type, boron doped, 1 Ω cm, prime grade wafer. The sample is mounted on a molybdenum sample holder. Both the sample and sample holder are out-gassed at 1000 K overnight. The sample is further cleaned by repeated sputtering (1 keV Ne^+ ions) and annealing (1200 to 1500 K) cycles.

It is generally accepted that the initial adsorption of H_2S on Si(111) is dissociative [7] even at low temperatures. HS initially adsorbs onto the center site silicon ad-atoms; at higher coverage, the corner silicon ad-atoms become populated. The detailed adsorption characteristics are temperature and coverage dependent and will be discussed elsewhere [8]. The dissociation results presented here are only concerned with the adsorbates on center sites at low coverage, typically 1 to 2 adsorbates per (7×7) unit cell. HS appears slightly darker than the surrounding Si atoms [Fig. 3.1(a)], even though it is above the silicon surface. This indicates that HS lowers the local density of states near the Fermi energy above its adsorption site.

3.3 STM Induced Dissociation

HS can be further dissociated into S and H. The dissociation can be STM induced and it also occurs thermally near room temperature. We will first discuss the STM induced dissociation results and then proceed with the thermal data. By characterizing the interaction of the STM with the adsorbate, we can choose the scanning parameters such that no dissociation occurs. This is important for the

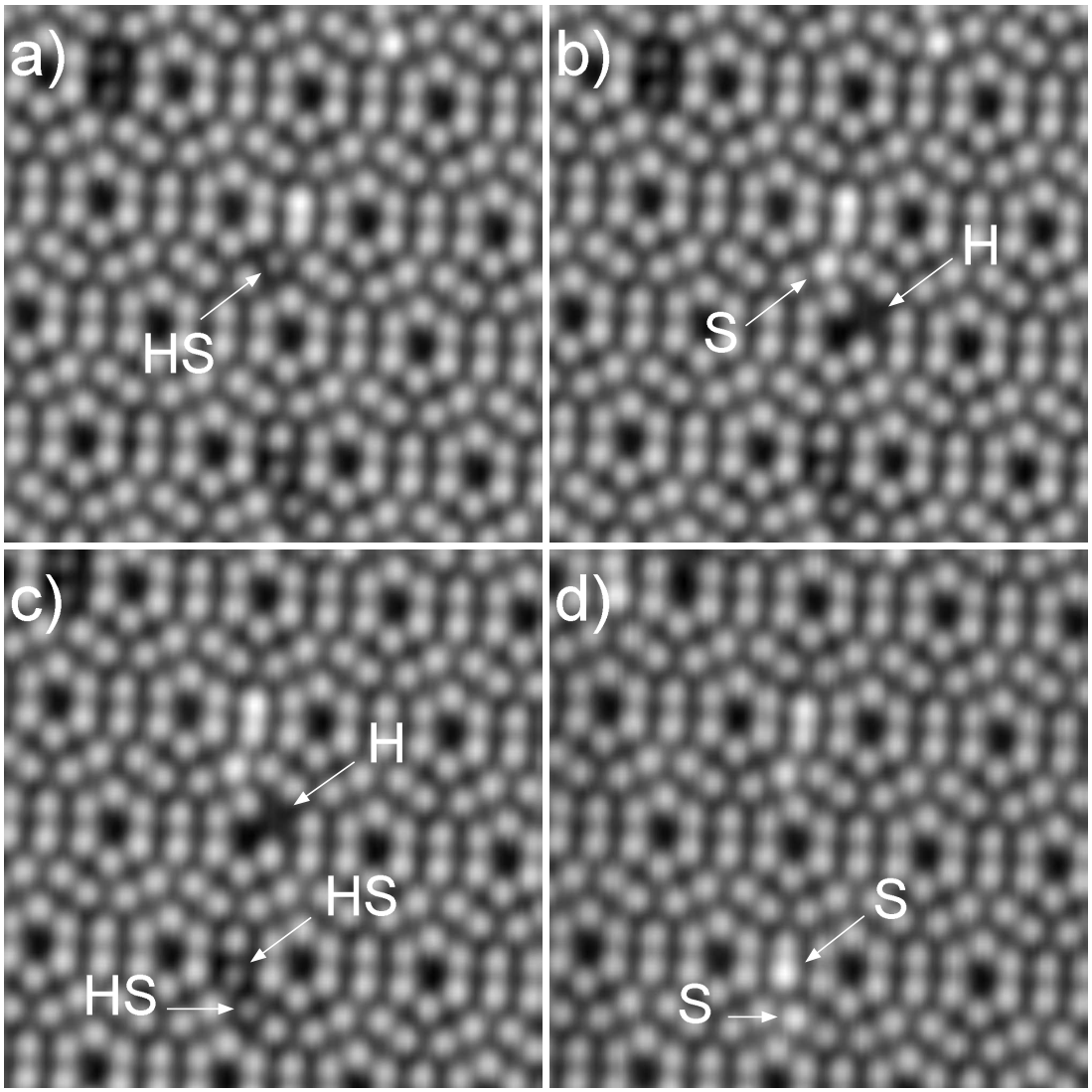

Figure 3.1: Dissociation induced by the STM, followed by desorption of H at 48 K. a) The STM tip is moved over a HS molecule. b) Image taken after a 2.5 V, 0.3 nA, 1 ms pulse; the HS molecule is dissociated into S and H. H sometimes desorbs entirely (not shown). c) The STM tip is centered over H. d) Image taken after a 3.5 V, 1.5 nA, 100 ms pulse; the hydrogen is desorbed. Several nearby HS molecules are dissociated as a result of the second pulse. The images were scanned at 1 V sample bias and 0.1 nA tunneling current.

thermal measurements, because we need a non-interacting probe to measure the pure thermal rates.

The surface is normally scanned at 0.7 to 1.0 V sample bias and 0.1 to 1 nA tunneling current, which does not disturb the adsorbates. If the voltage is raised above 2 V when the tip is above an HS molecule, the molecule dissociates. The hydrogen (or deuterium) atom either desorbs completely, leaving behind sulfur or it moves along the surface and bonds to a silicon atom; 55% ±8% of the hydrogen atoms do not desorb. The sulfur atom always appears at the same position as HS; it looks slightly brighter than a Si atom [Fig. 3.1(b)]. The hydrogen atom is identifiable because it appears as a very dark spot on the surface [9, 10] and it can be desorbed under suitable conditions of current and voltage [Fig. 3.1(d)] with the tip positioned over the atom [Fig. 3.1(c)]. The H and D desorption conditions are similar to results from previous experiments on Si(111) [11] and Si(100) [12]. Note that the conditions required for H desorption (in this case, 3.5 V, 1.5 nA) often lead to non-local dissociation of other, nearby HS adsorbates. If the dissociation is due to the current, as opposed to the electric field, these nonlocal events may be due to electrons propagating in a surface resonance band that exists in the range of 3 to 8 V [13]. Such non-local effects have been observed on Si(111) for other processes under similar conditions [14]. In the present paper, we are unable to unequivocally attribute the dissociation to the tunneling electrons or the electric field. Electric fields capable of breaking bonds are usually on the order of 1 V/Å. We estimate that the electric field at 2 V sample bias is about 0.5 V/Å in the tunneling junction, which may be large enough to induce dissociation.

The STM induced dissociation is very well controlled at lower voltages. It is accompanied with a change in current at the time of dissociation, similar to our

previous results on O_2 dissociation on Pt(111) [15]. The STM tip can be positioned to within 0.1 Å (laterally) of the top of the HS molecule. This is accomplished by a real time, computer controlled tracking process that eliminates effects due to thermal drift and piezo hysteresis. The dissociation can be induced locally without disturbing neighboring adsorbates. Figure 3.2(a) shows a pair of adsorbates on neighboring sites. Each adsorbate is dissociated separately. Unlike thermal dissociation, which is random, STM induced dissociation is bond specific. Since the dissociation is selective and the products can easily be identified, we can measure the distance that a hydrogen (or deuterium) atom travels. If multiple adsorbates were dissociated simultaneously, it would be difficult to attribute the hydrogen atoms to their original HS molecule, especially at moderate to high coverage.

Hydrogen binds strongly to silicon, with a calculated binding energy of 3.0 eV [16] to 3.1 eV [17, 18]. Unlike metallic systems with low diffusion barriers (typically 0.3 eV [19]), hydrogen does not diffuse very easily on silicon. The barrier to lateral motion of hydrogen has been measured to be 1.5 eV [20]. We have measured the distance traveled by H and D after a STM induced dissociation at 50 K. The dissociated hydrogen atoms can move very far and on average move 10 $\pm$ 2 Å. The deuterium atoms have a similar range (12 $\pm$ 3 Å). The distance between a center-site Si ad-atom and its nearest neighbor is 7.7 Å; in other words, H and D on average move one or two sites away from the original molecule. Isotope effects are normally kinetic (as opposed to chemical) in nature. If there were to be an isotope effect, it would be largest for hydrogen versus deuterium, because of the large difference in mass. Our data indicate that the potential energy surface and the dissipative forces at work are mostly chemical in character. It should be mentioned that hydrogen is known to adsorb at sites not visible to an STM: the

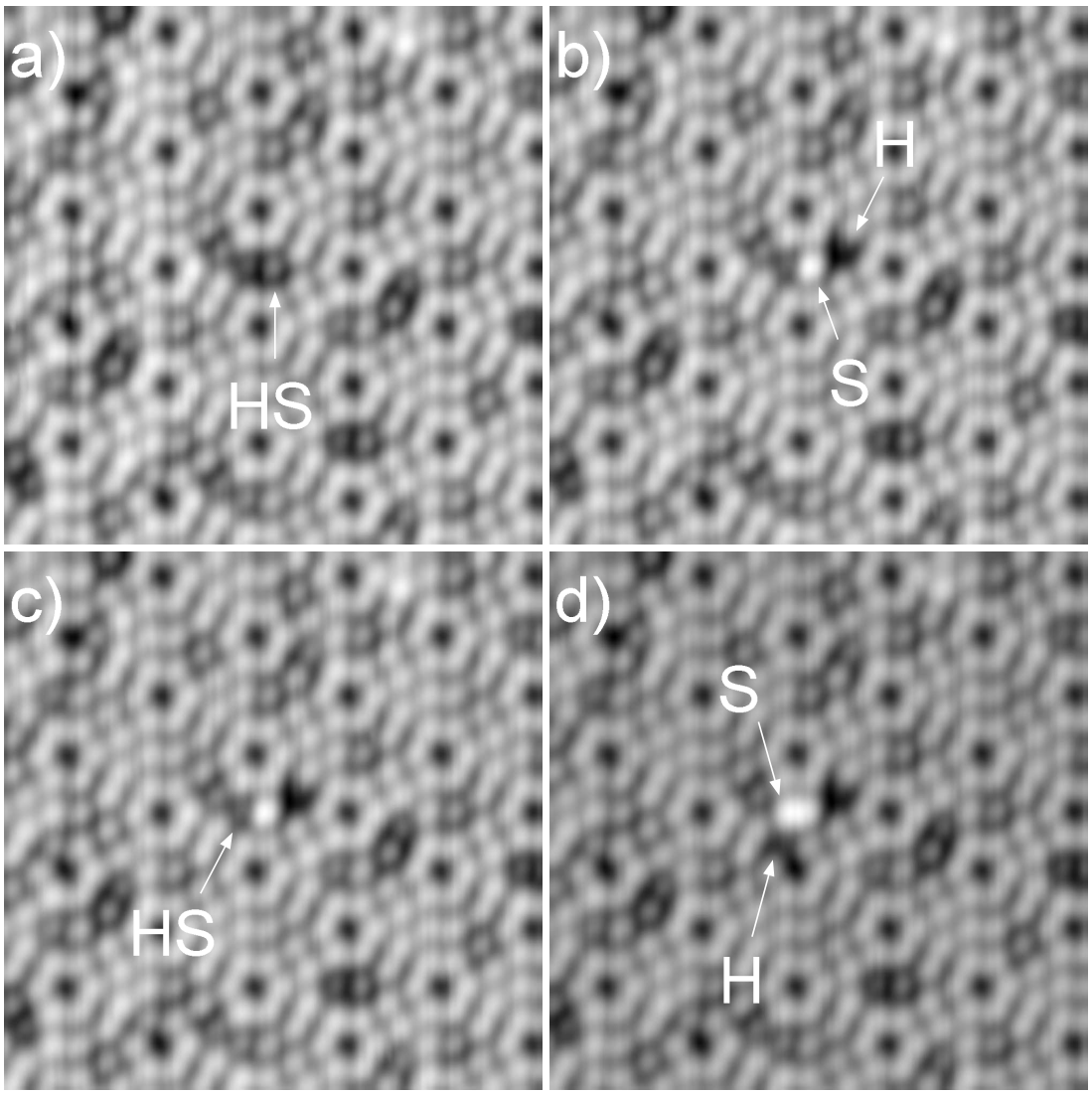

Figure 3.2: STM induced single molecule dissociation at 200 K: a) The tip is positioned over a HS molecule. b) Image taken after a 2.5 V, 0.7 nA, 100 ms pulse; the HS molecule is dissociated into H and S, without affecting the neighboring HS. c) The tip is moved over the second HS molecule. d) After another 2.5 V, 0.7 nA, 100 ms pulse, the second HS molecule is dissociated. The images were scanned at 1 V sample bias and 0.1 nA tunneling current.

dangling bonds in the second layer on the 7×7 reconstruction [9]. If some of the events that appear to be desorption are indeed adsorption to the second layer, then the distances calculated above may not be representative of the total population average.

3.4 Thermal Dissociation

The same dissociation process occurs thermally near room temperature. Since the STM can induce dissociation, we first established that the dissociations near room temperature are indeed thermal in nature. This was accomplished by measuring a rough lifetime by scanning the same area repeatedly and counting the dissociated species. Given this lifetime, we then waited for almost all the adsorbates to dissociate and then scanned an area far away that we had not scanned before. The adsorbates in this area were almost all dissociated as well, indicating that the process is independent of scanning. The lifetime at 297 K is much longer than the amount of time required for scanning an area, which is typically 1 to 2 minutes, making the above procedure possible.

Thermal dissociation experiments were performed at low coverage (1 to 2 adsorbates per 7×7 unit cell) to minimize nearest neighbor interactions. With other techniques, measuring events at such low coverage is often impractical. In particular, the adsorption characteristics change dramatically after the first monolayer: the molecules chemisorb without dissociation and form an ice layer at low temperatures [7]. In the present study, D_2S was used for all the thermal dissociation measurements. Isotope effects in thermal dissociation were not investigated, but are expected to be observable [21]. Figure 3.3 shows a typical thermal measure-

ment sequence for DS. The same area was scanned repeatedly until almost all the adsorbates had dissociated. The number of dissociations between each scan was then counted. The experiment was repeated for different temperatures, from 297 to 312 K. The dissociation rate is too fast above 312 K to be measured in this manner. Figure 3.4(a) shows the dissociation data as a function of time. The data are fitted to $\frac{N_0}{\tau}e^{-t/\tau}$, where N_0 is total number of dissociated molecules, t is the time and τ is the lifetime. The only fitted parameter is τ. Since the adsorption rate of D_2S onto faulted and unfaulted center sites differs at low temperature, the dissociation data were first compiled separately for the two adsorption sites. However, the measured lifetimes were not significantly different and therefore the data were combined into a single plot, yielding better statistics. The dissociation rate is calculated from the lifetime and is plotted in Fig. 3.4(b) as a function of temperature. The data are fitted to the Arrhenius equation, $R = \nu e^{-E/kT}$, where R is the dissociation rate, ν is the pre-exponential factor (attempt frequency), E is the dissociation barrier, k is Boltzman's constant and T is the temperature. From this plot, we have determined the dissociation barrier to be 0.73 $\pm$ 0.15 eV with a pre-exponential factor of $10^{11.9\pm2.4}$ s^{-1}. The dissociation barrier for free H_2S and thiols (RSH) are about 4 eV [22], which emphasizes the catalytic role of silicon. The pre-exponential is lower than the typical value of 10^{13} s^{-1}, but it is well within the error bounds. The dissociation barrier can be modified by isotope effects, but these effects are usually no more than 10%, which would be difficult to justify with our technique. To observe the isotope effect, we would also need a larger temperature range than is accessible with our experiment.

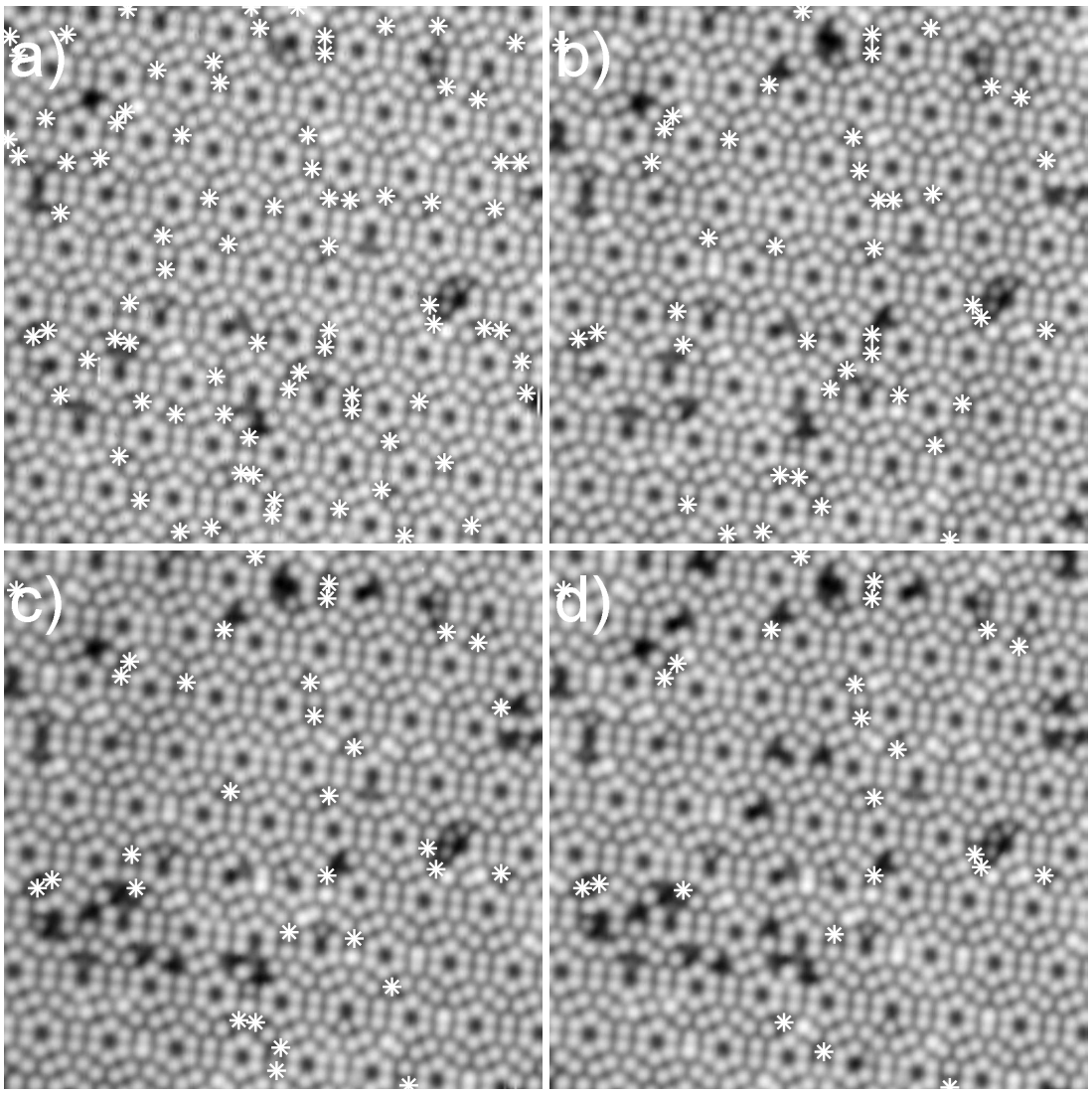

Figure 3.3: Typical thermal dissociation measurement sequence for DS at 297 K. The surface is scanned repeatedly every 1 to 2 minutes with a sample bias of 0.7 V and 0.1 nA tunneling current. The scanned area is 400 Å × 400 Å, but for clarity only 200 Å × 200 Å portion is shown. Adsorbates are marked with a white asterisk for clarity. The dark spots are deuterium atoms that were not desorbed after dissociation. a) First scan after dosing with D_2S, $t = 0$, total of 81 adsorbates. b) $t = 54$ minutes, 38 dissociations. c) $t = 111$ minutes, 49 dissociations. d) $t = 214$ minutes, 57 dissociations.

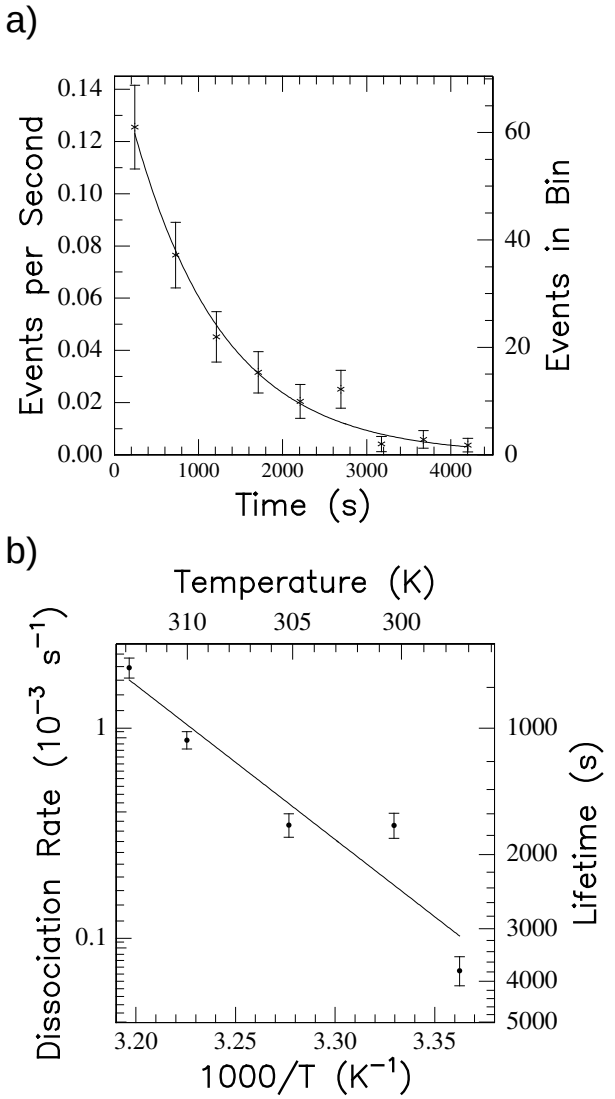

Figure 3.4: a) DS dissociation events at 310 K. Data were taken every 160 s. Three consecutive measurements were added and divided by the time interval to produce the bins. A total of 165 events were recorded at this temperature. The data are fitted as explained in the text. The same procedure was used at the other four temperatures (not shown). b) Dissociation rate of DS as a function of temperature. The slope of the linear fit determines the energy barrier and the intercept is the pre-exponential factor (attempt frequency) for thermally activated DS dissociation.

3.5 Discussion

Unlike the low temperature, STM induced dissociations, the data suggest that the deuterium atoms can move 100 Å or more. We arrive at this conclusion by looking at successive scans where the total number of dissociations is small (1 or 2) and a deuterium atom is also in the image. The deuterium atom is either the byproduct of a dissociation occurring inside or outside the imaged area. Since the distance traveled is on the order of the image size (400 Å × 400 Å), we take the minimum of the distance between the deuterium and the edge of the image and the distance to the nearest sulfur. By averaging five such events, we calculate the lower bound of deuterium movement at 300 K to be 68 Å. We are unable to determine the displacement length more accurately because of several factors. In a typical scan area of 400 Å × 400 Å, even at low dosage, multiple dissociations can occur between successive scans, which makes it difficult to attribute the deuterium atoms to their original molecule. Given that the displacement length is on the order of the scan length, it is also common to see deuterium atoms that have moved into the scan region from the periphery, making it even more difficult to identify the originating molecule. Conversely, deuterium atoms that originated in the scan region can move out of the scan region. If we increase the scan size to about 1000 Å × 1000 Å, we can no longer differentiate between the DS molecules and the silicon atoms.

There are three possible mechanisms by which the deuterium atom can move long distances. It is possible that the deuterium desorbs, bounces off the STM tip and adsorbs on the silicon surface. We can rule this out, because we have scanned areas far away from the scan region that clearly show the presence of deuterium on the surface. It may also be that at room temperature, deuterium can move longer distances after dissociation. Given the strong interaction between

silicon and deuterium, the large surface corrugation and large diffusion barrier, it seems unlikely that temperature is the only factor in the large distance traveled by deuterium atoms. The third possibility is that of a hot deuterium atom, which has significantly more energy than one produced by STM induced dissociation. The deuterium atom has to lose all the extra energy before it can chemisorb to silicon.

H_2O adsorbs similarly to H_2S on Si(111)-7×7: the initial adsorption is dissociative and the OH fragment is more likely to adsorb on the center ad-atoms compared to the corner ad-atoms [23]. OH, however, does not appear to dissociate like SH. The differences between OH and SH are of practical importance, especially in gas detector design. Under ambient conditions any detection scheme must be able to differentiate between the prevalent water vapor and H_2S.

3.6 Conclusion

Single molecule chemistry is an interesting and rapidly growing field with ramifications for both basic science and future technologies. Studying reactions on an atomic scale elucidates the local character of chemical interactions. Not only can we affect a single chemical bond without disturbing neighboring bonds, but we can make quantitative measurements that may further our theoretical understanding of the adsorbate-surface system. Our studies reveal the catalytic nature of silicon in the dissociation of DS and HS and the strong chemical interaction of H and D with Si.

Bibliography

[1] V. Jayaraman, G. Mangamma, T. Gnanasekaran, and G. Periaswami, Solid State Ionics, Diffusion and Reactions **86**, 1111 (1996).

[2] B. A. Akimov, A. V. Albul, A. M. Gas'kov, V. Yu. Il'in, M. N. Rumyantseva, L. I. Rybova, and M. Labeau, Semiconductors **31**, 335 (1997).

[3] H. U. Schutt and P. R. Rhodes, Corrosion **52**, 947 (1996).

[4] S. Conrad, D. R. Mullins, Q.-S. Xin, and X.-Y. Zhu, Appl. Surf. Sci. **107**, 145 (1996).

[5] D. R. DeBoer and P. G. Steffes, Icarus **123**, 324 (1996).

[6] N. Biver, D. Bockelee-Morvan, P. Colom, J. Crovisier, J. K. Davies, W. R. F. Dent, D. Despois, E. Gerard, E. Lellouch, H. Rauer, R. Moreno, and G. Paubert, Science **275**, 1915 (1997).

[7] D. V. Chakarov and W. Ho, Surf. Sci. **323**, 57 (1995).

[8] M. A. Rezaei, B. C. Stipe, and W. Ho, to be published.

[9] J. J. Boland, Surf. Sci. **244**, 1 (1991).

[10] H. Kuramochi, H. Uchida, and M. Aono, Phys. Rev. Lett. **72**, 932 (1994).

[11] R. S. Becker, G. S. Higashi, Y. J. Chabal, and A. J. Becker, Phys. Rev. Lett. **65**, 1917 (1990).

[12] T.-C. Shen, C. Wang, G. C. Abeln, J. R. Tucker, J. W. Lyding, Ph. Avouris, and R. E. Walkup, Science **268**, 1590 (1995).

[13] M. Schlüter and M. L. Cohen, Phys. Rev. B **17**, 716 (1978).

[14] B. C. Stipe, M. A. Rezaei, and W. Ho, Phys. Rev. Lett. **79**, 4397 (1997).

[15] B. C. Stipe, M. A. Rezaei, W. Ho, S. Gao, M. Persson, and B. I. Lundqvist, Phys. Rev. Lett. **78**, 4410 (1997).

[16] K. Hermann and P.S. Bagus, Phys. Rev. B **20**, 1603 (1979).

[17] B. M. Rice, L. M. Raff, and D. L. Thompson, Surf. Sci. **198**, 360 (1988).

[18] H. C. Akpati, P. Norlander, L. Lou, and Ph. Avouris, Surf. Sci. **372**, 9 (1997).

[19] R. Gomer, Rep. Prog. Phys. **53**, 917 (1990).

[20] G. A. Reider, U. Höfer, and T. F. Heinz, Phys. Rev. Lett. **66**, 1994 (1991).

[21] L. J. Richter and W. Ho, J. Vac. Sci. Tech. A **3**, 1549 (1985).

[22] D. F. McMillen and D. M. Golden, Ann. Rev. Phys. Chem. **33**, 493 (1982).

[23] Ph. Avouris and In-Whan Lyo, Surf. Sci. **242**, 1 (1991).

Chapter 4

Imaging the Atomically Resolved Dissociation of D_2S on Si(100) from 80 to 300 K[†]

4.1 Abstract

Using a variable-temperature, ultrahigh vacuum scanning tunneling microscope (STM), we have induced and imaged the dissociation of D_2S on Si(100). D_2S dissociates into DS and D below 200 K. Individual DS fragments can be dissociated with the STM at low temperatures. The deuterium atom attaches to a neighboring silicon dimer. At 200 K or above, D_2S dissociates into S and two D's. D_2S adsorption affects the surface reconstruction on Si(100), from the buckled dimer configuration to the dynamically flipping configuration and vice versa. We discuss our results in the context of other experiments on the same and similar systems.

[†]This chapter by M. A. Rezaei, B. C. Stipe, and W. Ho has been submitted to *Journal of Chemical Physics* under the same title for publication.

4.2 Introduction

Chemical reactions at solid surfaces play an important role in nature as well industrial applications. One avenue of research to understanding these processes is investigating the low coverage adsorption behavior on the atomic scale. A scanning tunneling microscope (STM) is a useful tool for observing gas-solid interactions with atomic scale resolution. Not only can an STM be used to observe the system, it can also be used to probe the molecules by inducing chemical changes. By performing experiments at different temperatures, reaction intermediates may be observed. To verify the interpretation of the data, the experimental results are compared to theoretical calculations of the same system [1]. Finally, by comparing the results to experimental results obtained for H_2S on Si(111) [2, 3] and H_2O on Si(100) [4, 5], we can construct a more complete and clearer picture for the adsorption and reaction of D_2S on Si(100).

Our STM is a home-made instrument which has been described in detail elsewhere [6]. It operates in an ultra-high vacuum system with a base pressure of 3×10^{-11} Torr. Liquid helium is used to cool the entire STM and two radiation shields that enclose it. Adjusting the cryogen flow rate changes the STM temperature. Due to small variations in flow rate, the temperature is regulated by a heater which is powered by a temperature controller. The temperature can be held constant from 8 to 350 K to within 0.1 K. The silicon used in these experiments is cut from a *n*-type, 10-25 Ω cm, prime grade wafer. The tips used for these experiments are polycrystalline tungsten or in a few cases polycrystalline Pt-Ir. The tips are 0.5 mm diameter wires that are chemically etched to a tip radius of 25 to 50 nm. No systematic difference was noted between the two tip materials. The sample is mounted on a molybdenum sample holder. Both the sample and sample holder are out-gassed

at 1000 K overnight. The sample is further cleaned by repeated sputtering (1 keV Ne^+ ions) and annealing (1200 to 1500 K) cycles. The final anneal is at 1500 K for 1 minute, followed by a rapid cool down to 1175 K and a slow (1 to 2 K/s) cool down to room temperature.

The adsorption of H_2S on Si(100) has been previously investigated theoretically [1] and by ultraviolet photoelectron spectroscopy (UPS) [7]. The UPS studies were conducted at 150 and 550 K. Our studies were conducted from 80 to 300 K. D_2S was used instead of H_2S because of our previous experiments with D_2S on Si(111) [2, 3]. Experiments using H_2S have shown no significant differences.

The Si(100) surface is a well studied and well understood surface [8–10]. The surface reconstructs into dimer rows that are buckled. At room temperature, the dimers appear symmetric because they are rapidly buckling back and forth. As the temperature is lowered to below 200 K [8], regions of centered 4×2 reconstruction appear. Theoretical [11–15] and experimental [16–18] results suggest energies between 1.5 and 2 eV lower per dimer relative to the unreconstructed surface. Figure 4.1a shows a large area scan of Si(100) at 300 K with a 2 V bias voltage. With a positive sample bias, the empty states are imaged and therefore, the dimer bonds appear dark and the remaining dangling bond on each surface atom appears bright. A close up view of the (2×1) reconstructed dimers [Fig. 4.1b] shows the dark dimer bond and the dangling bond on each Si atom. At low temperatures, domains of centered 4×2 reconstruction appear if the surface defect density is low enough [Fig. 4.1c]. Figure 4.1d shows the Si(100) surface scanned at 150 K with a 2 V bias. Silicon atoms that are buckled down are visible in this image. The effects of D_2S adsorption on the surface reconstruction as well as the role of the defects in the reconstruction will be discussed later.

Figure 4.1: a) Clean Si(100) scanned at 300 K, with 2 V sample bias. The dimers appear symmetric because they are dynamically flipping up and down at this temperature. b) High resolution scan at 300 K and 2 V sample bias. A silicon dimer is outlined. The dimer bond appears dark. c) Si(100) scanned at 150 K and 0.7 V sample bias. The c(2×4) reconstruction shows a typical "honeycomb" pattern because alternating Si atoms are not visible. The dynamically flipping dimers appear symmetric, much like the room temperature images. d) High resolution scan at 150 K and 2 V sample bias. A c(2×4) unit cell is outlined. At this bias voltage, all Si atoms are visible.

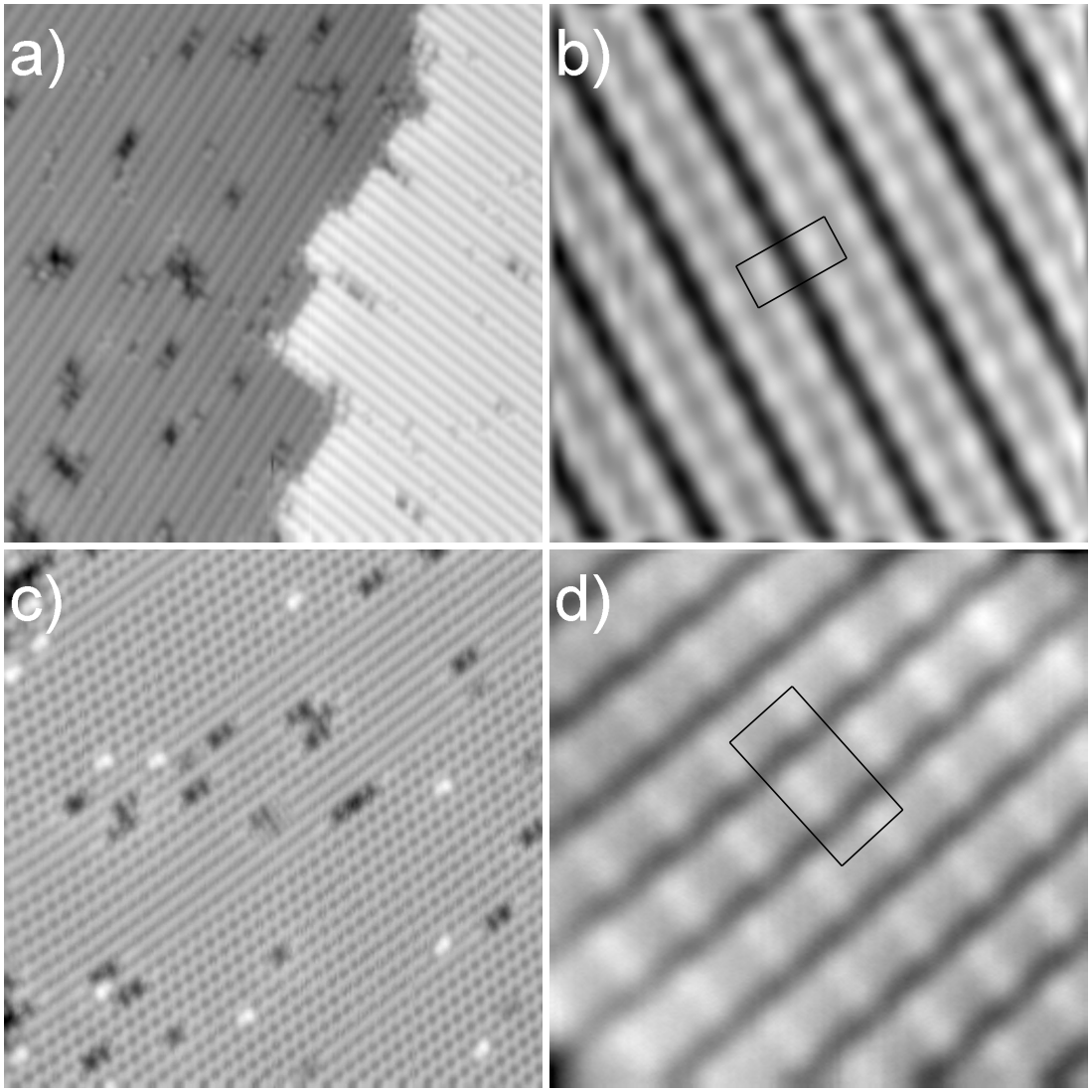
a)
b)
c)
d)

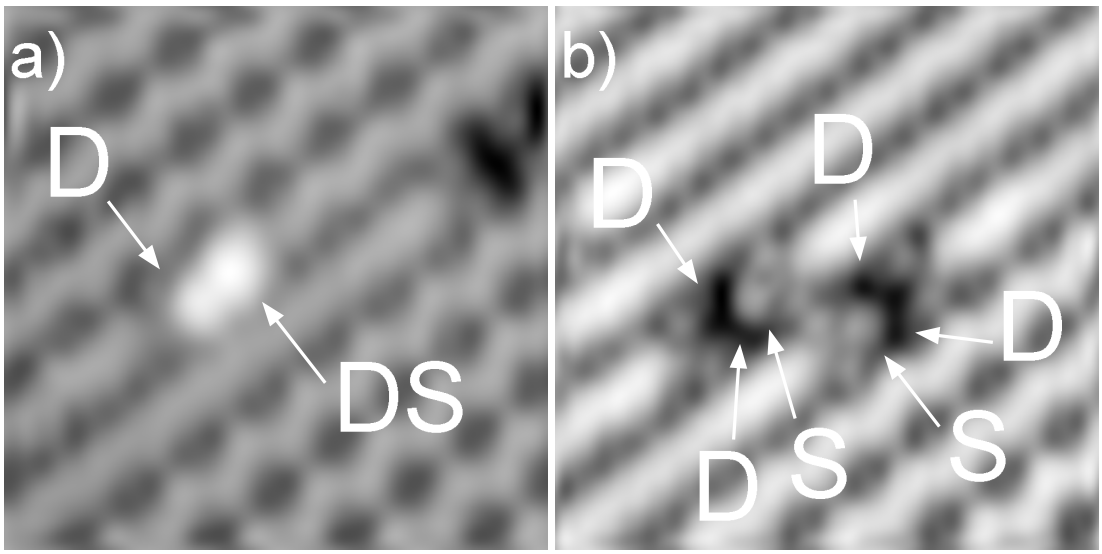

Figure 4.2: a) D_2S adsorbed on Si(100) at 150 K and dissociated into DS and D. Image was scanned at 1 V sample bias and 1 nA tunneling current. This is the only image shown in this paper that was taken with a Pt-Ir tip. b) Two D_2S molecules dissociated into S and two D's. The images were scanned at 1 V sample bias and 0.1 nA tunneling current at 130 K.

4.3 Experimental Results

Below 200 K, D_2S only partially dissociates on Si(100). The DS molecule is bonded in between dimer rows. The lone deuterium atom is bonded on the dimer next to DS. Figure 4.2a shows a picture of the dissociated D_2S (DS + D) at 150 K. Note that D appears slightly darker than the silicon atoms and the adjacent dangling bond is now brighter, making it more difficult to see the lone D.

DS can be dissociated during regular scanning. Figure 4.2b shows two such fully dissociated adsorbates. There are two dissociated molecules in the image and by the symmetry of the surface, the deuterium atoms can be on either side of the sulfur atom. The dissociation is an STM induced effect at low temperatures. Figure 4.3a

shows a large area scan taken at 1 V and 0.1 nA at 150 K before dosing. Figure 4.3b shows a closeup of the outlined area in Fig. 4.3a. The surface was dosed with D_2S and then the outlined square was immediately scanned [Fig. 4.3c]. This small area was scanned multiple times at 0.7 V and 0.1 nA, without scanning the periphery, then the entire area was scanned [Fig. 4.3d]. As can be seen, most of the adsorbates in that area have dissociated. We have been unable to tune the scanning parameters to avoid dissociation on Si(100), unlike our Si(111) studies [2, 3]. At around 200 K, the dissociation of DS occurs thermally at an appreciable rate. We have checked that the dissociation is not purely STM induced by taking two scans, one right after dose, which shows the bright species, and one after waiting a short while in an area far away from the tunneling junction, which shows the dissociated species as well. In the intermediate range of 150 to 200 K, both thermal and STM induced dissociations occur, but any particular dissociation cannot be easily attributed to one or the other mechanism.

At room temperature, D_2S adsorbs dissociatively into S and 2 D's. The sulfur atom is bonded to the dangling bonds of adjacent dimers, as is the DS at low temperatures. An adsorbate bonded in between two surface atoms is often labeled "bridge" as opposed to "on-top", where the adsorbate bonds on top of a single atom. There are two possible bridge adsorption sites: between two dimers or within the same dimer. The adsorption geometry of the dissociated products is identical to the adsorption geometry of molecules dissociated by the STM at low temperature [Fig. 4.2b]. The sulfur atom always bridge bonds between two dimers, with the deuterium atoms bonded to neighboring dimers with one D per Si atom. We have not observed any other modes of dissociation at low coverage, such as the deuterium atoms on different sides of S, or S bridge bonded in the dimer bond. The entire

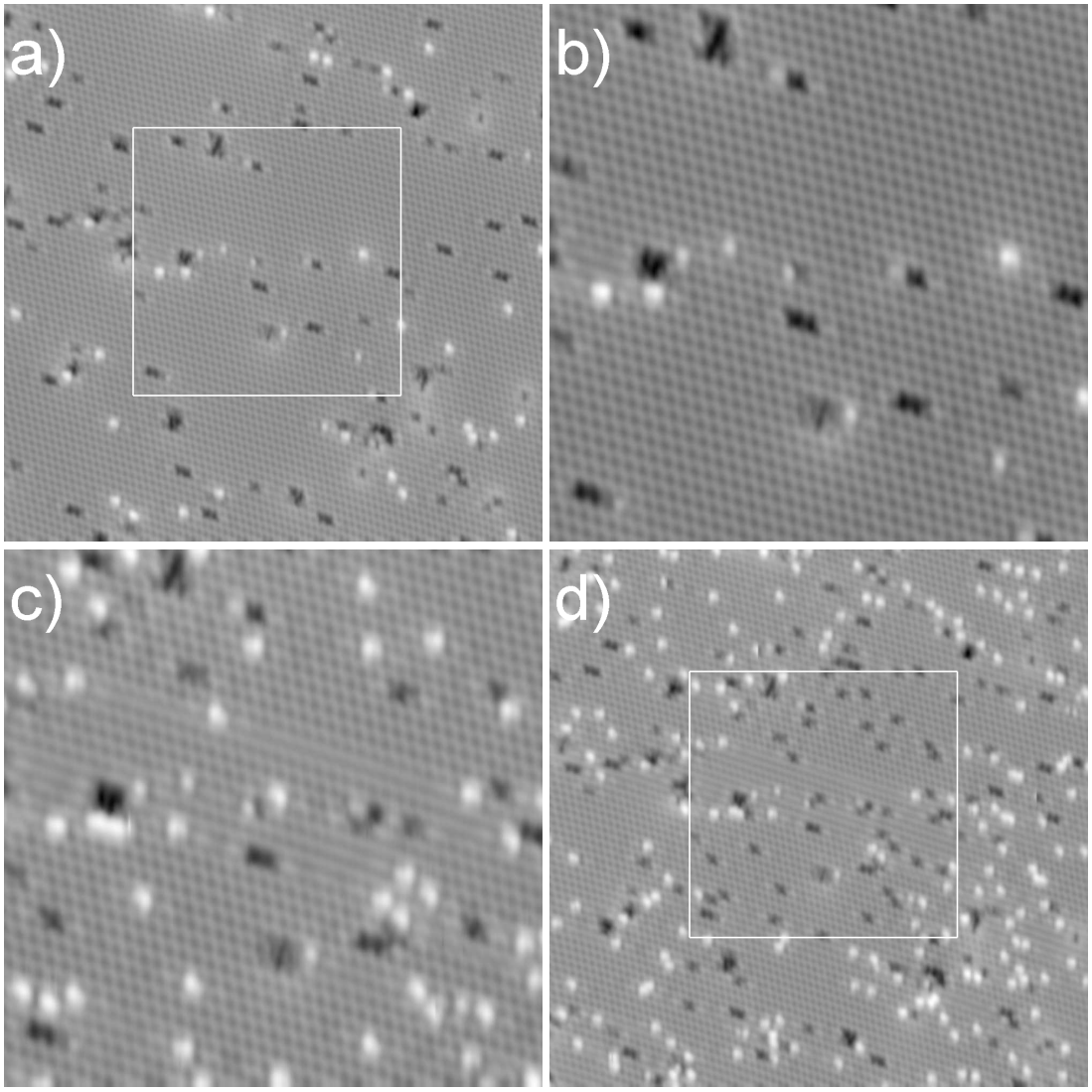

Figure 4.3: a) STM image of clean Si(100) surface taken at 150 K, 1 V sample bias and 0.1 nA tunneling current. b) Closeup view of the outlined area in (a), scanned at 0.7 V and 0.1 nA. c) Same area as (b) right after dosing with D_2S. This area was scanned at 0.7 V and 0.1 nA multiple times. d) Same area as (a) showing the STM induced dissociations in the outlined area, but not the surrounding area.

dissociated molecule (S+2 D) appears darker than the surrounding silicon, which is in contrast to the partially dissociated species (DS+D) which appears bright. With a negative sample bias, both species (S+2 D and DS+D) appear dark and are more difficult to distinguish. For this reason, all the images shown here were taken with positive sample bias.

Given this adsorption geometry at room temperature, we expect the single layer coverage to be saturated at 0.25 monolayer (ML), because sulfur bonds to two Si atoms and the deuterium atoms bond to one Si atom each. Figure 4.4 shows the same area at 300 K dosed successively with D_2S. As can be seen in Fig. 4.4d, at saturation, rows of sulfur appear very distinctly on the surface. Note that the size of the sulfur atoms appears rather large and there are four surface atoms for every adsorbed sulfur.

Below 200 K, STM induced DS dissociation occurs if the sample bias is 0.7 to 1.5 V. If the voltage is higher, DS does not dissociate but instead is forced into the dimer bond. Figure 4.5a shows a large area with many DS adsorbates at 130 K. After a 2 V scan, the same area was scanned and the image shows that many of the adsorbates appear to break up into two smaller bright spots [Fig. 4.5b]. Figure 4.5c shows a high resolution scan of such an adsorbate. The DS molecule has moved onto the dimer bond. Changing the adsorbate-surface bond arrangement to bridge bond on the dimer has been induced with the STM previously for benzene [19] and chlorine [20] on Si(100). Chlorine, like DS, does not naturally occupy the dimer bond. Benzene, however, bridge bonds on the dimer and between dimers naturally. Other adsorbates may require more energy in order to be inserted into the dimer bond. For instance, hydrogen bonds to the dangling bond of the Si atoms and only at elevated temperatures and high dosage does it attack the dimer

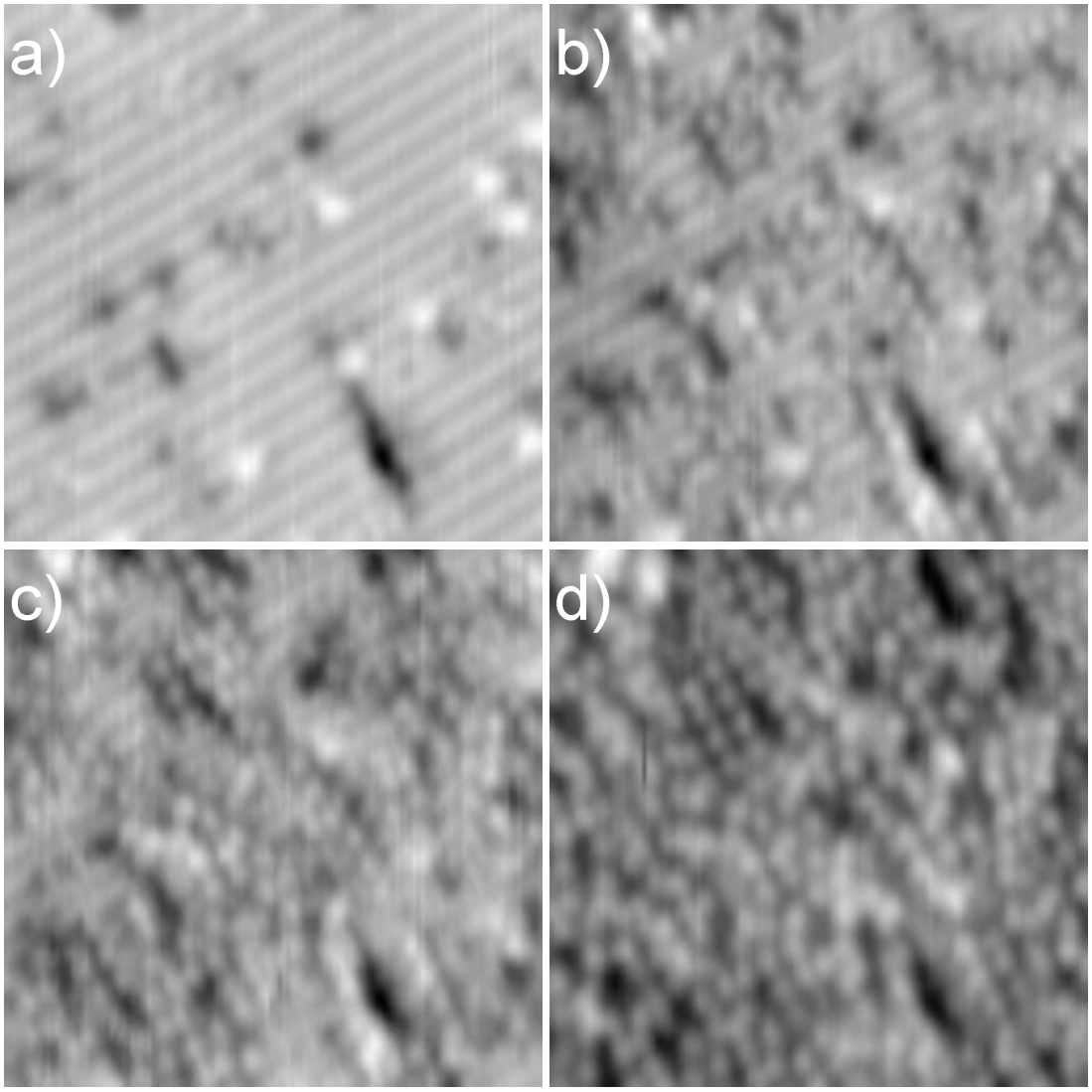

Figure 4.4: Successive doses of D_2S at 300 K. Same area is shown in all images at the same scale (125 Å×125 Å). The total dosing times are: a) 15 s. b) 60 s. c) 90 s. d) 210 s. The images were scanned at 2 V sample bias and 0.1 nA tunneling current. The surface defect (dark area) in the lower right of (a) is visible in all images.

Figure 4.5: a) D_2S on Si(100) at 130 K. The image was scanned with 1 V sample bias and 0.1 nA tunneling current. b) Same area as a), but after a 2 V scan. The image was scanned with 1 V sample bias and 0.1 nA tunneling current. Some of the adsorbates, three of which are indicated by arrows, appear to be split into two smaller bright dots. c) High resolution close up of the split adsorbate. The DS molecule has moved onto the dimer bond. The other bright spot is a Si dangling bond that results from D adsorption onto the neighboring site. The image was scanned at 2.45 V sample bias and 1 nA tunneling current. d) Schematic model of the adsorption of D_2S on Si(100). The initial adsorption is partially dissociative; DS can be dissociated with the STM or by heat. The STM can be used to move the DS onto the dimer bond. The sulfur atom does not stay on the dimer bond if the moved DS is dissociated.

bond [21]. Thermal CO also bonds to the dangling bond of a single Si atom. However, translationally energetic CO with 1.3 eV of energy can occupy the dimer bond [22].

DS can be dissociated with the STM from the dimer bridge site, but the sulfur atom then bonds in between dimers and not on top of the dimer. We have unable to move the sulfur into the dimer bond. The between dimer bridge configuration is possibly energetically more favorable because it does not involve breaking of the dimer bond and passivates the dangling bonds. Figure 4.5d shows a schematic of the different adsorption configurations as well as the effect of temperature and interaction with the STM.

Detailed studies [8, 9] of the reconstruction of Si(100) show that the c(4×2) reconstruction is the ground state and at low temperatures exists as either stabilized (asymmetric) or dynamically flipping (symmetric) dimer pairs. The symmetric

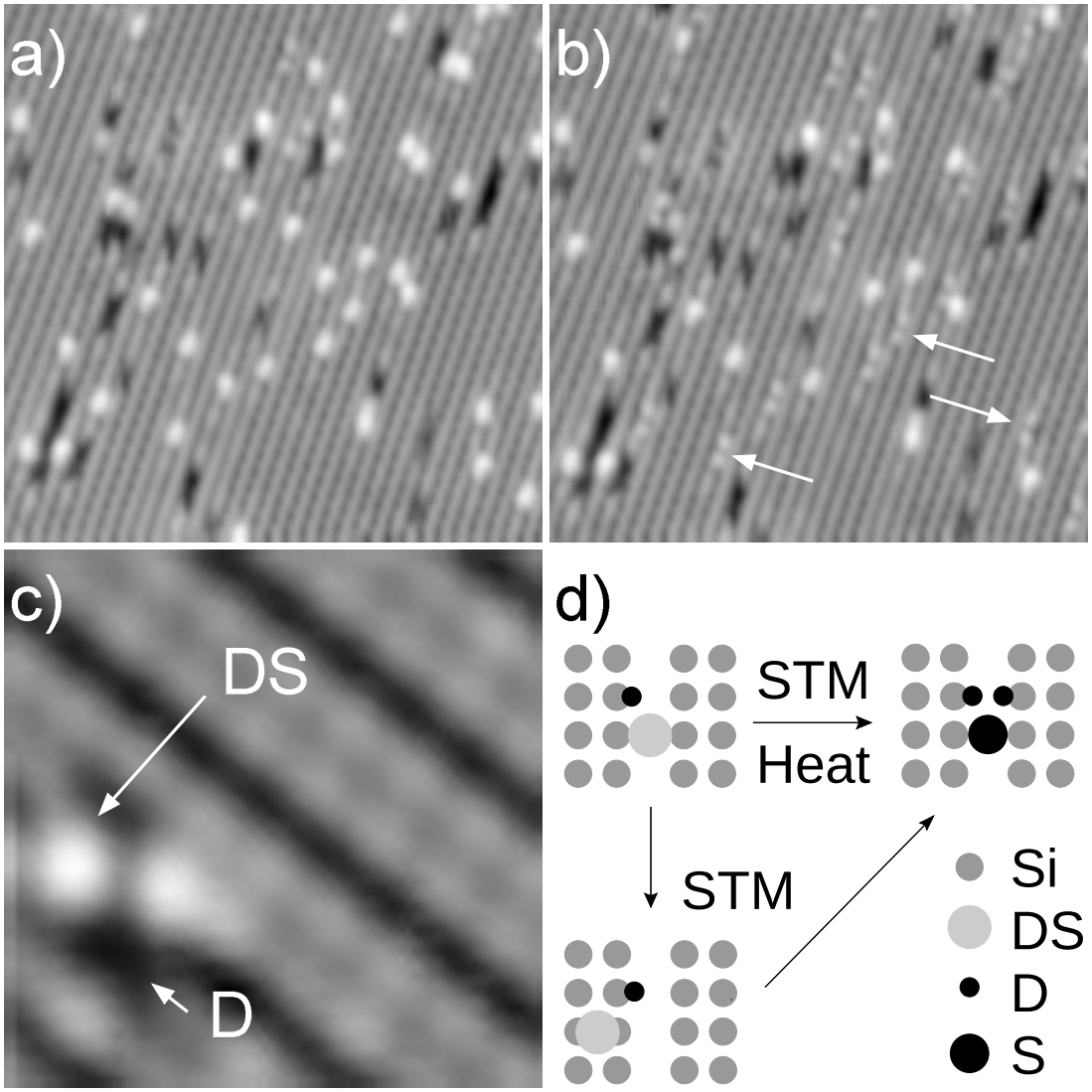
a)
b)
c)
DS
D
d)
STM
Heat
STM
Si
DS
D
S

dimers occur in the vicinity of surface defects, and are often pinned between two defects. Defects on Si(100) are usually attributed to missing dimers, although it has been suggested that some of the defect-like features on the surface are due to adsorbed water [4]. We have found that the reconstruction can be changed both by the adsorption of D_2S and the dissociation of DS. In most cases the adsorbates do not disturb the surface reconstruction, but if an adsorbate is close enough to a defect it can influence the appearance of dimers. We have not, however, seen a difference in surface reconstruction even for closely spaced adsorbates that are far away from defect sites. Figure 4.6a shows the surface at 150 K and before dose. After dosing, the reconstruction is changed to the asymmetric dimer configuration due to the adsorbed DS and D [Fig. 4.6b]. The dissociation DS causes the reconstruction to revert to the symmetric configuration [Fig. 4.6c]. The length over which the dimers are affected (about 10 dimers) is consistent with previous experiments studying the effect of surface defects [10]. Recent experiments [23] show that perturbing the surface defects with voltage pulses can have temporary and permanent long range effects on the reconstruction. Our experiments demonstrate that the symmetric and asymmetric buckling configurations can be changed with adsorbates.

4.4 Discussion

Our STM results agree well with the UPS studies [7] of the same system and can be used to understand some of the features found using UPS. The UPS studies suggest that the adsorption is partially dissociative ($D_2S \rightarrow DS + D$) at 150 K and fully dissociative ($D_2S \rightarrow S + 2\ D$) at 550 K, which agrees with our interpretation of the STM images. We have found, however, that the full dissociation temperature is

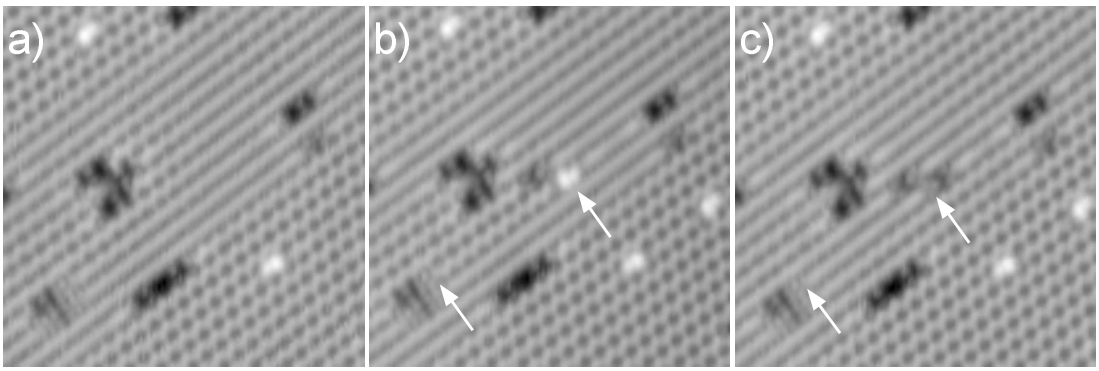

Figure 4.6: Effect of D_2S adsorption and dissociation on the surface reconstruction at 150 K: a) The clean surface. b) Surface after a light dose. Note the change in the reconstruction from symmetric to asymmetric in the marked row. c) The STM induced dissociation of the adsorbate causes the reconstruction to revert to the symmetric configuration. The images were scanned with 1 V sample bias and 1 nA tunneling current.

about 200 K. No attempt was made to find the dissociation temperature with UPS. According to the UPS data at 150 K, the adsorption has a fast and slow phase, with the slow phase starting after 1/3 monolayer coverage. Our experiments suggest that DS is bonded to two silicon atoms and D is on a Si atom of the next dimer. This bonding structure requires three Si atoms per adsorbate and the saturation of available sites explains the onset of the slow adsorption.

Theoretical calculations for H_2S on Si(100) have been performed using the MNDO (modified neglect of differential overlap) semiempirical method [1]. The results suggest that molecular adsorption is not favored. Three dissociative adsorption geometries were found to be close in energy: H(on-top)+HS(bridge) at -2.9 eV, 2H(on-top)+S(bridge) at -3.1 eV and 2H(dihydride)+S(bridge) at -3.4 eV relative to the unreacted gas/surface system. It should be noted that the calculations were

performed for an unreconstructed surface, with two dangling bonds per surface atom. From studies of hydrogen on Si(100) [24], it is clear that only one H bonds to each Si atom and therefore, we can rule out the last configuration. The first two configurations are in agreement with our observations below and above 200 K, respectively.

We have studied the adsorption of D_2S on Si(111) [2, 3]. The adsorption behavior is similar in that there are two dissociation steps: partial dissociation ($D_2S \rightarrow DS + D$) at low temperatures and full dissociattion ($D_2S \rightarrow S + 2\ D$). However, for Si(111), DS does not dissociate until about 295 K, whereas it dissociates around 200 K on Si(100). Furthermore, we were able to lower the tunneling current and sample bias so that the STM did not influence the DS dissociation on Si(111), but we were not able to do the same for Si(100). These results suggest that the dissociation energy for DS is lower on Si(100).

We have determined the dissociation energy of DS to be 0.73 eV on Si(111) by measuring the dissociation rate as a function of temperature. Breaking the DS bond requires 4 eV of energy for D_2S in the gas phase [25]. The surface, therefore, acts as an effective catalyst in the dissociation process. The thermal dissociation of D_2S on Si(111) produces hot D atoms that can move up to 100 Å. On Si(100), the D atoms are always adjacent to the adsorbed sulfur. This behavior suggests a concerted bond formation/bond breaking mechanism that involves the Si(100) surface atoms. On Si(111), the top layer atoms are 6 to 7 Å apart, whereas adjacent Si(100) atoms are only 3.8 Å apart and can therefore participate more readily in the dissociation of D_2S and DS.

The adsorption of D_2S on Si(111)-(7×7) is more complicated than its adsorption on Si(100). There are four distinct adsorption sites on Si(111) with different sticking

probabilities, but there is only one adsorption site on Si(100). The adsorption behavior on Si(111)-7×7 is related to the complicated reconstruction of the surface. There are strong nearest neighbor effects on Si(111) which we have not observed on Si(100).

Another system that is often studied in conjunction with H_2S is H_2O on Si(100). H_2O dissociates into OH and H at room temperature on Si(100). Although there is some STM evidence for molecular adsorption at low coverage [4], molecular adsorption has not been confirmed with any other methods. In contrast to D_2S, both OH and H attach to the same dimer. OH does not dissociate even up to 400 K [5], indicating a higher barrier to dissociation as compared to DS. The difference between the two systems may stem from the different bonding arrangements that O and S favor. S bonds more readily in the bridge configuration, whereas O prefers the on-top position.

4.5 Conclusion

We have studied the adsorption and dissociation of D_2S on Si(100) at various temperatures. D_2S partially dissociates below 200 K and is fully dissociated above 200 K. S and DS bond in a bridge configuration between two dimers with the remaining D on a neighboring dimer. DS can be dissociated with the STM and it can also be forced into the dimer bond. Our results are in good agreement with previous UPS studies and theoretical calculations of adsorption geometry. Our studies reveal the catalytic nature of silicon in the dissociation of DS and the strong chemical interaction of D with Si.

The interaction with the surface changes the energy barrier to dissociation.

Not only does the surface influence the adsorbate, but the adsorbate may affect the energetics of the surface as well. The adsorption of single D_2S molecule on Si(100) can change the reconstruction of the surface for as many as 15 dimer pairs away. Observing such effects is difficult with other methods. Investigating the adsorption and dissociation of gases on surfaces at the atomic scale is a powerful method for understanding chemical reactions. Performing these experiments at various temperatures can provide a window into the reaction pathway as well as the energies involved.

4.6 Acknowledgment

Support for this research by the Division of Chemical Sciences, Office of Basic Energy Sciences, Office of Energy Research, U.S. Department of Energy under Grant No. DE-FG02-91ER14025 is gratefully acknowledged.

Bibliography

[1] V. Barone, Surf. Sci. **189/190**, 106 (1987).

[2] M. A. Rezaei, B. C. Stipe, and W. Ho, J. Chem. Phys., (to be published).

[3] M. A. Rezaei, B. C. Stipe, and W. Ho, (to be published).

[4] M. Chander, Y. Z. Li, J. C. Patrin, and J. H. Weaver, Phys. Rev. B **48**, 2493 (1993).

[5] W. Ranke, Surf. Sci. **369**, 137 (1996).

[6] B. C. Stipe, M. A. Rezaei, and W. Ho, Rev. Sci. Instrum., (to be published).

[7] E. Schröder-Bergen and W. Ranke, Surf. Sci. **236**, 103 (1990).

[8] R. A. Wolkow, Phys. Rev. Lett. **68**, 2636 (1992).

[9] D. Badt, H. Wengelnik, and H. Neddermeyer, J. Vac. Sci. Technol. B **12**, 1872 (1994).

[10] J. A. Kubby and J. J. Boland, Surf. Sci. Rep. **26**, 61 (1996).

[11] J. Fritsch and P. Pavone, Surf. Sci. **344**, 159 (1995).

[12] Z. Jing and J. L. Witten, Surf. Sci. **274**, 106 (1992).

[13] F. F. Abraham and I. P. Batra, Surf. Sci. **163**, L752 (1985).

[14] J. A. Appelbaum and D. R. Hamann, Surf. Sci. **74**, 21 (1978).

[15] S. Y. Tong and A. L. Maldonado, Surf. Sci. **78**, 459 (1978).

[16] J. P. Levine, Surf. Sci. **34**, 90 (1973).

[17] B. W. Holland, C. B. Duke, and A. Paton, Surf. Sci. **140**, L269 (1984).

[18] M. T. Yin and M. L. Cohen, Phys. Rev. B **28**, 2049 (1983).

[19] G. P. Lopinski, T. M. Fortier, D. J. Moffatt, and R. A. Wolkow, J. Vac. Sci. Technol. A **16**, 1037 (1998).

[20] J. J. Boland, Science **262**, 1703 (1993).

[21] J. J. Boland, Surf. Sci. **261**, 17 (1992).

[22] D. Hu, W. Ho, X. Chen, S. Wang, and W. A. Goddard III, Phys. Rev. Lett **78**, 1178 (1997).

[23] K. Hata, M. Ishida, K. Miyake, and H. Shigekawa, Appl. Phys. Lett. **73**, 40 (1998).

[24] J. J. Boland, Surf. Sci. **244**, 1 (1991).

[25] D. F. McMillen and D. M. Golden, Ann. Rev. Phys. Chem. **33**, 493 (1982).

Chapter 5

Atomically Resolved Adsorption and STM Induced Desorption on a Semiconductor: NO on Si(111)-(7×7)

5.1 Abstract

Using a variable-temperature, ultrahigh vacuum scanning tunneling microscope (STM), we have studied the adsorption and STM induced desorption of NO from Si(111)-(7×7). NO adsorbs preferentially on faulted corner sites, followed by faulted center sites, unfaulted corner sites and unfaulted center sites. The preference for the different adsorption sites is independent of temperature and correlates well with the local density of states at these sites. NO can be desorbed from Si(111) with the

[†]This chapter by M. A. Rezaei, B. C. Stipe, and W. Ho has been submitted to *Journal of Chemical Physics* under the same title for publication.

STM. We present data that suggest the desorption is induced by the electric field under the STM tip. The threshold positive electric field for desorption of NO is 0.114 ± 0.009 V/Å. For sufficiently small tip-surface distances, NO can be desorbed locally without affecting the neighboring adsorbates.

5.2 Introduction

Investigating the reaction of nitric oxide (NO) on Si(111)-(7×7) is important for both basic science and industrial applications. NO is produced during combustion and is therefore a major concern in power plant emissions [1, 2]. It is also produced by photochemical processes in the upper atmosphere [3] and other natural phenomena such as lightning [4]. As NO is toxic, the detection and conversion of NO into harmless chemicals is essential for a healthy environment and a safe industry. Research into silicon based NO detectors strives towards this need [5]. NO is also used for thermal nitridation and oxy-nitridation of silicon in semiconductor processing [6]. It has been predicted that NO can be desorbed from Si(111) by the electric field produced by an STM [7]. This mechanism is quite distinct from the one involving electron-hole pairs which has been proposed for photon induced NO desorption [8, 9]. There have been no experiments to verify the electric field mechanism in the desorption of NO.

Our instrument is a home-made STM based on the Besocke design [10]. It operates in ultrahigh vacuum (UHV) with a base pressure of 3×10^{-11} Torr. The STM temperature can be held constant from 8 to 350 K to within 0.1 K. The tips used in these experiments are chemically etched from polycrystalline tungsten wire. The tips are 0.5 mm thick with a tip radius of 25 to 50 nm. The tips are cleaned in

UHV by repeated sputter and anneal cycles. The silicon used in these experiments is cut from a *p*-type, boron-doped, 1 Ω cm, prime grade wafer. The sample is mounted on a molybdenum sample holder. Both the sample and sample holder are out-gassed at 1000 K overnight. The sample is further cleaned by repeated sputtering (1 keV Ne^+ ions) and annealing (1200 to 1500 K) cycles.

The adsorption, dissociation and desorption of NO on Si(111) has been investigated previously by other methods. Temperature programmed desorption (TPD) and electron energy loss spectroscopy (EELS) [11] have been used to identify the surface species at various temperatures and coverages. At 90 K there are two molecular NO species; one is labeled "bridge" and the other "atop". The bridge species is found at all coverages; the atop species only occurs at higher coverage. The bridge species desorbs or dissociates at 147 K. The atop species dissociates between 200 and 300 K.

Photon and electron induced desorption of NO have also been investigated [8, 12, 13]. The data suggest that the desorption mechanism is mediated by electron-hole pair excitation in silicon and not a direct photon process. Although the results based on photon irradiation are not directly related to our studies and the electron energy used (350 eV) is much higher than tunneling electron energies, the proposed desorption mechanisms are relevant. These mechanisms, as well as electric field induced desorption are discussed later.

The Si(111)-(7×7) surface is schematically depicted in Fig. 5.1a [14]. There are twelve atoms on the top (adatom) layer. The unit cell has two halves, one faulted and the other unfaulted, which refer to the stacking fault of the adatom layer with respect to the bulk layer. The two halves of the unit cell cannot be distinguished in the positive bias STM image of the clean surface (Fig. 5.1b). The faulted half,

however, appears brighter in the negative bias (filled state) STM image (Fig. 5.1c), because the local density of states (LDOS) is higher in the faulted half [15, 16]. There are two types of adatoms in each half: the center and corner adatoms. The LDOS on the Si(111)-(7×7) surface varies from site to site. Within each half the corner sites have higher LDOS than the center sites. The four different adatom sites on the surface show different adsorption behavior for NO.

5.3 Adsorption Characteristics

We have studied the low coverage adsorption of NO on Si(111)-(7×7) from 32 to 160 K. NO adsorbs molecularly below 150 K. Figure 5.2a shows the clean silicon surface at 50 K. After dosing, adsorbed NO appears darker than the silicon atoms (Fig. 5.2b,c). It binds in an on-top configuration on both center and corner adatoms. The adsorption probability depends on the adsorption site and it is independent of temperature. The probability for sticking is highest for the faulted corner adatoms, followed by the faulted center adatoms, unfaulted corner adatoms and unfaulted center adatoms. According to EELS data [11], the only low coverage species above 150 K are atomic N and O. The STM image at 160 K shows species very distinct from NO: the adsorbates appear darker (Fig. 5.2d) and unlike NO, we cannot desorb them with the STM. NO desorption will be discussed in detail later. We cannot distinguish between N and O in STM images. Furthermore, in some cases the adsorbates do not appear pairwise, which one might expect from dissociated NO. It is possible that either N or O is bonded to the dangling bond on the rest atom layer and is not visible in the STM images. It is also possible that the dissociated atoms travel longer distances along the surface, either in a cannon ball type trajectory or

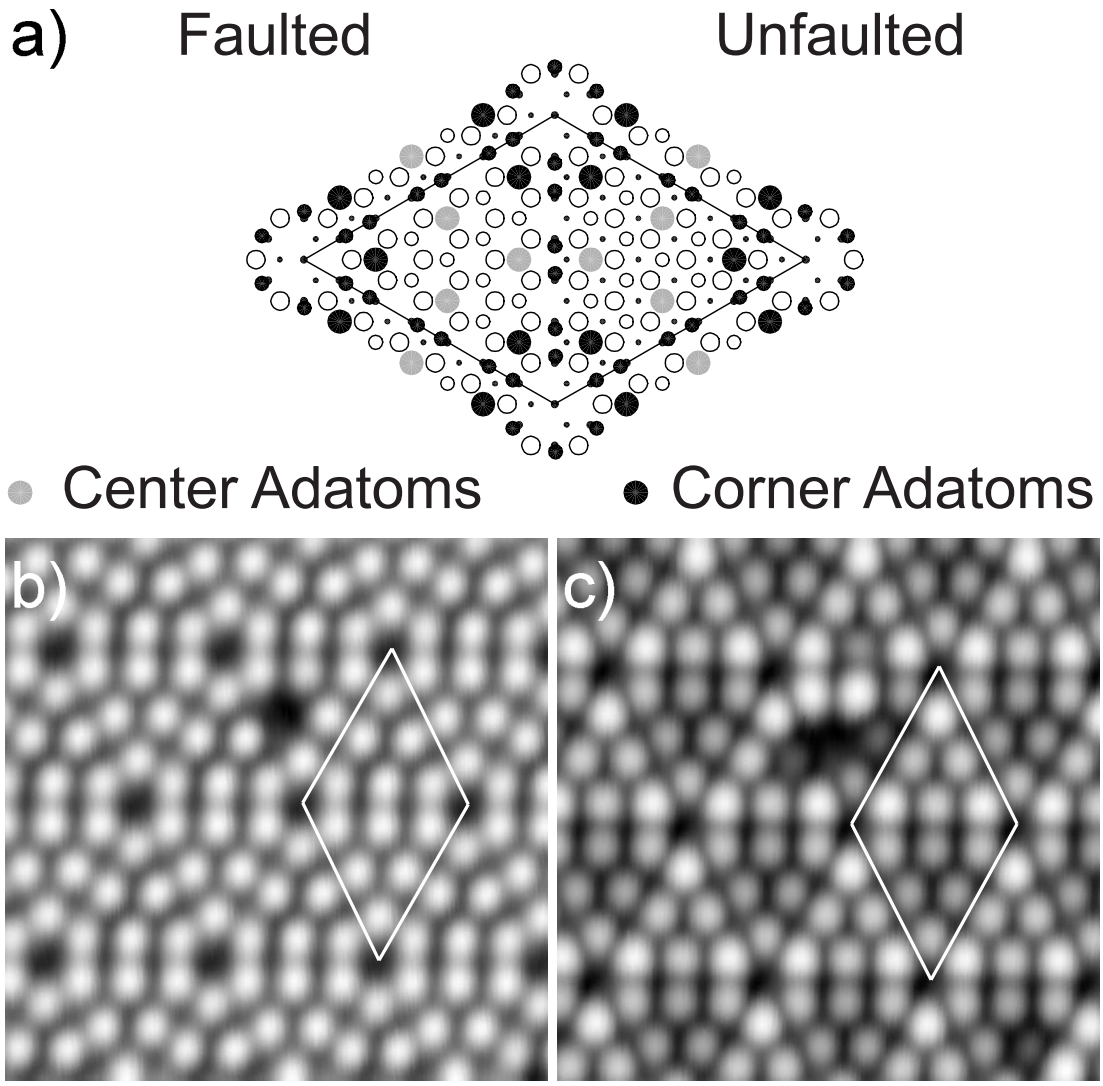

Figure 5.1: a) Schematic drawing of the Si(111)-(7×7) surface. b) Clean Si(111) scanned at 200 K with 0.7 V sample bias and 1 nA tunneling current. The unit cell is outlined. c) The same area as (b), scanned at -0.7 V sample bias and 1 nA tunneling current. The unit cell is outlined. The brighter half of the unit cell is the faulted half.

parallel to the surface.

The molecular NO species detected with EELS [11] and labeled "bridge" appears to be the on-top position as identified in our experiments. According to the EELS data, these adsorbates dissociate and desorb at 150 K, which is consistent with our experiment at 160 K. The EELS data also suggest that there may be two "bridge" type species, which may be accounted for by the different adsorption sites on the surface, that is, corner versus center or faulted versus unfaulted sites. In the coverage ranges studied here (1 to 10 adsorbates per 100 surface adatoms), we have not observed the "atop" NO species as determined by EELS [11].

Table 5.1 shows the percentages of adsorbates on the four possible adsorption sites at 50, 92, and 120 K. The adsorption probability on different sites is found to be independent of substrate temperature. The incoming NO molecules have the same mean kinetic energy for all the experiments, as the doser was kept at room temperature. It is likely that the barrier to adsorption at the different sites, if any, and the final state energies of the chemisorbed molecule are different at the four sites. The data suggest that NO does not reach thermal equilibrium with the surface before adsorption, because otherwise one would expect a population distribution that varies as a function of substrate temperature. The LDOS variations over the surface match the adsorption preference of NO. As mentioned earlier, the LDOS is highest at the faulted corner sites, followed by the faulted center sites, unfaulted corner sites and unfaulted center sites [15, 16]. Similar site preferences has been observed for O_2 on Si(111), although the temperature dependence of this effect was not investigated [17].

It has been suggested that O_2 looses its kinetic energy by becoming charged as it approaches the surface [17]. NO has a comparable electronegativity and except

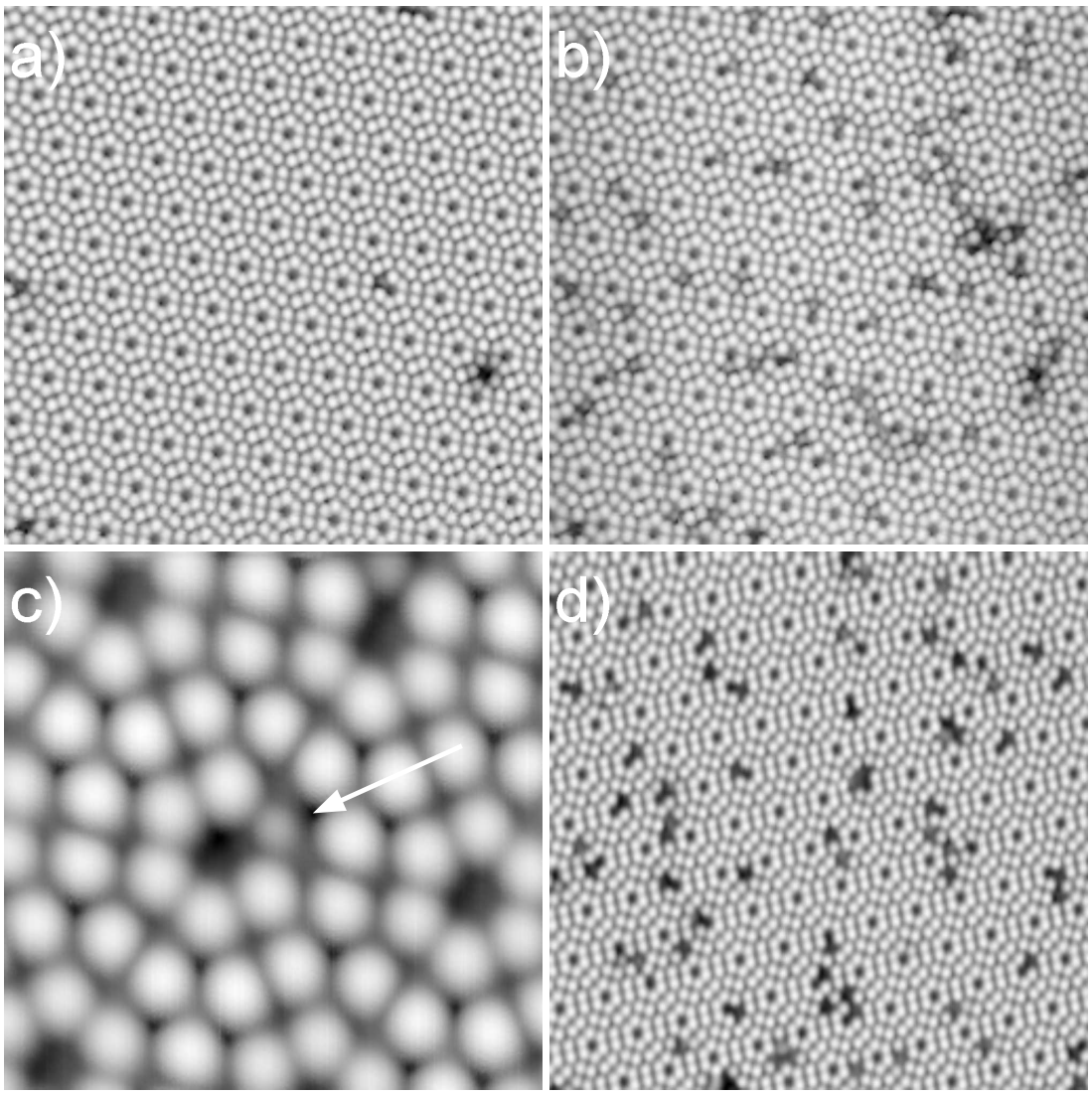

Figure 5.2: a) Clean Si(111)-(7×7) surface scanned at 0.85 V sample bias and 0.1 nA tunneling current at 48 K. b) Same area as (a) after dosing with NO. c) High resolution scan of NO (indicated by the arrow) at 50 K, scanned at 0.85 V sample bias and 0.1 nA tunneling current. d) Si(111) dosed with NO at 160 K. There is no molecular NO on the surface. N and O appear darker than NO. The image was scanned at 0.7 V sample bias and 0.1 nA tunneling current.

Table 5.1: The percentage of NO adsorbates on different sites. To avoid saturation effects, the data were collected at low coverage (less than one adsorbate per 10 surface adatoms). There is no temperature dependence in the site distribution from 50 to 120 K.

		Temperature (K)		
		50	92	120
Site	Faulted Corner	44 ± 2	40 ± 3	40 ± 3
	Faulted Center	25 ± 2	26 ± 3	25 ± 3
	Unfaulted Corner	20 ± 2	21 ± 2	21 ± 2
	Unfaulted Center	11 ± 1	13 ± 2	14 ± 2

for one less electron, a similar molecular orbital structure to O_2 and it is likely that the same mechanism is involved in the dissipation of the NO kinetic energy. The resulting charge transfer from Si to NO provides a pathway for the dissipation of the NO kinetic energy. The positive electronegativity of adsorbed NO causes the molecule to be partially negatively charged [7], which is consistent with adsorption kinetics involving electron exchange between the gas molecule and the surface. Since the LDOS is independent of temperature, so is the sticking probability at the different sites. Other excitation, such as phonons, are also likely to be involved in the dissipation of the NO kinetic energy prior to adsorption. The interaction with the substrate phonons, however, is not the primary pathway for the loss of kinetic energy, as a strong interaction would likely introduce substrate temperature dependence in the adsorption population at the different sites. The LDOS does not strongly influence the adsorption characteristics of other gases. H_2S, for example,

does not follow the same adsorption kinetics as NO [18]. H_2S shows a preference for the center sites within the same half of the unit cell and the sticking probability at various sites is dependent on temperature. The adsorption behavior of H_2S can best be described as a thermally activated process with different energy barriers at different sites.

5.4 NO Desorption

There are many mechanisms by which the STM can interact with an adsorbate or substrate [19, 20]. Van der Waals forces between the tip and the adsorbate have been used to move adsorbates on surfaces [21]. Tunneling as well as field emitted electrons have been used to excite adsorbate vibrational states and cause desorption [22], dissociation [23], or rotation [24] of adsorbates. The electric field under the STM tip has also been used to manipulate the adsorbate [25]. It is often difficult to discern the mechanism responsible for a particular effect, especially when trying to distinguish electron induced and field induced effects. The electron parameters (bias and current) cannot be changed independently of the electric field and therefore it is difficult to attribute the effect to one or the other mechanism.

To probe the mechanism of NO desorption from Si(111), we applied voltage pulses to the molecules at various tip-surface distances. The tunneling current was measured during the pulse and a characteristic step increase in the current indicated the moment of desorption. For consistency, only NO molecules adsorbed on faulted corner sites were used in the pulsing experiments. In addition to desorption, NO can move along the surface and bond to a different Si atom. NO desorbs $60 \pm 14\%$ of the time. Figure 5.3 shows an example of desorption of two neighboring NO adsorbates,

one at a time, indicating that the low voltage desorption is well controlled and local. The tip can be positioned directly on top of each of the NO molecules to desorb them separately. We can also desorb large numbers of NO adsorbates by scanning at 1.5 V. Figure 5.4 illustrates the desorption of many NO adsorbates by scanning. In some cases, NO does not desorb, but rather moves along the silicon surface. Figure 5.5 shows an NO molecule that moved after a voltage pulse. It is not clear whether NO actually moves along the surface, or desorbs, is reflected by the STM tip, and then re-adsorbs. The silicon surface corrugation is high and the barriers to diffusion are correspondingly high. For example, the barrier to diffusion of hydrogen on Si(111) is 1.5 eV [26]. In some cases we have observed that the STM tip will undergo a change after a pulse which may be attributed to NO that is bonded to the tip.

With the same tip, we can generally obtain consistent results that show a decrease in the desorption time with increasing voltage or increasing current. The desorption characteristics appeared to change, however, even when all measurable variables, that is temperature, voltage and current were kept the same. For example, we measured the desorption time at 1.2 V bias voltage and 0.3 nA tunneling current to be 129 $\pm$ 39 ms. With a different tip, we measured the desorption time at 1.2 V bias voltage and 0.9 nA tunneling current to be 5.1 $\pm$ 2.5 s. The same sample was used for both experiments and it was prepared identically on both days. The only difference was the tip. Given these results and the theoretical prediction that NO desorption can be induced by the electric field under the STM tip, we changed our pulsing technique to explore the field dependent characteristics.

To minimize the possibility of electron induced desorption, we moved the STM tip far away from the sample to reduce the current. We measured the current to be

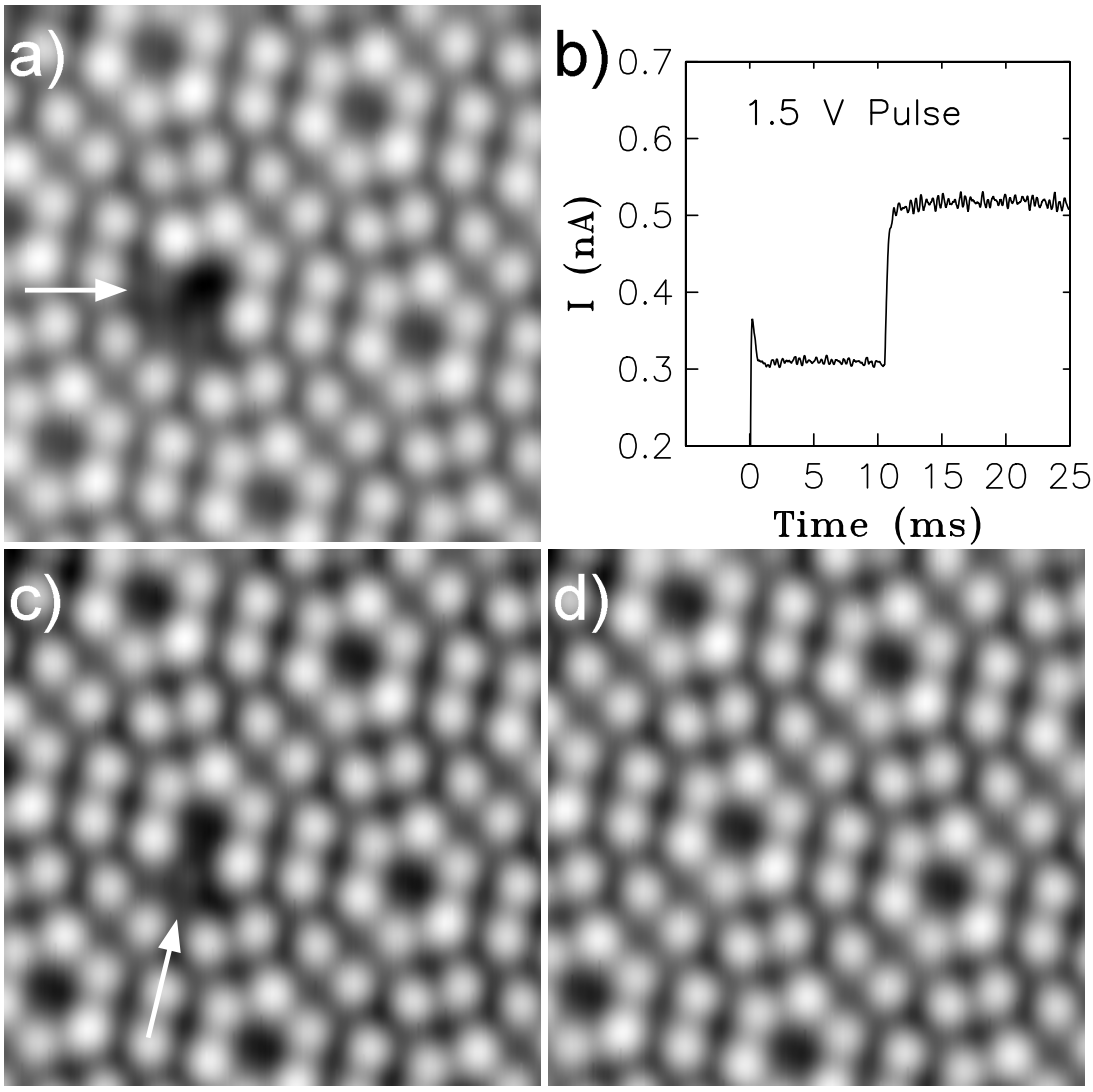

Figure 5.3: a) Two NO adsorbates at 50 K. The tip is positioned on the marked molecule and a voltage pulse is applied with the feedback turned off (fixed tip-sample distance). b) During the voltage pulse of 1.5 V and 0.3 nA, the current suddenly jumps, indicating the moment of desorption. c) Only the targeted NO molecule is desorbed. The tip is positioned on the next molecule and a similar voltage pulse is applied. d) The NO molecule is desorbed. The STM images were scanned at 0.7 V sample bias and 0.1 nA tunneling current.

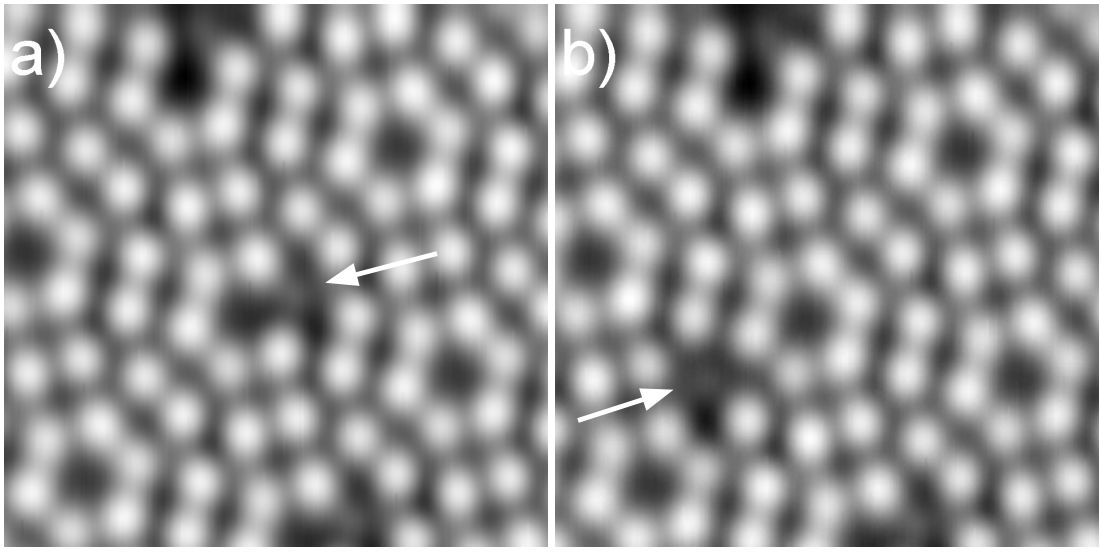

Figure 5.4: a) Clean Si(111) at 92 K. A phase boundary is visible in the lower left of the image. b) Same area as (a) after dosing with NO. c) After a 1.5 V and 1 nA scan, almost all the NO molecules have desorbed. The same location is marked in all three images. The images were scanned at 1 V sample bias and 1 nA tunneling current.

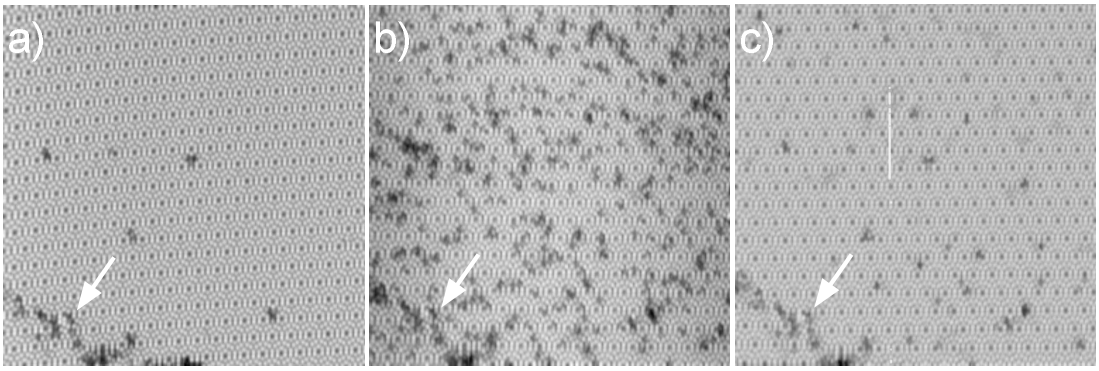

Figure 5.5: NO moving on Si(111) at 50 K. a) Before a 1.25 V and 2 nA voltage pulse. b) After the voltage pulse. NO has moved, and not desorbed. The images were scanned with 1 V sample bias and 0.05 nA tunneling current.

less than 1 pA in these experiments. Since we could no longer measure the current and therefore could not measure the desorption time, we looked for a threshold voltage at a given distance from the surface where the probability for desorption in one second for an adsorbate is 50%. The tip was was held directly over a single isolated NO molecule and the desorption probability of that molecule was noted by repeating the experiments several times. For each distance, the experiment was performed at least four times per voltage in 0.25 V steps. Because the height of the tunneling gap is not known and also depends slightly on the tip, we have to approximate the tip-surface distance. We can measure the height of the tunneling gap by bringing the tip closer to the surface at zero bias voltage until we see a perturbation in the surface under the tip. Figure 5.6a shows the threshold voltage as a function of distance to the surface at various temperatures. The fitted line has a slope of 0.144 ± 0.009 V/Å. We expect the y-intercept to be zero, but we could not determine it accurately from our data. The calculated least squares intercept is 0.5 ± 0.5 V. Even though the N-O bond is weakened by the electric field, we have not been able to dissociate NO with the STM [7]. The electronegativity of adsorbed NO causes a charge rearrangement, leading to $Si^{+\alpha}$:$N^{-\beta}O^{-\gamma}$ so that both N and O have a slightly negative charge [7], thus the N-O bond is not as strongly influenced by the electric field as the NO-Si bond. It is therefore consistent with our observation that NO desorbs rather than dissociates as the result of the applied electric field.

The electric field under the STM tip depends on the shape of the tip [27, 28]. This may explain the inconsistency in our low voltage results, wherein the desorption rate varied by more than an order of magnitude. For our high voltage, low current experiments, we can approximate the electric field by V/d, where V is the

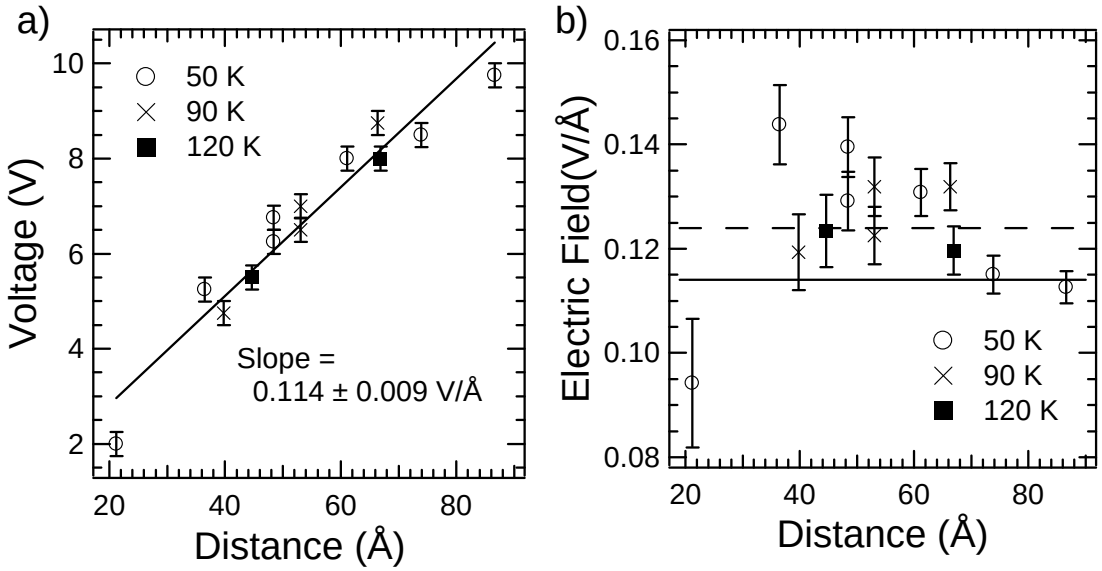

Figure 5.6: a) Threshold voltage for desorption plotted versus tip-surface distance at various temperatures. The error in distance (not shown) is 0.85 Å, 1.21 Å, and 1.49 Å for 50 K, 90 K, and 120 K, respectively. b) Same data as (a) displayed as approximate electric field (voltage/distance) versus distance. The dashed horizontal lines is the average field (0.12 ± 0.02 V/Å) and the solid line is the slope of the least squares fit from (a), 0.144 ± 0.009 V/Å.

bias voltage and d is the tip-surface distance. This approximation is valid directly under the tip in the limit that the tip radius is much larger than the tip-surface separation. We estimate our tip radius to be 25 to 50 nm. Because of the asperity at the end of the tip, the field is more perturbed from the V/d approximation if the STM tip is closer to the surface. A positive electric field is defined by a positive bias on the sample. Figure 5.6b shows the approximate threshold electric field for desorption as a function of distance at various temperatures. The average field is calculated to be 0.12 ± 0.02 V/Å, which is in good agreement with the slope of the least squares fit of 0.114 ± 0.009 V/Å [Fig. 5.6a]. We should note that when the tip is far away from the surface, the electric field is more uniform over a large area, and therefore the probability of nonlocal desorption of NO is higher.

For sufficiently high fields (1 V/Å or higher), NO can be desorbed by field evaporation, which is insensitive to temperature [29]. The electric fields in our experiments, however, are not large enough to justify this mechanism. The effect of the electric field on the adsorbate-surface bond has been treated theoretically [7]. As mentioned earlier, the electronegativity of NO causes a charge rearrangement, leading to $Si^{+\alpha}$:$N^{-\beta}O^{-\gamma}$. The electric field affects the charge distribution, which can weaken or strengthen the NO-Si bond. According to calculation of the vibrational energy of the adsorbate-surface system, positive electric fields decrease the energy, that is, weaken the adsorbate-surface bond. NO desorbs thermally at about 150 K. The electric field weakens the NO-Si bond and the desorption occurs at a lower temperature. Ideally, one should be able to measure the threshold electric field as a function of the temperature. As can be seen from the data in Fig. 5.6, the results are insensitive to temperature to within our error values. To understand this result, we have to explore the relationship between the electric field and the bond energy.

The effect of a positive electric field (defined for a positive sample bias) is to weaken the NO-Si bond. The higher the electric field, the weaker the bond becomes. Negative electric fields, however, do not affect the NO-Si bond monotonically. For electric fields between -0.5 and 0 V/Å, the bond is strengthened. Below -0.5 V/Å, the bonds is weakened again. The adsorbate-surface vibrational frequency has a quadratic dependence on the electric field [7] and can be expressed as:

$$\nu = \nu_0 - c(E - E_0)^2, \tag{5.1}$$

where ν is the vibrational frequency, E is the magnitude of the electric field with the appropriate sign, and ν_0, E_0 and c are constants. The vibrational frequency can be empirically related to the desorption barrier (that is, the NO-Si bond energy):

$$\epsilon \propto \nu^2, \tag{5.2}$$

where ϵ is the barrier to desorption [30]. The rate of desorption depends on the desorption barrier by the Arrhenius law:

$$R \propto e^{-\alpha},\ \alpha = \epsilon/kT, \tag{5.3}$$

where R is the desorption rate. Combining Eqs. 5.1, 5.2, 5.3, we obtain:

$$\alpha \propto (\nu_0 - c(E - E_0)^2)^2/kT, \tag{5.4}$$

that is, α has a quartic dependence on E. This sharp dependence on the electric field can be described as a threshold behavior that is insensitive to temperature for our temperature range.

According to the theoretical calculations [7], the maximum vibrational energy occurs for a negative electric field at -0.5 V/Å. To verify this effect, we investigated the desorption of NO with negative electric fields. We are able to desorb NO with

an electric field of -0.2 to -0.25 V/Å, which is about twice the magnitude required for positive field desorption. However, we measured current (0.01 to 0.1 nA at -6 to -10 V) during these experiments because of the smaller tip-surface separation. According to the calculation results, for electric fields between 0 V/Å and -0.5 V/Å, the NO-Si bond is strengthened, which does not agree with our results. The calculations, however, are based on the unreconstructed surface and therefore may not be quantitatively correct. It is also possible that the desorption is caused by another mechanism, such as electron-hole pair excitations that are involved in photon induced desorption of NO.

The Fermi levels of both the surface and NO have been shifted with respect to the tip Fermi level because of the potential difference. With a negative sample bias, electrons flow from the sample to the tip, leaving holes in the substrate that may annihilate by interacting with a NO filled state, leading to desorption. Photon induced NO desorption from Si(111) has been the subject of several studies [8, 12, 13]. It has been proposed that the desorption of NO is caused by carrier excitations across the band gap [8] or involving surface states [12] in silicon. Although this mechanism is unlikely to be involved in the STM induced desorption with a positive sample bias, it may be responsible for the desorption with negative bias due to the measurable current from the sample to the tip.

5.5 Conclusion

The adsorption of NO on Si(111) illustrates the effect of local atomic and electronic structures on chemical bonds. The (7×7) reconstructed silicon surface provides four different adsorption sites for NO at low coverage. Faulted corner adatoms are

the most favorable adsorption sites, followed by faulted center adatoms, unfaulted corner adatoms and unfaulted center adatoms. The adsorption characteristics are independent of temperature, and are due to variations in the local electron density on the surface. By varying the temperature, we can probe different aspects of the adsorption behavior and differentiate thermal vs nonthermal processes.

The STM induced desorption of NO at positive sample bias can be attributed to the electric field under the STM tip. This mechanism is quite different from the photogenerated hole process that is responsible for the photon induced desorption of NO from Si(111). We can desorb NO locally or over large areas with the STM. A single chemical bond can be affected without disturbing neighboring bonds and we can make quantitative measurements that may further our theoretical understanding of adsorbate-surface systems.

5.6 Acknowledgement

Support for this research by the Division of Chemical Sciences, Office of Basic Energy Sciences, Office of Energy Research, U.S. Department of Energy under Grant No. DE-FG02-91ER14025 is gratefully acknowledged.

Bibliography

[1] V. R. Kotler, Thermal Engineering **45**, 253 (1998).

[2] F. J. Marx and U. Johanntgen, VBG Kraftwekstechnik **78**, 127 (1998).

[3] P. K. Swaminathan, D. F. Strobel, D. G. Kupperman, C. Krishna Kumar, L. Acton, R. DeMajistre, J.-H. Yee, L. Paxton, D. E. Anderson, D. J. Strickland, and J. W. Duff, J. Geophys. Res. **103**, 11579 (1998)

[4] F. Coppens, R. Berton, A. Bondiou-Clergerie, and I. Gallimberti, J. Geophys. Res. **103**, 10769 (1998).

[5] M. B. A. Fontes, J. Santiago-Aviles, and R. Furlan, Proc. SPIE - Int. Soc. Opt. Eng. (USA) **3223**, 64 (1997).

[6] J. Kuehne, S. Hattangady, J. Piccirillo, G. C. Xing, G. E. Miner, and D. Lopes, Rapid Thermal Integrated Processing VI, 381 (1997).

[7] H. C. Akpati, P. Norlander, L. Lou, and Ph. Avouris, Surf. Sci. **401**, 47 (1998).

[8] Z. C. Ying and W. Ho, Phys. Rev. Lett. **60**, 57 (1988).

[9] L. J. Richter, S. A. Buntin, D. S. King, and R. R. Cavanagh, Phys. Rev. Lett. **65**, 1957 (1990).

[10] B. C. Stipe, M. A. Rezaei, and W. Ho, Rev. Sci. Instrum., (to be published).

[11] Z. Ying and W. Ho, J. Chem. Phys., **91**, 2689 (1989).

[12] L. J. Richter, S. A. Buntin, D. S. King, and R. R. Cavanagh, Phys. Rev. Lett. **96**, 2324 (1992).

[13] K. Sakamoto, K. Nakatsuji, H. Daimon, T. Yonezawa, S. Suga, H. Namba and T. Ohta, J. Electron Spectrosc. Rel. Phenom. **80**, 125 (1996).

[14] K. Takayanagi, Y. Tanishiro, M. Takahashi, and S. Takahashi, J. Vac. Sci. Tech. A **3**, 1502 (1985).

[15] G. Binnig, H. Rohrer, Ch. Gerber, and E. Weibel, Phys. Rev. Lett. **50**, 120 (1983).

[16] R. M. Tromp, R. J. Hamers, and J. E. Demuth, Phys. Rev. B **34**, 1388 (1986).

[17] Ph. Avouris, I.-W. Lyo, and F. Bozso, J. Vac. Sci. Technol. B. **9**, 424 (1991).

[18] M. A. Rezaei, B. C. Stipe, and W. Ho, (to be published).

[19] J. A. Stroscio and D. M. Eigler, Science **254**, 1319 (1991).

[20] Ph. Avouris, Acc. Chem. Res. **28**, 95 (1995).

[21] D. M. Eigler and E. Schweizer, Nature **344**, 524 (1990).

[22] T.-C. Shen, C. Wang, G. C. Abeln, J. R. Tucker, J. W. Lyding, Ph. Avouris, and R. E. Walkup, Science **268**, 1590 (1995).

[23] B. C. Stipe, M. A. Rezaei, W. Ho, S. Gao, M. Persson, and B. I. Lundqvist, Phys. Rev. Lett. **78**, 4410 (1997).

[24] B. C. Stipe, M. A. Rezaei, and W. Ho, Science **279**, 1907 (1998).

[25] L. J. Whitman, J. A. Stroscio, R. A. Dragoset, and R. J. Cellota, Science **251**, 1206 (1991).

[26] G. A. Reider, U. Höfer, and T. F. Heinz, Phys. Rev. Lett. **66**, 1994 (1991).

[27] C. Girard, C. Joachim, C. Chavy, and P. Sautet, Surf. Sci. **282**, 400 (1993).

[28] T. M. Mayer, D. P. Adams, and B. M. Marder, J. Vac. Sci. Technol. B **14**, 2438 (1996).

[29] T. T. Tsong, *Atom-Probe Field Ion Microscopy* (Cambridge University Press, Cambridge, 1990).

[30] D. C. Harris and M. D. Bertolucci, *Symmetry and Spectroscopy* (Dover, New York, 1989), p. 108.

Chapter 6

Conclusion and Future Prospects

6.1 Concluding Remarks

As stated in the introduction, the major thrust of this work has been to understand the atomic scale chemical behavior of a few selected adsorbates on silicon surfaces. To that end we have studied the adsorption of H_2S, D_2S, and NO on Si(111)-(7×7) and the adsorption of D_2S on Si(100).

We can begin to understand the chemical behavior of adsorbates on silicon by determining the reaction site and adsorption geometry. By analyzing our STM images, probing the adsorbates by STM induced chemical changes and comparing our results to previous work, we have determined the reaction sites and adsorption geometries of H_2S, D_2S, and NO on Si(111)-(7×7) and D_2S on Si(100). The most complicated system studied here is H_2S on Si(111)-(7×7), where the adsorption requires the participation of two surface dangling bonds, one of which is not visible in STM images.

The interaction of the gas molecule with the surface prior to chemisorption is critical in determining the adsorption characteristics. Although we cannot directly

observe this interaction with the STM, we can infer several aspects of the interaction based on the adsorption pattern. For H_2S and D_2S on Si(111)-(7×7), the temperature dependence of the adsorption site populations points to a mobile precursor state, which is in thermal equilibrium with the surface. For NO on Si(111)-(7×7), however, we observe no temperature dependence in the adsorption site populations. NO adsorption is dictated by the local density of states at the particular Si sites. We have also established that nearest neighbor effects can be very important in some systems, such as H_2S on Si(111), but are not very critical in other systems, such as D_2S on Si(100) and NO on Si(111).

Silicon surfaces are highly reactive and can easily make the barrier to dissociation thermally accessible. For example, 4 eV of energy is required to break one of the hydrogen-sulfur bonds in H_2S in the gas phase, but this dissociation occurs on Si(111) and Si(100) even at 50 K. The dangling bonds on Si(111) play an important role in the adsorption of H_2S, D_2S, and NO. H_2S and D_2S adsorb dissociatively on Si(111). Two surface dangling bonds are involved in the adsorption and dissociation process, one in the adatom layer and the second in the rest atom layer. HS (DS) is bonded to an adatom and H (D) is bonded to a rest atom. This adsorption geometry is dictated by the location of the dangling bonds as well as the charge distribution on the surface. All the adsorbates that we have studied show a preference for the faulted half of the unit cell. By varying the temperature, we can probe different aspects of the adsorption behavior. The site selectivity is more evident at low temperatures. H_2S and D_2S prefer the center sites, especially at low temperatures.

The reconstruction of the Si(100) surface also affects the adsorption behavior of various substances. DS and D bond to the dangling bonds and not the dimer bond. The surface reconstruction can also be affected by the adsorbates: regions

of symmetric dimers can become asymmetric as a result of DS adsorption. The Si(100) reconstruction, however, is not nearly as complex as the Si(111)-(7×7) reconstruction and does not lead to the same rich chemical behavior we have seen on Si(111).

The ability of the STM to cause chemical changes in the adsorbate-surface system has been used throughout this work. On Si(100), DS can be dissociated or moved into the dimer bond which is not thermally accessible. On Si(111), DS can also be dissociated. We have also verified that the desorption characteristics of the deuterium atoms are consistent with previous experiments and have thereby differentiated D from S. We have verified that NO dissociates above 150 K by trying to desorb the adsorbates without success; both N and O are more strongly bonded to Si than NO is, and do not desorb as easily.

To understand the physics that underlies the chemical behavior of adsorbates, quantitative measurements have to be made. STM images do not directly measure simple properties of a system, such as vibrational energies. Nevertheless, we have been able to extract quantitative data from STM images. The activation barrier to the thermal dissociation of DS on Si(111) was determined to be 0.73 ± 0.15 eV. The mechanism for NO desorption is attributed to the electric field under the STM tip. The threshold electric field for the desorption of NO was measured to be 0.114 ± 0.009 V/Å from 50 to 120 K. By varying the temperature, we have also been able to estimate the difference in the energy barrier to adsorption at different sites on Si(111) for D_2S. The effect of adsorbate-adsorbate interaction was also explored quantitatively for D_2S on Si(111) where nearest neighbor interactions lead to non-Langmuir kinetics.

6.2 Future Prospects

The STM is a rather versatile instrument and can be used in many different settings; we will not attempt to cover all possible experiments that can be performed with our instrument. There are two groups of future experiments that can be related to the work presented here: specific experiments that provide additional information on the systems studied here and more general prospects that go beyond the topics covered but can be related to study of chemistry on silicon surfaces.

6.2.1 H_2S and D_2S on Si(111)-(7×7)

There are several interesting effects that were not investigated but merit further work:

- The distance that deuterium atoms move after thermal dissociation was measured to be roughly 50 to 100 Å (Ch. 3). To study the isotope effect, this value should be measured more accurately and then compared to the same value for hydrogen, which should be measured as well.

- The distance that deuterium and hydrogen atoms move after STM induced dissociation was measured at 50 K (Ch. 3). The temperature dependence of the distance traveled was not investigated. Since the thermal deuterium atoms move 5 to 10 times more at 300 K, it would be interesting to know whether deuterium and hydrogen atoms move longer distance at temperatures higher than 50 K after STM induced dissociation.

- The energy barrier to dissociation for DS was measured to be 0.73 ± 0.15 eV. As stated in Ch. 3, an isotope effect is expected to be measurable and should be investigated.

6.2.2 NO on Si(111)-(7×7)

There are three aspects of our NO experiments (Ch. 5) that can be further studied:

- The substrate-temperature independence of the NO adsorption probability on different sites may be because NO does not reach thermal equilibrium with the surface prior to chemisorption. To verify this conjecture, molecular beams of NO with varying energies can be made to adsorb on silicon and the resulting populations on the various sites studied.

- The electric field desorption of NO is critically dependent on the negative charge that a chemisorbed NO acquires. Other diatomic molecules have a different charge configuration on the surface: Si^{+e}:$O^{-f}H^{+g}$ and Si^{-h}:$Be^{+i}H^{-j}$ [1]. These molecules behave differently as a function of the polarity and magnitude of the electric field and have not been studied experimentally to date.

- Our experimental results for electric field induced NO desorption do match the theoretical results quantitatively [1]. We attribute this to the unreconstructed surface that was used in the theoretical calculations. The reconstructed surface has very different properties and it would be instructive to perform the same calculations for a reconstructed surface.

6.2.3 Future Directions

We have successfully performed tunneling spectroscopy on a single molecule on metal surfaces with our instrument [2]. One of the biggest problems in performing spectroscopy on metal surfaces is the weak bond between adsorbates and the surface: the adsorbates are often mobile or move because of interactions with the STM. Silicon surfaces, on the other hand, form strong bonds with many adsorbates but

present many difficulties that must be overcome in order for spectroscopy to be possible. Some of these problems are:

- Spectroscopy is best performed below 15 K because the width of the spectroscopic peak becomes too broad above 15 K. It is possible to tunnel on highly doped silicon at very low temperatures, even at 6 K [3]. However, we have been unable to clean highly doped silicon in our UHV chamber (App. C).

- It is not clear whether tunneling current can flow for low voltages (below 0.7 V) where we've traditionally performed spectroscopy because of the silicon band gap. There are other vibrational peaks at higher energies, but the signal to noise ratio is also lower at higher energies.

- Metal surfaces have a close to linear I-V curve which results in almost zero d^2I/dV^2. Silicon surfaces have a nearly exponential I-V curve which can make the adsorbate signal to background ratio even lower.

Overcoming these problems is a difficult task, but can be very rewarding.

Bibliography

[1] H. C. Akpati, P. Norlander, L. Lou, and Ph. Avouris, Surf. Sci. **401**, 47 (1998).

[2] B. C. Stipe, M. A. Rezaei, and W. Ho, Science **280**, 1732 (1998).

[3] H. Shigekawa, K. Miyake, M. Ishida, S. Ozawa, and K. Hata, Sci. Rep. Res. Inst. Tokohu Univ. A **44**, 67 (1997).

Appendix A

STM Software Design

This section is not intended to be a software manual. The purpose of this section is to explain the software design philosophy, provide some examples of how the philosophy was actually applied and highlight the novel approaches taken to solve physics problems. Emphasis is put on problems and solutions that are specific to data acquisition software and will not arise for other programs, such as word processors.

The software is written entirely in C. It is over 30,000 lines of code. From a programming perspective, the software is composed of three major sections: low level digital I/O, data acquisition and data analysis. The graphical user interface (GUI) is the glue that holds the various parts together. The software was designed to maximize user friendliness without compromising the access to the available instrument functions. Although the STM hardware has not changed significantly since it was first designed, the software has evolved constantly, allowing us to perform novel experiments and extending the capabilities of the instrument.

A.1 Low Level I/O

For the purposes of this discussion, the term "hardware" is used for the digital I/O board (AT-DIO-32F) inside the computer. The low level I/O routines are separated into a single file for modularization purposes. Unlike most data acquisition software, the I/O routines do not use any drivers; the routines interact directly with the hardware. There are advantages and disadvantages to this approach. The advantages are:

- Without any driver calls, the I/O routines are faster. An I/O instruction is a single instruction, whereas calls to drivers functions requires stack manipulation and function call overhead. Additionally, many drivers tend to perform extra, and often unnecessary tasks (such as range checking and hardware queries) that slow down the I/O even further.

- Drivers are operating system dependent. It is not always the case that drivers for older hardware exist for newer operating systems. Furthermore, it may take a while before drivers are completed for newer operating systems, even for new hardware.

- Driver bugs can be hard to track down and fix. If a problem with a driver exists, fixing it requires cooperation of the driver authors, who may not always be forthcoming.

The disadvantages of this approach are also important to note:

- The software becomes hardware dependent. Since newer hardware can radically change the underlying protocol, the software can be incompatible with the new hardware. Since the start of this project, National Instruments has

introduced two new models of the I/O board that are incompatible with our software.

- Under protected operating systems (such as Windows NT and Unix), user level programs are forbidden from interacting with the hardware directly. Therefore, our software will not work under these operating systems. Hardware manufacturers usually provide drivers for many operating systems.

The modularization of the I/O routines can alleviate problems associated with the above disadvantages. For the software to work with a new board, just a few routines have to be modified. The software modification is simple, but learning the new hardware protocols and testing the new software is time consuming. For the software to work with protected operating systems, low level system drivers have to be written.

A.2 Accurate Timing

The STM electronics have very strict timing requirements. Wherever possible, the timing is performed using the real time clock on board the digital I/O card. The clock has a 2 MHz frequency, and therefore a theoretical resolution of 0.5 μs. However, the reading and writing of the clock registers on the I/O board take longer than 0.5 μs. The initial clock start up takes about 8 μs. The checking of the clock takes 3 μs.

To test the repeatability of the timing routines and gain some insight into the timing variations, we performed a simple measurement, where data was taken as quickly as possible and the time was recorded for every data point. Figure A.1a shows the histogram of time intervals between data points when the computer

interrupts were not disabled. Notice the long tail that extends to 120 μs. When interrupts are disabled, the timing is much better and there is no tail, as seen in Fig. A.1b. The small variation (about 2 μs) is due to subtle timing of the ISA bus. The ISA bus runs on an 8 MHz clock, but there is also a latency that is more difficult to measure. It is unlikely that this variation is caused by the 333 MHz CPU, as the CPU timings involved are much faster.

Since there is only one real time clock on board the I/O card, it is sometimes necessary to use another delay mechanism. These delays are all generated by reading and writing null data to the I/O card. Since the delay associated with these instructions is due to the communication with the I/O card and because the I/O card is sitting on a fixed clock bus (the ISA bus), the delays are processor independent. This is quite important, because we have switched computers many times since the beginning of the project (from a 66 MHz 486 to a 333 MHz Pentium II), without having to change the delays significantly. It is always a good idea to test the timing when the computer is changed. There are also a few self timing routines that determine certain hardware delays automatically.

A.3 Choice of Operating System

When the project was started, we wanted the program to run under IBM OS/2. We could not, however, write directly to the hardware and after many failed attempts, we abandoned OS/2 for Microsoft Windows 3.1. Since OS/2 is a preemptively multi-tasked operating system, it can also interfere with precise timing. Under Windows 3.1, the program has complete control over the CPU, if need be. Interrupts can be disabled as well.

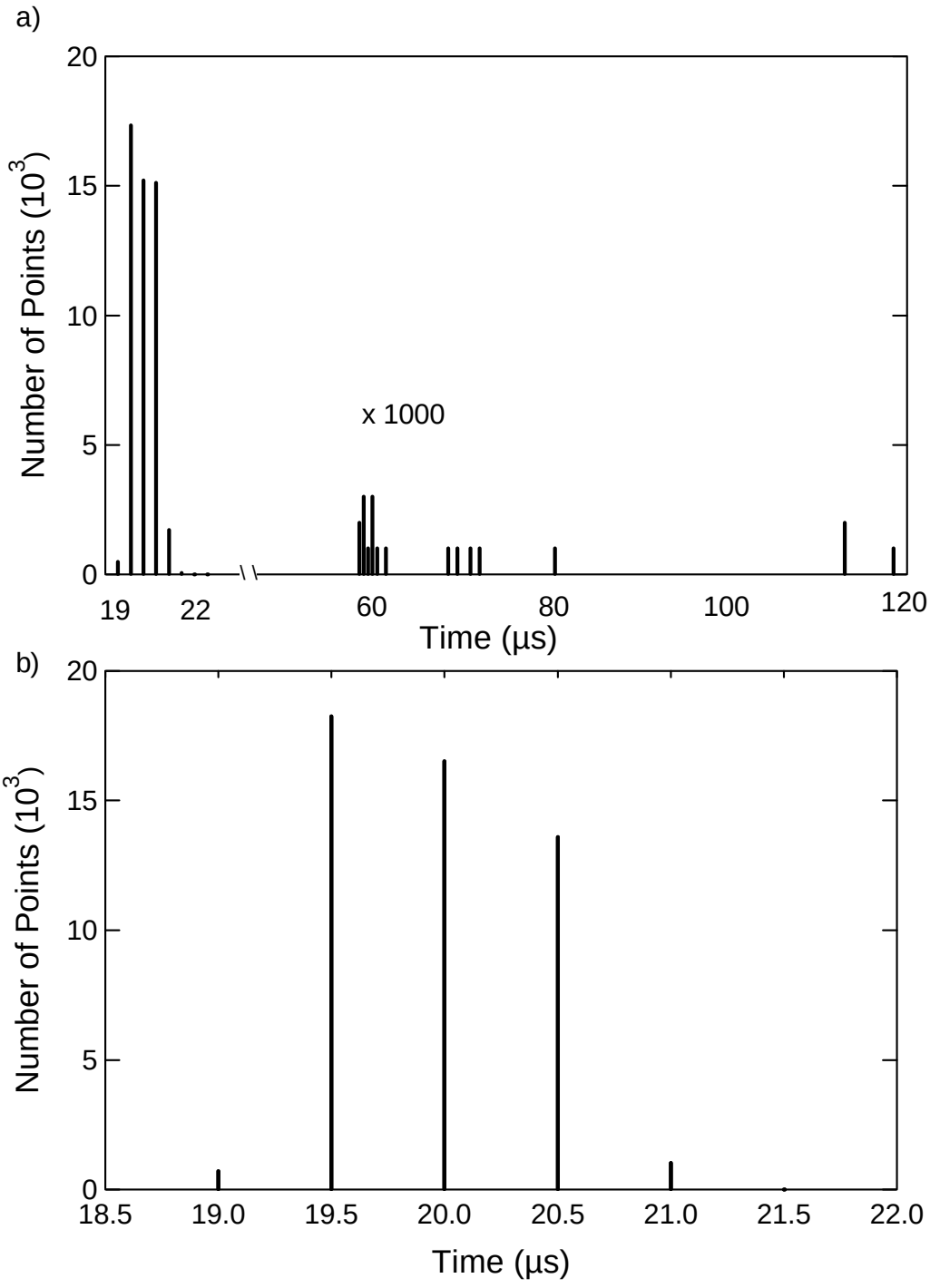

Figure A.1: a) Histogram of time intervals between successive data points under Windows 3.1. b) Histogram of time intervals between successive data points under Windows 3.1 with interrupts disabled.

Although the program is written as a Win32 application, and therefore can run natively under Windows 95, it should be run under Windows 3.1 for data acquisition purposes. Windows 95 can take over the CPU for milliseconds at a time [1], which is not acceptable for our purposes.

To demonstrate this problem, we used the program to take data as quickly as possible, and record the time at which each data point was taken. This was performed twice under Windows 95. The first time, no other programs were running. The histogram (Fig. A.2a) shows a longer tail compared to the Windows 3.1 results (Fig. A.1) with delays up to 180 μs. The test was performed a second time, while another computer was used to ping the data acquisition machine. A ping packet is a small network packet sent from one machine to another; the recipient machine sends an acknowledge packet back. Network responses of this sort are very simple and do not require many CPU cycles or I/O time. The results (Fig. A.2b) show a large peak at 60 to 70 μs, which is the result of the CPU responding to network requests. The tail of the histogram now extends to 230 μs. Simple operations, such as minimizing a window, can cause large real time delays which are not appropriate in a data acquisition setting. The delays are not necessarily created by the user. For example, Windows 95 periodically synchronizes the hard drives with its disk cache data. Such an event can take hundreds of milliseconds because of the slow hard drive response. There is no way to disable the multitasking capabilities of Windows 95 and therefore we use Windows 3.1 for our data acquisition.

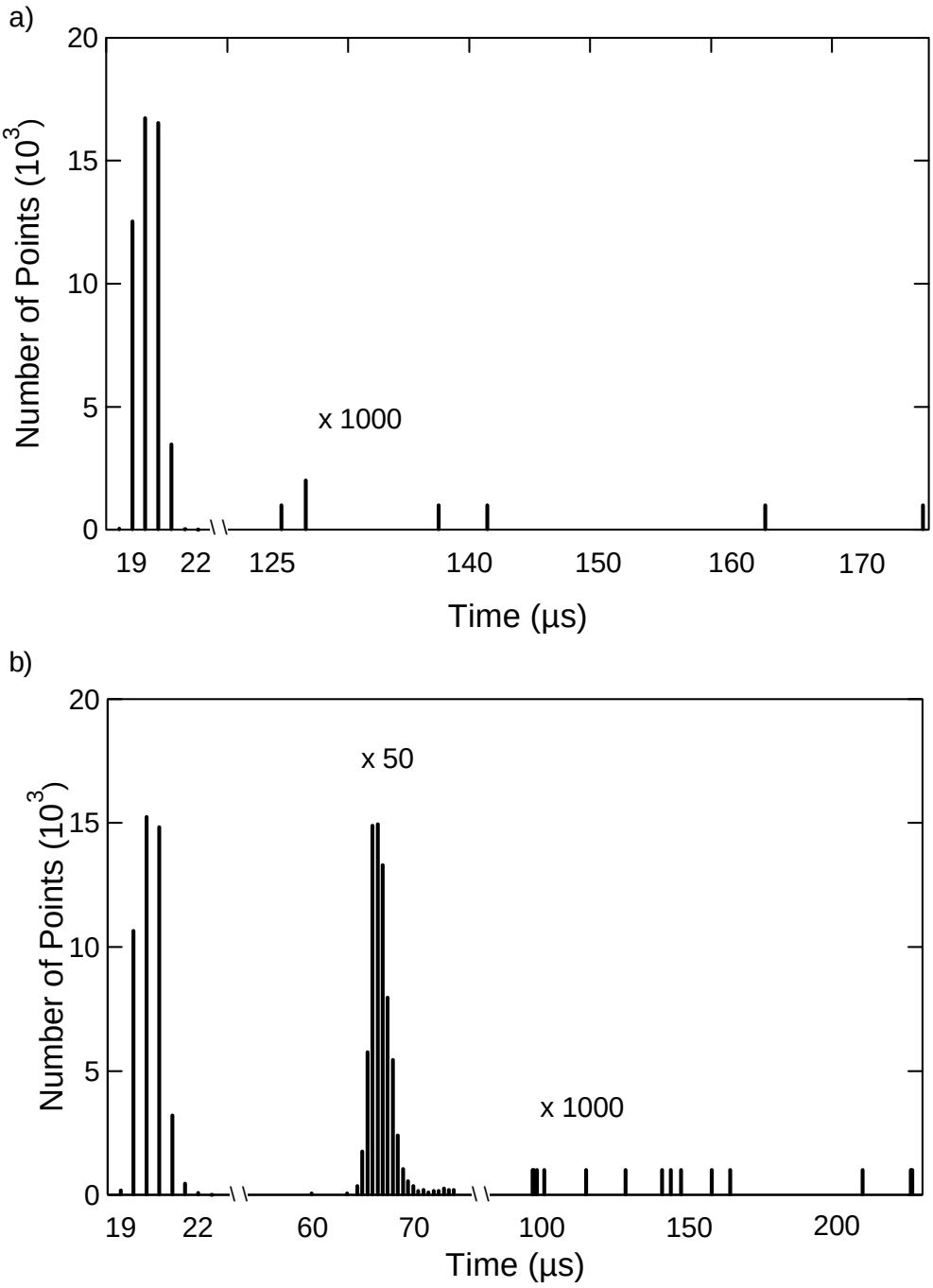

Figure A.2: a) Histogram of time intervals between successive data points under Windows 95. b) Histogram of time intervals between successive data points under Windows 95 with another computer pinging the data acquisition machine.

A.4 Safety Features

The middle piezo tube on the STM is responsible for keeping a fixed distance between the tip and the sample. This is accomplished by a feedback loop that controls the voltage on the piezo. The voltage on the z piezo is the sum of two signals: the z-offset channel and the feedback z channel. Changing the z-offset channel will change the total voltage on the piezo and the feedback loop will respond by changing the feedback z channel in the opposite direction. The z-offset channel always has a gain of ten, whereas the feedback z channel can be selected to have a gain of 0.1, 1 or 10. When the z-gain is changed, if the z-channel value is not close to zero, the actual voltage going out to the piezo can change by a factor of 10, which essentially jerks the z-piezo, and possibly crashes the tip.

During scanning various safety features are available to the operator. On rough or steep terrain, with a low z-gain, it is possible that the feedback loop will reach the limit of the z-voltage, and if left unchecked, the tip will crash into the surface. When the z-offset safety feature is enabled, the computer can perform one of several actions to ensure the tip does not crash. If the z-channel is within 5% of its limits, the computer can either

- Stop scanning.
- Change the z-offset so that the z-channel is no longer close to the limit by three times the settable limit, i.e. 15% if the limit is set to 5%.
- Use the range of z that has been measured so far and change z-offset such that the z-channel is exactly centered about zero.

The limit at which the crash protection will be activated defaults to 5%, but it can be changed by the operator.

Another safety feature that is available during scanning is the digital feedback in addition to the hardware (analog) feedback. The computer can monitor the current at each step and ensure that the analog feedback has had enough time to compensate for the movement. If the current is not within a prescribed range of the ideal (equilibrium) position, the computer will wait longer to allow the feedback loop time to adjust z.

A.5 Data Manipulation and Analysis

One of the most important aspects of the data manipulation routines is its close integration with the rest of the program. While acquiring data, an STM requires constant attention and decision making. These decisions may be based upon data that has just been taken. During the experiment, the operator has to resolve certain problems which include simple problems (such as "where is a large terrace to perform the experiment?") and more complex issues (such as "does the adsorbate have more than one adsorption site?"). Traditionally, data analysis is done after all the data are collected. The latter approach works well if the system is well understood, but is less flexible for unknown systems.

Figure A.3 shows four images that are produced from the same data; the system is Cu(100) dosed with pyridine (C_5H_5N) [2]. Figure A.3a is the raw data scaled linearly to the grey palette. The structure is very difficult to make out, as the pyridine molecules are rather tall compared to the rest of the features on the surface and the surface is sloped. Figure A.3b is the image after a plane has been fitted to the data. Usually, fitting a plane reveals most of the structure and therefore the STM program defaults to showing plane fitted data in the main scan view. The data

are always saved in raw form and the operator may turn off the plane fitting. Again, for this system, plane fitting is not enough to reveal all the features. Figure A.3c shows the data with an equalized palette. An equalized palette allocates the same number of pixels to each color and therefore has maximum contrast. Subtle feature are usually revealed when the palette is equalized. We have often used this feature to locate areas on surfaces such as copper that are free from defects, as these areas appear much brighter compared to the rest of the image. Figure A.3d shows the data as if it were illuminated. The surface defects and pyridine molecules are easy to see, but the effect of the extent of the defects in the LDOS that can be seen in Fig. A.3c is not visible. The operator can view up to four different representation of the data (not limited to the representations listed above) at once to better understand the experiment.

One other aspect of the data manipulation routines is the custom routines written to analyze specific experimental data. These routines are used just like any of the other tools available in the program. Three of these tools have been used extensively for the analysis of data. One of these analysis routines is the trace analysis feature. With this feature, current traces that have multiple, well defined levels with sudden shifts (telegraph noise) can be analyzed. The average time spent in a given state and the average current in that state are calculated.

The counting toolbox was written specifically to analyze thermal dissociation data, but has been used in many settings. The counting toolbox allows the user to place colored circles on an image. The STM data are not modified, as would be the case if circles were added in an image manipulation program. Up to four different colors are available. The circles can be erased or converted from one color to another. The number of circles of each color is summed and reported. The

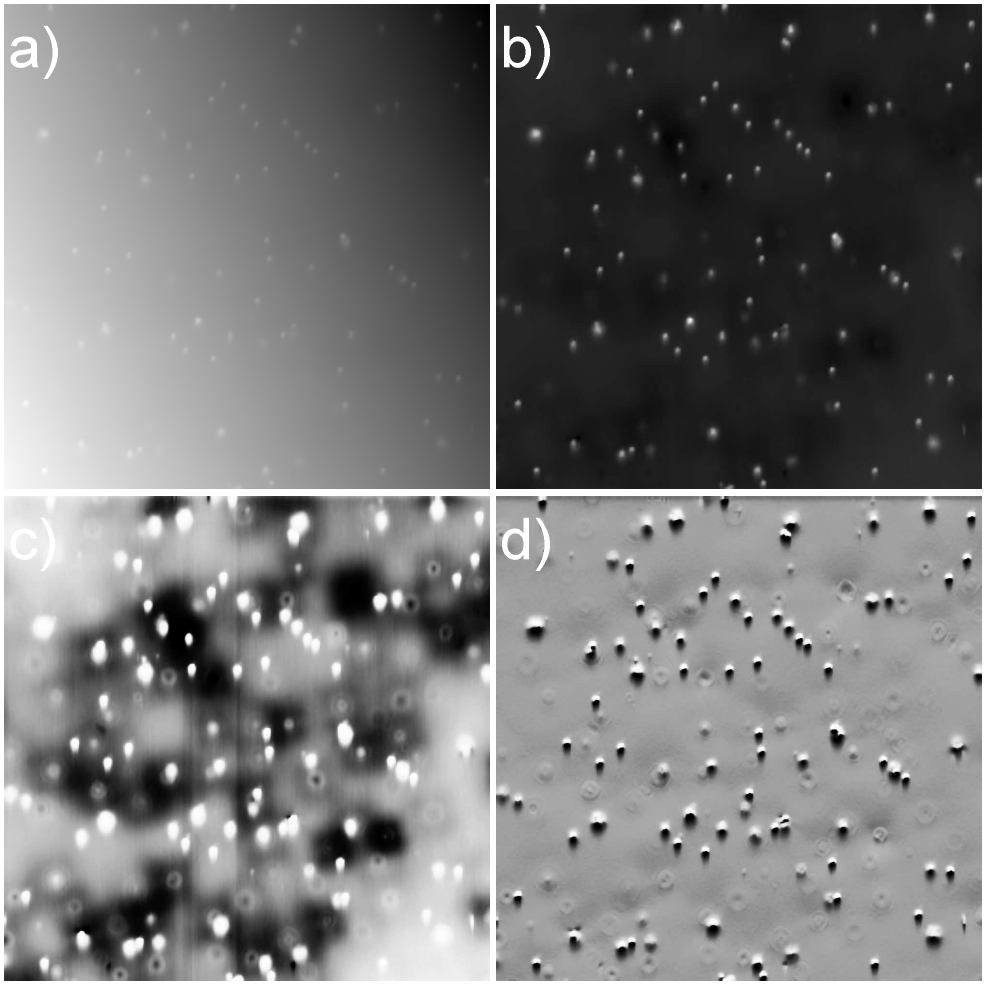

Figure A.3: All four images show the same data. The surface is Cu(100) and it is dosed with pyridine. a) Raw data. b) Plane fitted data. c) Equalized data. d) Illuminated data.

thermal dissociation of DS on Si(111) [Ch. 3] was studied by scanning the surface as quickly as possible and looking for changes from image to image. With over 400 DS molecules to track per image, it becomes difficult to count the events properly. Only 1 to 20 events occur from image to image. By keeping track of the events in each image using the counting feature, it is possible to double check the data and ensure no events were missed or double counted. The analysis of the results would have been significantly more difficult without the counting toolbox.

The counting toolbox has also been used to keep track of the different adsorption sites on Si(111) [Ch. 2]. Perhaps more importantly, it is used to quickly mark new features on the surface after dose while performing an experiment. It is often the case that two isotopes of the same chemical are used in the same experiment. By marking the different isotopes, one can quickly distinguish them, even though they appear identical in STM images.

Another analysis tool that is specific to this program is the grid fitting toolbox. Up to three sets of parallel lines can be displayed on top of the STM data at arbitrary angles and inter-line distances. This feature can readily be used to find adsorption sites and the surface orientation.

It should be noted that the STM program is a work in progress and the ability to add custom analysis routines that can used even while taking data is an important asset that should be taken advantage of.

A.6 Extending Instrument Capabilities

Computer control of the STM allows for a flexible framework that can be changed to suit the need of the instrument in general or a specific experiment. The safety

features discussed earlier (section A.4) is an example of making the instrument more reliable.

Two of the limitation of current STM piezo actuators are drift and creep. Drift is caused by thermal mismatch between the actuators and other parts of the instrument. The piezo response to a voltage change is not instantaneous. The response as a function of time has a slow component that causes STM images to appear warped because the piezos are not at their final equilibrium position. This effect is called creep. Without creep and drift, a wider range of experiments can be performed.

Creep is easily noticed moving long distances or scanning too fast. With a little patience creep can be avoided, but it is sometimes necessary to take data as quickly as possible. Creep is most noticeable in the fast scanning direction; the image becomes visibly warped. To minimize this problem, the tip is moved an extra distance before the beginning of the scan in the fast raster direction. Although the effect is not entirely eliminated, it is reduced. In commercial STM programs especially those written for metrology applications, creep is dealt with more rigorously. These programs keep track of the history of the piezo tube and by knowing the creep parameters change the actuation voltage to move the piezo to the proper location. We have not had the need to implement such a system, but doing so is not difficult. There are also hardware solutions that use a separate distance measuring device, such an interferometer, to locate the actual position of the piezo and change the voltage such that the the piezo is positioned properly. The correction to the actuation voltage is usually regulated by a feedback loop . It would be very difficult to modify our current STM to accommodate such a correction system.

Thermal drift changes the relative position of tip and surface. For experiments

that need a stationary tip, thermal drift can be a serious problem. One such experiment is spectroscopy [3]. We can measure the current, I, as a function of voltage, V and also the first two derivatives, dI/dV and d^2I/dV^2, by rastering the voltage in a specific range and recording the three signals. The derivatives are measured by a lock-in amplifier. It takes several minutes to measure the derivatives in a useful voltage range (0 to 0.5 V) because of the slow oscillation frequency (several hundred Hz). Many such spectra have to be averaged to get good signal to noise ratio. Thermal drift can make it impossible to take more than a few spectra over the same position. To solve this problem, the computer is instructed to search for a local minimum or maximum in the immediate vicinity of the tip position between spectra. By tracking a maximum or minimum, the relative position of the tip and surface can be kept fixed. We have taken spectra over the same molecule for 10 or more hours [3]. Thermal drift is no longer the limiting factor in these experiments.

Bibliography

[1] Microsoft online developer documentation,
http://www.microsoft.com/directx/pavilion/dsound/timerlatency.htm

[2] B. C. Stipe, M. A. Rezaei, and W. Ho, unpublished.

[3] B. C. Stipe, M. A. Rezaei, and W. Ho, Science **280**, 1732 (1998).

Appendix B

STM Construction

The STM head is made of many pieces that are glued together using UHV compatible epoxy. The materials used are listed in table B.1. The assembled head is schematically depicted in Fig. B.1. The metal parts are machined from Al (spring hooks), Mo (base plate) and OFHC copper (cross piece and magnet holders). The STM with springs and copper cross piece is schematically depicted in Fig. B.2. The materials were chosen for their high thermal conductivity at low temperatures. The base plate is the same material as the sample holder to minimize the thermal expansion mis-match. The springs provide vibrational isolation for the STM. The three magnets that are attached to the copper cross piece dampen any oscillations by creating eddy currents in the surrounding copper shield.

Since the STM will be used in UHV, care should be taken to clean all parts appropriately, which usually entails cleaning with acetone and isopropyl alcohol. Powder free gloves and a clean work environment are essential to keeping the parts clean.

Table B.1: STM parts.

Item	Description/ Part Number	Quantity	Vendor
Tungsten Balls	0.125" diameter, Grade 50, pure	3	Bal-Tech
Epoxy, conductive	H21D, 1 oz. eval. kit	1	Epo-tech
Epoxy, insulating	H74F, 3 oz. test kit	1	Epo-tech
Sapphire rings	R152.4 ring jewel, straight	9	Swiss Jewel Co.
Sapphire disks	W6.36 sapphire window	6	Swiss Jewel Co.
SmCo disk magnets	18DRE2008 0.3121" D 0.125" T	3	Magnet Sales & Manufacturing
Piezo Tubes	EBL2, radial polarization, 4 Au electrodes	3	Staveley Sensors, Inc.
Piezo Tube	EBL2, radial polarization, 1 Au electrode	1	Staveley Sensors, Inc.
Mo Rod	1.5" diameter ground rod (baseplate)	2	Schwartzkopf Tech Corp.

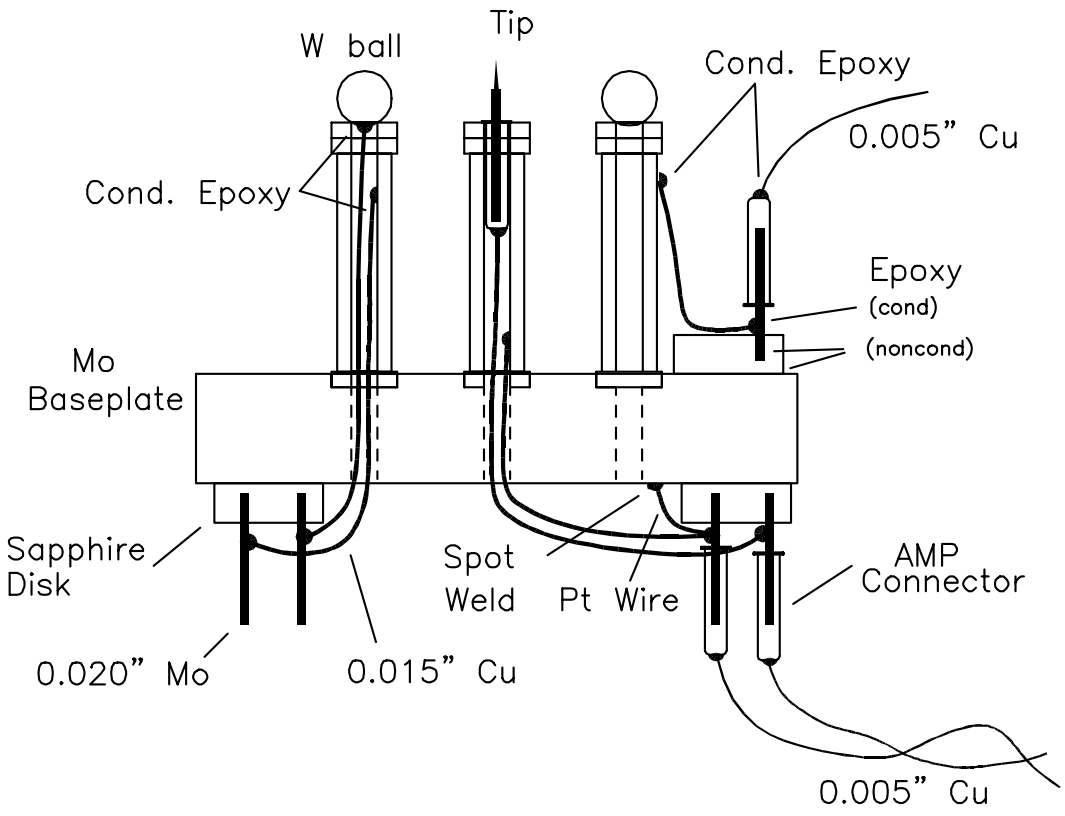

Figure B.1: STM head showing the piezo connections and glue joints.

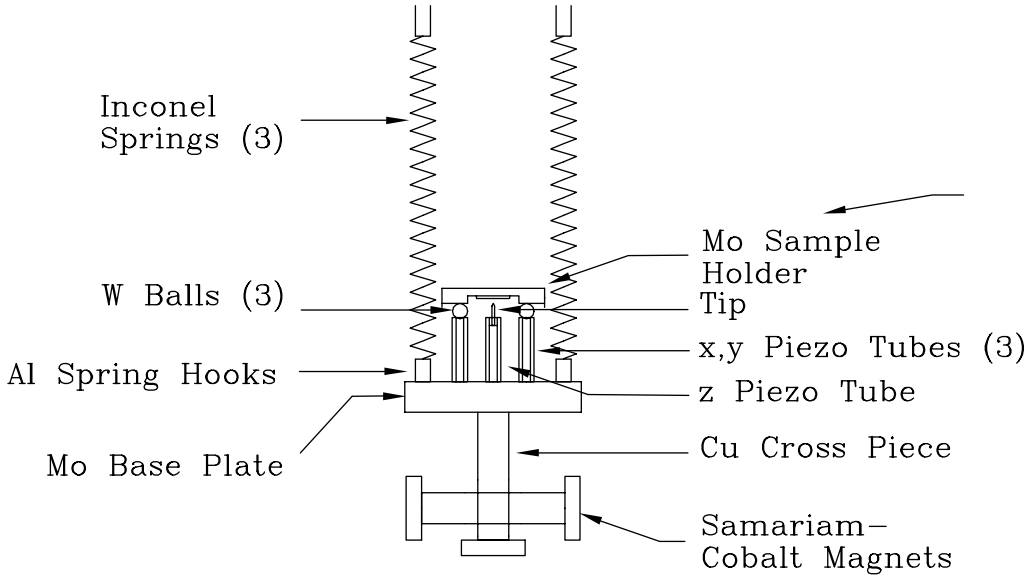

Figure B.2: Schematic diagram of STM with copper piece, magnets and springs.

B.1 Gluing the STM Head

The first three STM's were glued with conductive and nonconductive epoxy. We have since used Eutectic 157 UHV compatible solder in place of the conductive epoxy. The conductive epoxy can sometimes have large resistances and is prone to peeling off the piezo electrodes. For the details of using solder refer to L. Lauhon's Ph.D. thesis [1]. We will describe the gluing technique here.

The STM base plate (Fig. B.3) is machined from molybdenum. Four piezo tubes are glued onto the base plate. The piezo tube electrodes are connected to molybdenum posts that are insulated from the base plate by a sapphire disks. There are four posts per disk. The piezos are assembled first and then glued onto the base plate (Fig. B.4). The three outer piezos are used for lateral (x and y) motion and are identical. The inner piezo, which is used for z motion, has the tip socket mounted in the middle.

The epoxy has to be cured in an oven at 120° C for 30 minutes. Since the epoxy is not very strong before curing, it is cured at each step of the construction. To properly align the pieces and to avoid possible movement during the curing process, the pieces are held together in teflon jigs or by other means. The jigs have to be machined to closely match the different pieces. Machining teflon can be difficult because of the softness of the material. A sharp cutting tool (drill bit, lathe cutting tools, etc.) is necessary for proper machining of the jigs. The final jig has to be tested against the pieces to insure proper fit; merely measuring the jig while machining can be misleading because the dimensions can change under the pressure used to hold the piece. The jigs are shown in Fig. B.5.

The wires used on the STM head are 0.015" thick polyamide coated copper wires listed in table B.2. The wires are first cut to about 3" pieces and only in

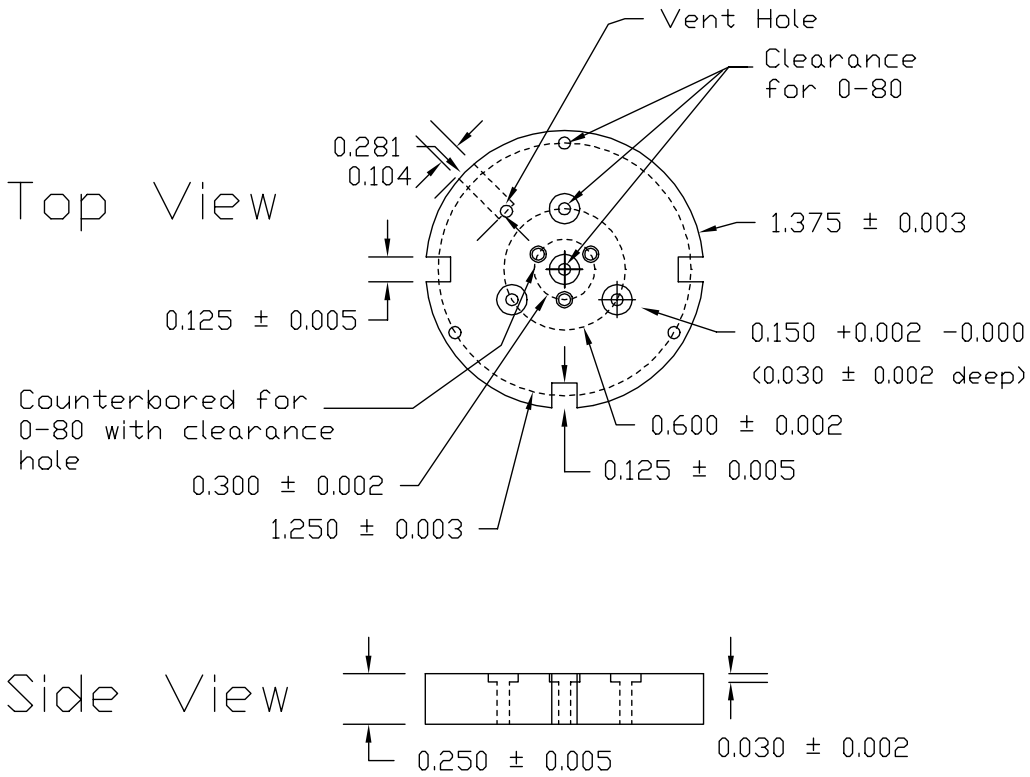

Figure B.3: STM molybdenum base plate. All dimensions are in inches.

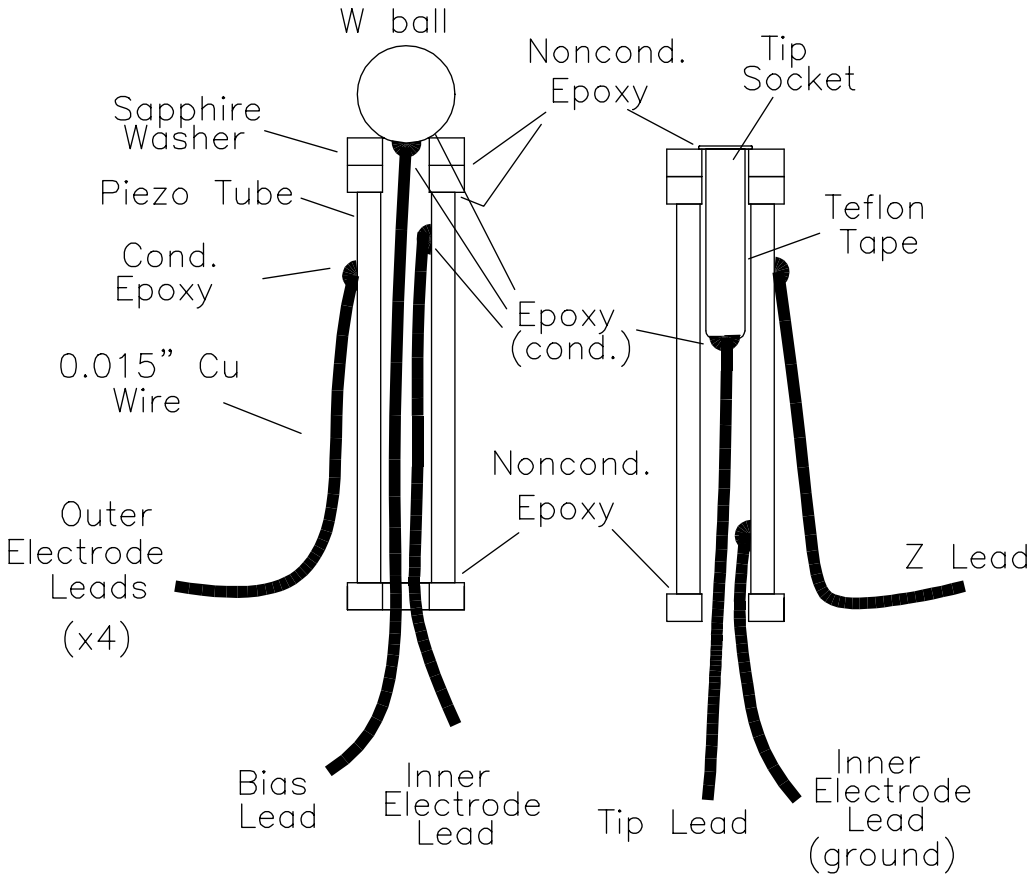

Figure B.4: STM piezo tubes. The tube shown on the left is used for the outer piezos. The other tube is the inner piezo tube.

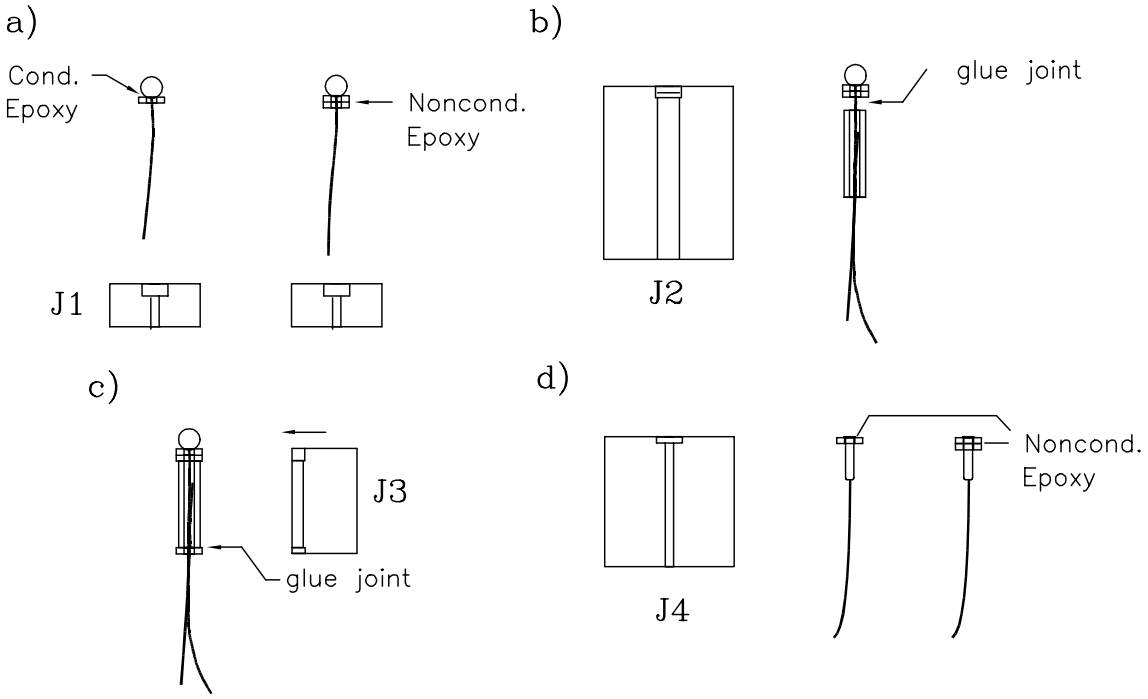

Figure B.5: Jigs used for gluing. a) J1 is used for gluing the wire to the ball and the second sapphire washer. b) J2 is used for gluing the ball assembly to the piezo tube. c) J3 is used for gluing the bottom sapphire washer to the piezos and also for centering the inner piezo on the base plate. d) J4 is used for gluing the tip socket to the sapphire washer.

Table B.2: Wires and connectors used in STM construction. All wires are polyamide coated and bought in 100 ft reels.

Item	Description/ Part Number	Quantity	Vendor
Connectors	AMP 50863	100	AMP
Cu wire	0.015”	1	California Fine Wire Co.
Cu wire	0.005”, 99.99% pure	1	California Fine Wire Co.
Stainless steel wire	0.010”	1	California Fine Wire Co.

the final stage are cut again to the proper length. Stripping the polyamide can be difficult. A sharp, small utility knife can be used to scrape the coating. We have had little success with chemical strippers.

B.1.1 Outer Piezo Tubes

The outer piezo tubes are glued from the top to bottom as follows:

- To glue the W ball to the sapphire washer , place some conductive epoxy on the ball and lay it on the washer.
- Using jig J1, glue the 0.015” Cu wire to the ball with conductive epoxy.
- Using jig J1, glue the next washer to the ball assembly with nonconductive epoxy.
- Glue the inner piezo wire to the piezo using conductive epoxy.
- Using jig J2, glue the ball assembly to the piezo tube with nonconductive epoxy.

- Using jig J3, glue the bottom sapphire washer to the piezo tube with nonconductive epoxy.

- Attach the four outer electrode wires with conductive epoxy. A small copper alligator clip can be used to hold the wire in place while the epoxy is being applied and later cured.

B.1.2 Inner Piezo Tube and Tip Socket

The tip socket is prepared first and then glued to the piezo tube as follows:

- Attach the tip wire to the AMP socket using conductive epoxy. Test the socket to insure glue did not destroy the spring mechanism inside.

- Glue teflon tape around the tip socket with nonconductive epoxy. Test the socket to make sure the outside wall of the socket is nonconductive.

- Using jig J4, glue the two sapphire washers to the tip socket with nonconductive epoxy, one at a time.

- Glue the inner piezo wire to the piezo using conductive epoxy.

- Using jig J2, glue the tip socket to the piezo tube with nonconductive epoxy.

- Using jig J3, glue the bottom sapphire washer to the piezo tube with nonconductive epoxy.

The outer electrode wire will be attached after the piezo is glued to the base plate.

B.1.3 Sapphire Discs with Posts

The sapphire discs have to prepared by drilling four non-through (blind) holes. Use the ultrasonic impact grinder for drilling the holes with 0.019" drill bits. The end of the drill bit has to be ground flat after each use. Grinding the long, thin drill bit can be difficult. Use two fingers to support the bit while grinding, leaving only a few millimeters between fingers and the grinding wheel. The holes are spaced on the washer using an aluminum mask. The sapphire is attached to a glass substrate using paraffin or xtal bond. After the holes have been ground, attach molybdenum posts onto the disk using nonconductive epoxy. To ensure the posts are straight, use two teflon discs with four holes with the same spacing as the disc holes at the two ends of the posts. After curing, scrape the extra nonconductive epoxy with a small utility knife to ensure good electrical conduction.

B.1.4 Preparing the Base Plate

Aluminum posts can be attached to the plate in place of the spring hooks to lift the base plate so that the wires running through the base plate won't have to be bent. All parts are glued to the base plate with nonconductive epoxy as follows:

- The inner piezo is glued first. Using jig J3, make sure the piezo is placed at the proper angle (90° to the base plate). After the curing, attach the outer electrode with conductive epoxy.

- Place the three outer piezo tubes on the base plate with a small amount of epoxy. Rotate the tubes until the small spaces between electrodes matches the scratch lines on the plate. Place a 0.25" thick glass plate on top of the piezos and realign the piezos if they shifted. With the glass on top of the

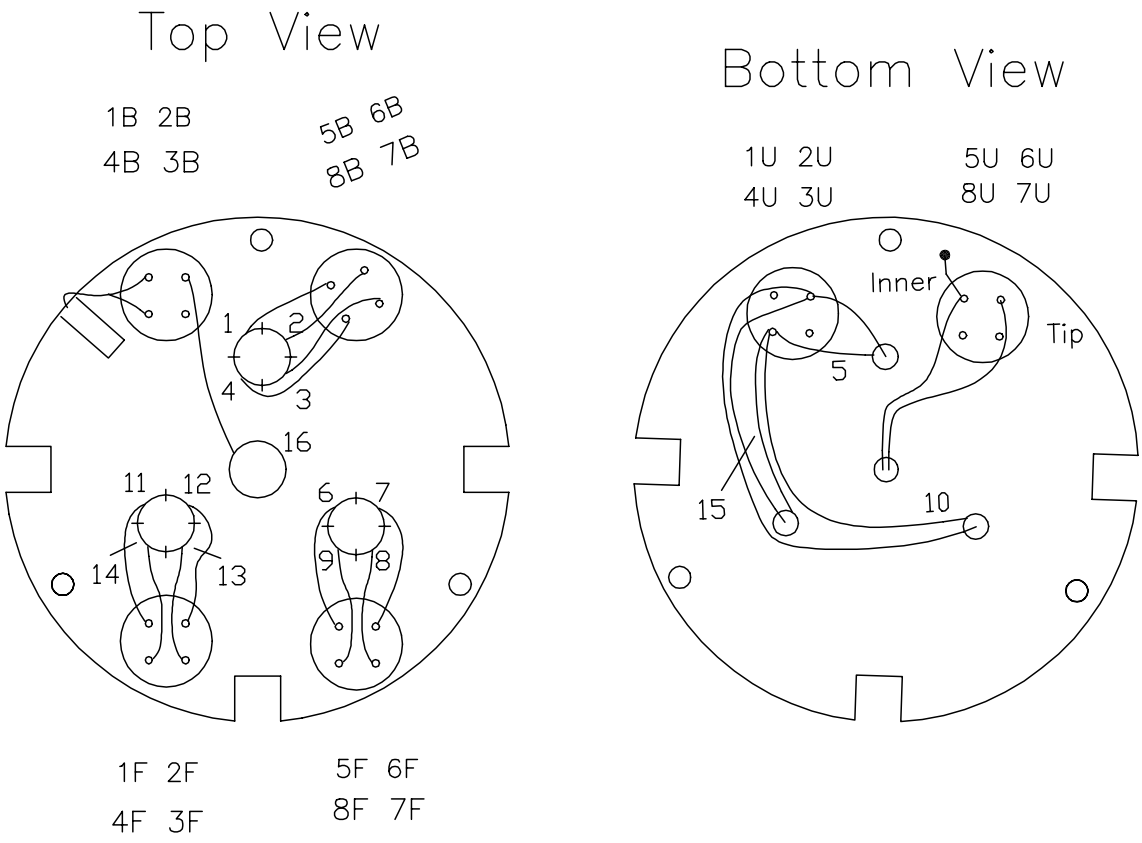

Figure B.6: Wiring labels and connections on the STM.

piezos, cure the entire assembly.

- Glue six sapphire disks to the base plate, 4 on top, 2 on the bottom as shown in Fig. B.6.

The electrical connections have to be glued next. Using the wiring diagram (Fig. B.6), carefully cut each wire to length, strip the end and attach it to the proper Mo post with conductive epoxy. Check the electrical connections from the post to the piezos, tip socket and W balls.

B.2 Wiring

The STM connections start from the components on the STM base. These components are connected by 0.015" Cu wire to Mo posts on the base. The posts are connected to a sapphire feedthrough on the inner shield with 0.005" Cu wires that have AMP connectors on both ends. The connectors are attached using conductive epoxy. The wires are cut to minimize slack before the connectors are attached. These thin wires were chosen to minimize the mechanical connection, but provide some thermal conduction. The sapphire feedthrough connections are then routed with 0.010" stainless steel wires to the vacuum feedthroughs. The stainless steel wire is a poor thermal conductor, which is ideal for our purposes, because the vacuum feedthrough is at room temperature, but the sapphire feedthrough is cold (8 K minimum temperature). The stainless steel wires are heat sunk to the outer shield, which is below room temperature, but warmer than the inner shield (100 K minimum temperature). The wiring is schematically represented in Fig. B.7, including the grounding configuration.

Since the tunneling current is typically 0.1 to 10 nA, the tip wire has to be treated with care. It is separated from the rest of the wires by ground shielding and distance as much as possible. It is connected to its own vacuum feedthrough. The connections from the STM to the electronics rack are listed in table B.3. The numbering scheme used in table B.3 is depicted in Fig. B.6 for the STM connections and Fig. B.8 for the sapphire and vacuum feedthroughs.

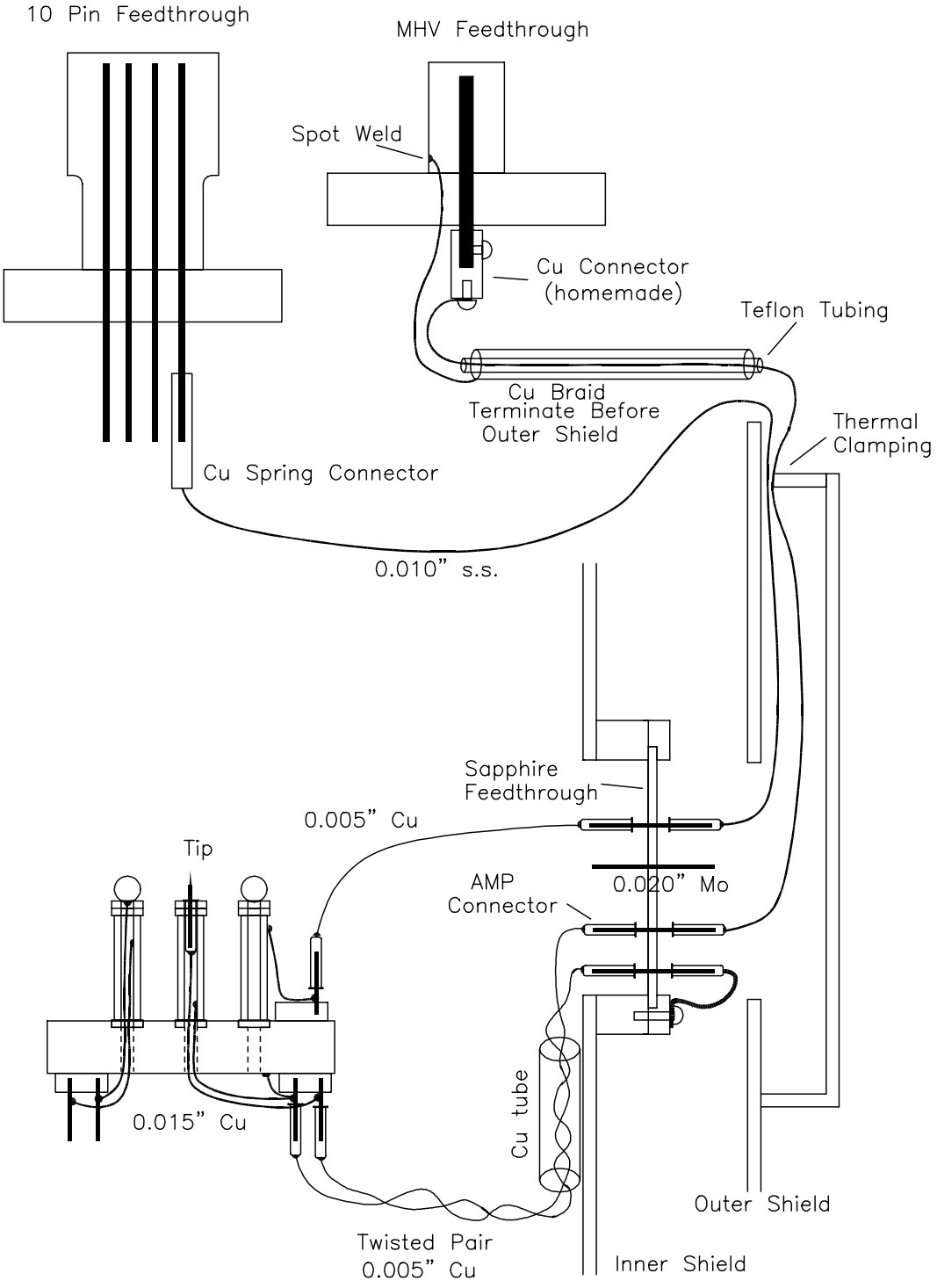

Figure B.7: Schematic wire connections from the STM to the vacuum feedthroughs, including the grounding scheme.

Table B.3: Electrical connections from the STM to the electronics rack.

STM	Sap. Feed.	Vac. Feed.	Electronics	Description
5F	18	1R	1	Piezo 1
6F	19	2R	2	Piezo 1
7F	14	3R	3	Piezo 1
8F	13	4R	4	Piezo 1
5B	9	5R	6	Piezo 2
6B	10	6R	7	Piezo 2
7B	5	7R	8	Piezo 2
8B	4	8R	9	Piezo 2
1B	6	3L	11	Piezo 3
2B	7	4L	12	Piezo 3
3B	2	5L	13	Piezo 3
4B	1	6L	14	Piezo 3
3U	24	7L	5,10,15	OPIE
5U	22	Shield		IPIE
6U	21	MHV		Tip
1U	25	2L	B	Balls
1F	17	10R	16 (Z)	IPOE
2F	20	10C		STM Diode Red
3F	15	9C		STM Diode Black

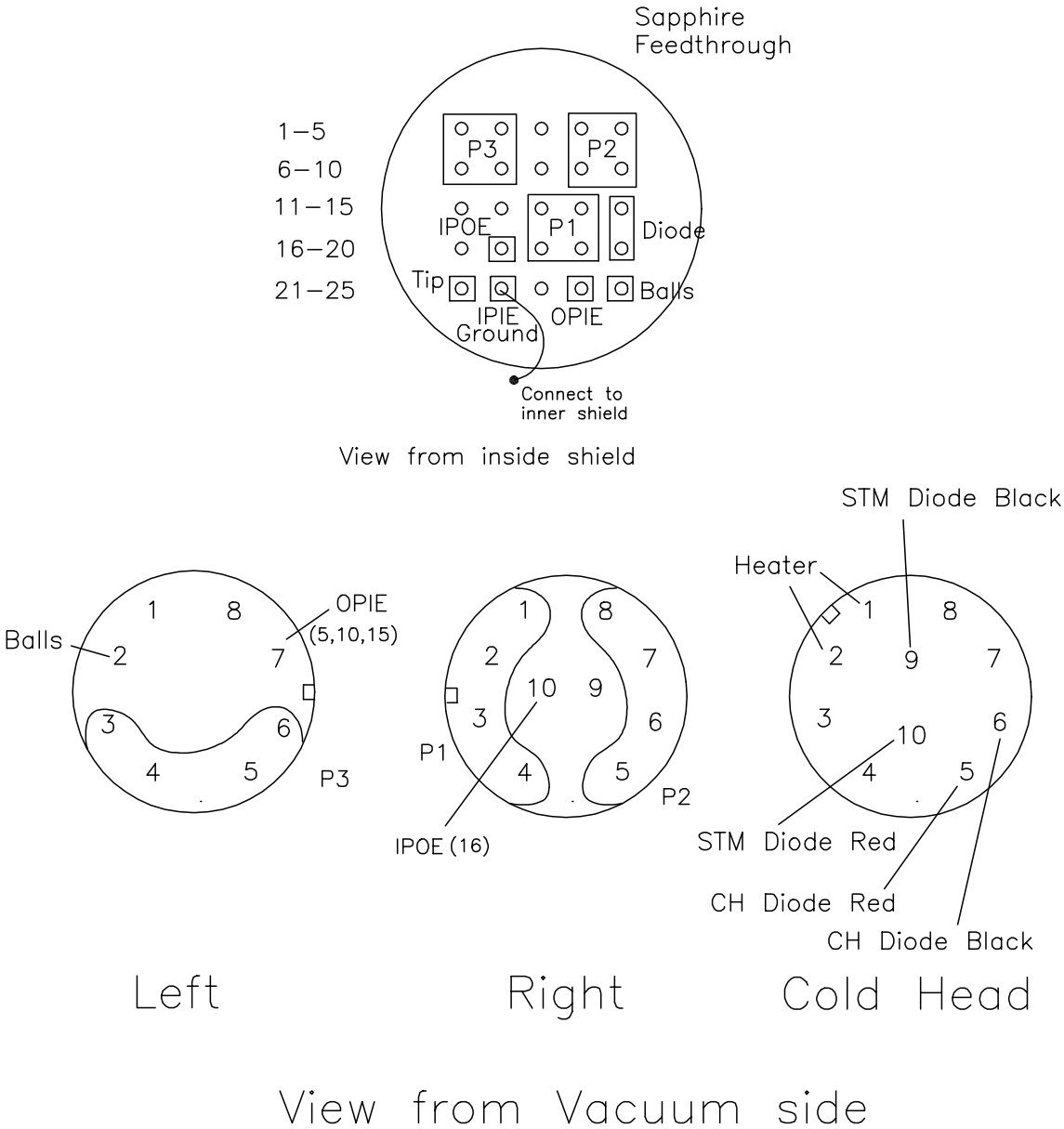

Figure B.8: Connections labels on the sapphire (top) and vacuum (bottom) feedthroughs.

Table B.4: Tantalum screw parts.

Item	Description	Quantity	Vendor
Ta hex nuts	0-80	72	Thermo Shield
Ta Threaded Rod	0-80, 1 ft	2	Thermo Shield

B.3 Making Tantalum Screws

Tantalum 0-80 screws are used on the sample holder to hold the rails and clips in place. Tantalum was chosen because it is a refractive metal and can withstand high temperatures, yet it is easier to machine than molybdenum or tungsten. The tantalum parts used in making the 0-80 screws are listed in table B.4. A water wheel is used for grinding and cutting the tantalum parts. All grinding is performed while holding the piece with stainless steel forceps. To make screws from the threaded rod and hex nuts, follow these steps:

- The hex nut has to be ground down to the size of a real 0-80 screw head. Place the nut on a stainless steel socket head bolt and grind down the sides (Fig. B.9a).
- Grind down the shaft of the stainless steel bolt and some of the Ta nut until the nut is as thick as the bolt head (0.05") (Fig. B.9b).
- Cut the Ta threaded rod into small pieces, about 0.25" long.
- Grind down the ends of the threaded rod so they are flat.
- Place the Ta nut on the end of the threaded rod, and using tungsten leads, spot weld the nut to the rod at 100 Watt s setting (Fig. B.9c). Multiple spot

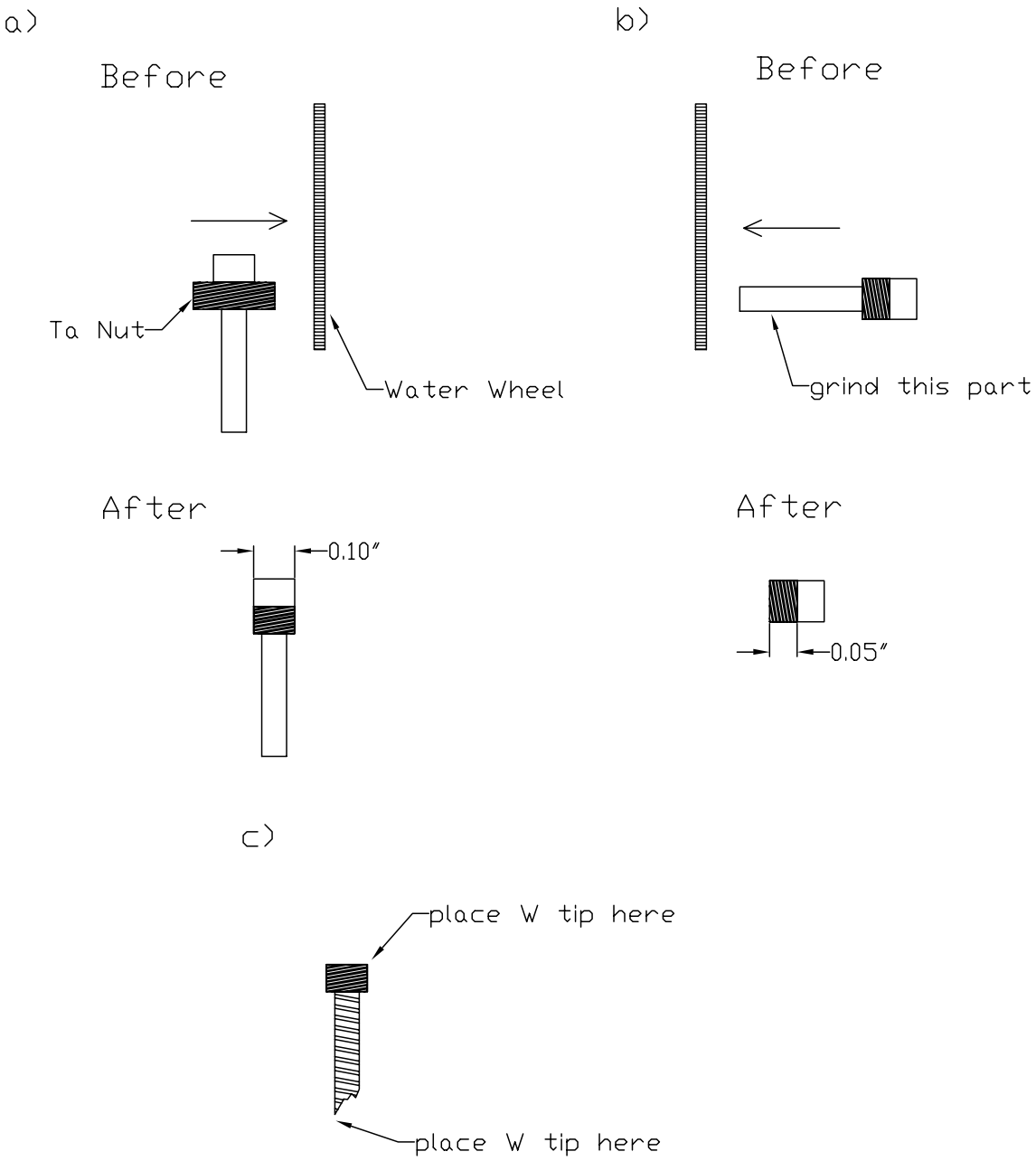

Figure B.9: a) Grinding the Ta nut so it is as wide as a regular screw head. b) Grinding the Ta nut so that it is as thick as a regular screw head. c) Spot welding the Ta nut and threaded rod.

welds are often necessary. After welding, apply torque to the nut to make sure it is welded properly.

- Place a stainless steel nut on the Ta bolt next to the Ta bolt head. Grind down the part of the rod that is sticking out of the nut.
- Make slots in the Ta bolt heads with a 0.012" slotting saw on the milling machine. The bolt is best held in a plate with a 0-80 tapped hole.
- Test the screw one last time to make sure the grinding and slotting has not loosened the head.

B.4 Making Inconel Springs

The STM is hung from three springs, whose primary function is to provide vibrational isolation. The resonance frequency of a mass and spring system is given by

$$\omega = \sqrt{k/m}, \tag{B.1}$$

where ω is the frequency, k is the spring constant and m is the mass of the STM. Since the mass of the STM is fixed (120 g), to lower the resonance frequency, and thereby increase the vibrational isolation, we need to reduce k as much as possible. From Hook's law ($F = kx$) we can deduce that increasing the stretched length, x, will decrease k, because the weight of the STM, F, is constant.

The spring constant of a real spring is given by

$$k = \frac{Gd^4}{8nD^3} \tag{B.2}$$

where G is the torsion modulus, d is the diameter of the wire, D is the mean diameter of the spring and n is the number of active coils [2]. To reduce k, we

can reduce d, increase D or increase n. There are natural limits to d, dictated mostly by what wire is commercially available and is strong enough to hold the STM. There are also geometrical constraints on D. Increasing n, however, causes the stretched length of the spring to be smaller because the length of the stretched spring is constrained by the shield design and therefore the vibrational frequency will be higher. G does not vary tremendously from material to material.

The springs are made from Inconel. This material was chosen because every other material that we tried (W, stainless steel, and music wire) did not perform well after temperature cycling. The STM is heated to 420 K during chamber baking and reaches 8 K during low temperature experiments. Inconel 718 is made of 52.7% Ni, 18.3% Cr, 18.1% Fe, 3.1% Mo, 1.1% Ti and a few impurities. It is particularly resistant to shape changes as a function of temperature. Inconel is suitable for high temperature applications for up to 593° C [2].

The 0.07" thick Inconel wire was wound on a custom made threaded rod 0.25" in diameter with approximately 125 threads per inch. The rod was mounted on a rotating lathe and one end of the wire was clamped onto the end of the rod. The other end of the wire was clamped to a large aluminum weight (1.2 kg). The wire was carefully wound on the threaded rod. When sufficient wire was wound, the end of the wire was clamped to the rod and cut, without ever losing the tension in the wire. The rod assembly (rod, wire and two clamps) was then heated to 500° C in an air oven for 1 hour. The assembly was then quickly cooled down by dropping it in liquid nitrogen. The fashioned springs are of very high quality: they are resistant to sagging as a result of temperature cycling and they extend up to ten times their unstretched length without deforming.

After the springs were fashioned, they were cut to the appropriate size and

mounted in the copper shield with the STM. The natural frequency of the STM was measured with no damping by letting the STM oscillate up and down and measuring the oscillation frequency. Our STM has a natural frequency of 2 to 3 Hz. The STM head is small and all the parts are well anchored so that no piece can oscillate near this natural frequency. We have not measured the natural frequency of the STM head. Based on oscillations observed in our tunneling current, we estimate the lowest oscillation frequency of STM head to be 5 to 10 kHz. The springs provide good vibrational isolation because of the disparity between their oscillation frequency and the high frequency oscillations of the STM head.

Bibliography

[1] L. Lauhon, PhD Dissertation, Cornell University, not yet published.

[2] Century Spring Corporation Catalog.

Appendix C

Cleaning Silicon Surfaces in UHV

Silicon surfaces can be difficult to clean. We have had little success in cleaning low resistivity silicon samples. The purpose of this appendix is to document the procedure used to clean our silicon surfaces.

C.1 Si(111)

We have found that boron doped, 1 Ω cm, prime grade Si(111) wafers are well suited for cleaning in our chamber. Other dopants such as phosphorus or lower resistivity wafers can produce rough surfaces, which might be due to dopant precipitation. Unfortunately, 1 Ω cm resistivity can only conduct above 50 K due to carrier freeze out. Figure C.1 shows an example of a rough surface. The following procedure was used to clean Si(111) to obtain large, flat, (7×7) reconstructed surfaces:

- The initial chamber pressure was 3×10^{-11} Torr. The sample was slowly heated to 700° C while keeping the chamber pressure below 1×10^{-9} Torr. The sample was outgassed overnight (10 to 12 hours) at 700° C. The final chamber pressure was 2×10^{-10} Torr.

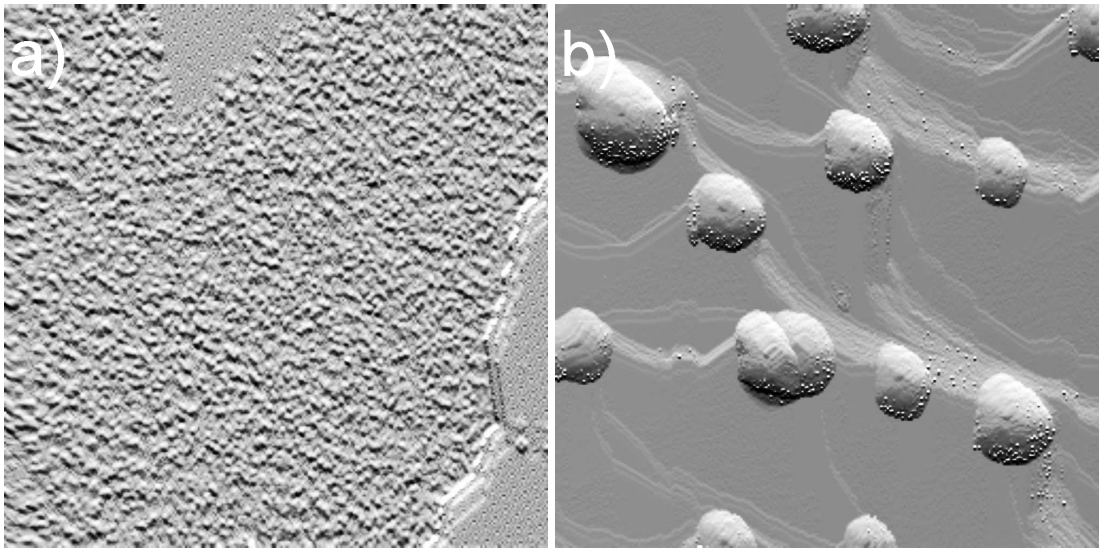

Figure C.1: Si(111) roughened surface. The sample was cut from a phosphorus doped, 0.02 Ω cm wafer. There are large, disordered mounds as well as disordered terraces on the surface. a) The close up view (1000×1000 Å) shows a mostly disordered terrace with some (7×7) reconstructed parts in the top and right of the image. b) Large scale view (4000×4000 Å) shows large disordered mounds that pin the steps.

- The sample was cooled to 400° C at a rate of 2-3 degrees per second and left to cool to room temperature for about an hour.

- After the sample had cooled down to room temperature and the chamber pressure dropped, the sample was annealed to 900° C for 3 minutes. The pressure while at 900° C was 2×10^{-10} Torr. The sample was cooled down at the same rate as before.

- The sample was sputtered with 1 keV Ne^{+} ions at a background pressure of 8×10^{-5} Torr for 5 minutes.

- The sample was annealed to 930° C for 5 minutes. The pressure while at 930° C was 2.5×10^{-10} Torr.

- The sputter-anneal cycle was repeated two more times. The final chamber pressure at 930° C was 2.2×10^{-10} Torr.

- The sample was sputtered at a background pressure of 8×10^{-5} Torr for 10 minutes.

- The sample was annealed to 1130° C for 5 minutes. The pressure while at 1130° C started at 2.5×10^{-9} Torr and dropped to 2×10^{-9} Torr. The sample was quickly cooled to 850 to 900° C and then slowly cooled as before.

- The sample was sputtered at a background pressure of 8×10^{-5} Torr for 10 minutes.

- The sample was annealed to 1215° C for 2 minutes. The pressure while at 1215° C was 3×10^{-9} Torr. The sample was quickly cooled to 850 to 900° C and then slowly cooled as before.

- The sample was sputtered at a background pressure of 8×10^{-5} Torr for 10 minutes.

- The sample was annealed to 1240° C for 1 minute. The pressure while at 1240° C was 3×10^{-9} Torr. The sample was quickly cooled to 850 to 900° C and then slowly cooled as before.

- The sputter-anneal cycle at 1240° C was repeated 4 more times. The final pressure at 1240° C was 1.1×10^{-9} Torr.

At this point, the sample was clean and could be used after one sputter-anneal cycle at 1240° C. The sample may be slightly hazy at this point, but the haze does not affect the atomic scale (7×7) reconstruction. Haze is usually attributed to large steps separated by large terraces. The terrace length is on the order of the visible light wavelength and therefore causes the haze.

C.2 Si(100)

Cleaning Si(100) is very similar to Si(111). The sample that has worked consistently for our experiments is n-type, 10-25 Ω cm, prime grade wafer. It was cleaned as follows:

- The sample was outgassed at 678° C overnight. The final chamber pressure was 1.8×10^{-10} Torr. The sample is cooled down slower than Si(111) at 1 degree per second.

- The sample was annealed to 750° C for 20 minutes. The pressure at 750° C was 2×10^{-10} Torr.

- The sample was sputtered at a background pressure of 8×10^{-5} Torr for 15 minutes.
- The sample was annealed to 920° C for 10 minutes. The maximum pressure was 2.6×10^{-9} Torr; the final pressure was 1.2×10^{-9} Torr.
- The sample was sputtered at a background pressure of 8×10^{-5} Torr for 10 minutes.
- The sample was annealed to 1035° C for 5 minutes. The maximum pressure was 3.6×10^{-9} Torr; the final pressure was 2×10^{-9} Torr.
- The sample was sputtered at a background pressure of 8×10^{-5} Torr for 10 minutes.
- The sample was annealed to 1100° C for 4 minutes. The maximum pressure was 1.9×10^{-9} Torr; the final pressure was 1.6×10^{-9} Torr.
- The sample was sputtered at a background pressure of 8×10^{-5} Torr for 10 minutes.
- The sample was annealed to 1225° C for 1 minute. The final pressure was 3.8×10^{-9} Torr.
- The sputter-anneal cycle at 1225° C was repeated 5 more times. The final pressure was 3.4×10^{-9} Torr.

At this point, the sample was clean and could be used after one sputter-anneal cycle at 1225° C.